NASA CR-66262

SPACE PROBE RADAR ALTIMETER STUDY

Volume I

TECHNICAL REPORT

November 1966

Prepared under Contract No. NAS 1-5953

by

WESTINGHOUSE ELECTRIC CORPORATION
Aerospace Division
Baltimore, Maryland

for

NATIONAL AERONAUTICS AND SPACE ADMINISTRATION
Langley Research Center
Hampton, Virginia

SPACE PROBE RADAR ALTIMETER STUDY

Volume I

TECHNICAL REPORT

November 1966

Prepared under Contract No. NAS 1-5953

by

WESTINGHOUSE ELECTRIC CORPORATION
Aerospace Division
Baltimore, Maryland

for

NATIONAL AERONAUTICS AND SPACE ADMINISTRATION
Langley Research Center
Hampton, Virginia

FOREWORD

Westinghouse Electric Corporation, Aerospace Division, Baltimore, Maryland, has investigated the system requirements of a radar altimeter applicable to deep space probes. The study has been conducted under contract NAS 1-5953 with the National Aeronautics and Space Administration, Langley Research Center, Hampton, Virginia. The Westinghouse order number was AAD-53449.

The results of the study are presented in three volumes. Volumes II and III are the development and reliability plans, respectively. This document, Volume I, is a discussion of the operational requirements and a technical discussion of the radar to meet these needs.

TABLE OF CONTENTS

LIST OF TABLES

INTRODUCTION

Westinghouse Electric Corporation, Aerospace Division, has conducted a Space Probe Radar Altimeter (SPRA) Study under contract NAS 1-5953 for NASA's Langley Research Center. Under this program was developed an altimeter conceptual design and a plan for further development. This technical report is one of three volumes which, together with a set of drawings, constitute the contract final report. Other volumes are: Volume II, "Development Plan"; and Volume III, "Reliability and Quality Assurance Plan".

The altimeter design presented here has been based on the requirements of first-generation planetary landers such as that considered for Mars in mid-1971. Altitude information would be used for such purposes as correlation of atmospheric measurements taken during descent and initiation of parachute deployment. The postulated vehicle would be a small, semi-hard lander, and the volume, weight, and power available for an altimeter would be limited. Thus size, weight, and power consumption are critical items. Additionally, anti-contamination considerations require sterile equipment, so that components and materials must withstand sterilization heat soaks without detrimental effects.

The impact of requirements for an advanced, more elaborate mission has also been considered. This report discussed modifications to the basic altimeter for attaining higher altitudes, greater accuracy, etc.

This document is divided generally into the needs and their fulfillment. First, design goals are given and a typical trajectory presented. Several radar requirements are derived from the trajectory model. Then, based on the established operational specifications, various types of radar systems are considered and compared. The report then develops in detail the design of the most favorable of these for this application, a pulse radar. Advanced requirements and growth potential are also discussed.

SUMMARY

A number of representative generic altimeter types were investigated during the SPRA Study. The conclusion was that a pulse radar is best suited for the altimeter application. Power consumption and complexity of FM/CW and ICW systems make them unattractive relative to conventional pulse radar. This is largely because doppler shifts and doppler smearing of the return signal denies use of the narrowband, coherent processing upon which the high duty cycle and cw techniques depend for efficient operation. Considering weight, volume, reliability, and power consumption, a pulse radar is clearly favored.

The pulse radar design is conceptually a conventional, closed loop, pulse tracking system. Unique features are a digital range tracker, and TWT transmitter. Another is a stepped scan, phased array antenna employing a modified Butler beam-forming network.

The digital range tracking system offers higher accuracy and greater environmental stability than does its analog counterpart. Reliability considerations, as well as magnetic cleanliness, led to the choice of a TWT transmitter, the TWT amplifier being driven by a solid-state X-band source. The antenna configuration is the smallest, lightest, and most reliable of all electronically scanned antennas capable of covering the required 120° x 120° field of view. Reliability, plus compatibility with flush mounting, favor an electronically scanned antenna over a mechanical scanner.

The altimeter weight and volume exceed the contract guideline design goals (weight, 13.88 pounds; volume, 474 cubic inches). Power consumption is approximately 20 watts. A significant portion of the total weight and volume is due to the antenna (3.35 pounds and 236 cubic inches). Antenna size could be reduced considerably with a restricted scan angle. For example, a 40% reduction could be realized by reducing the scan angles to 60° x 120°.

In view of the available development time, a smaller altimeter is not believed practical unless performance or reliability is degraded.

With respect to the sterilization requirement, it was concluded that the sterilization heat soaks do not present a significant problem. Materials, components, and fabrication techniques must be selected, but the altimeter design can be made compatible with sterilization temperatures without difficulty.

REQUIREMENTS

The space probe radar altimeter must be a compact, low power consuming, light-weight, sterilizable device. It must have a high probability of successful operation after a long storage period while in transit (9 months for a Mars mission). The altimeter during atmospheric entry will provide altitude markers for parachute deployment. Also it will provide continuous altitude readings for correlation of atmospheric measurements by instruments in the lander scientific payload.

Parameters

Operational parameters and performance characteristics as specified in the Contract Work Statement are listed in Table I.

TABLE I. - CONTRACTUAL REQUIREMENTS

Parameter	Performance
Altitude range	300 m to 15.5 km
Accuracy	±10 m or ±2 %
Frequency	X-band (8-10 GHz)
Velocity (max)	3.0 km/sec
Acceleration (max)	200 g
Antenna (max)	6" dia paraboloid or equivalent
Power required (max)	15 W
Size (max)	300 cu in
Weight (max)	6 lb
Data rate and format	One reading every 5 seconds minimum; 10 readings per second max., least significant bit = 10 meters; 11 - bit binary code.
Radar reflectivity	Similar to extremes of earth (-20 to -30 dB)
S/N in automatic range track	20 dB
Mission lifetime	Approximately 9 months total (9 months inactive, 30 minutes operating).

Trajectory

To more closely define some of the constraints on the lander altimeter it is necessary to estimate the capsule trajectory. The needed values are the likely extremes of flight angle, vertical and horizontal velocity, and vertical acceleration as functions of altitude. From these we can establish antenna coverage, doppler shift and bandwidth, acqusition time, and range track loop parameters. Of course, uncertainties in the knowledge of Martian atmospheric characteristics and the preliminary nature of Voyager studies to date preclude exact trajectory determination. However, typical extremes can be established. Accordingly, the altimeter design and performance calculations have been based on the curves of Figures 1 through 6, which describe a typical capsule trajectory.

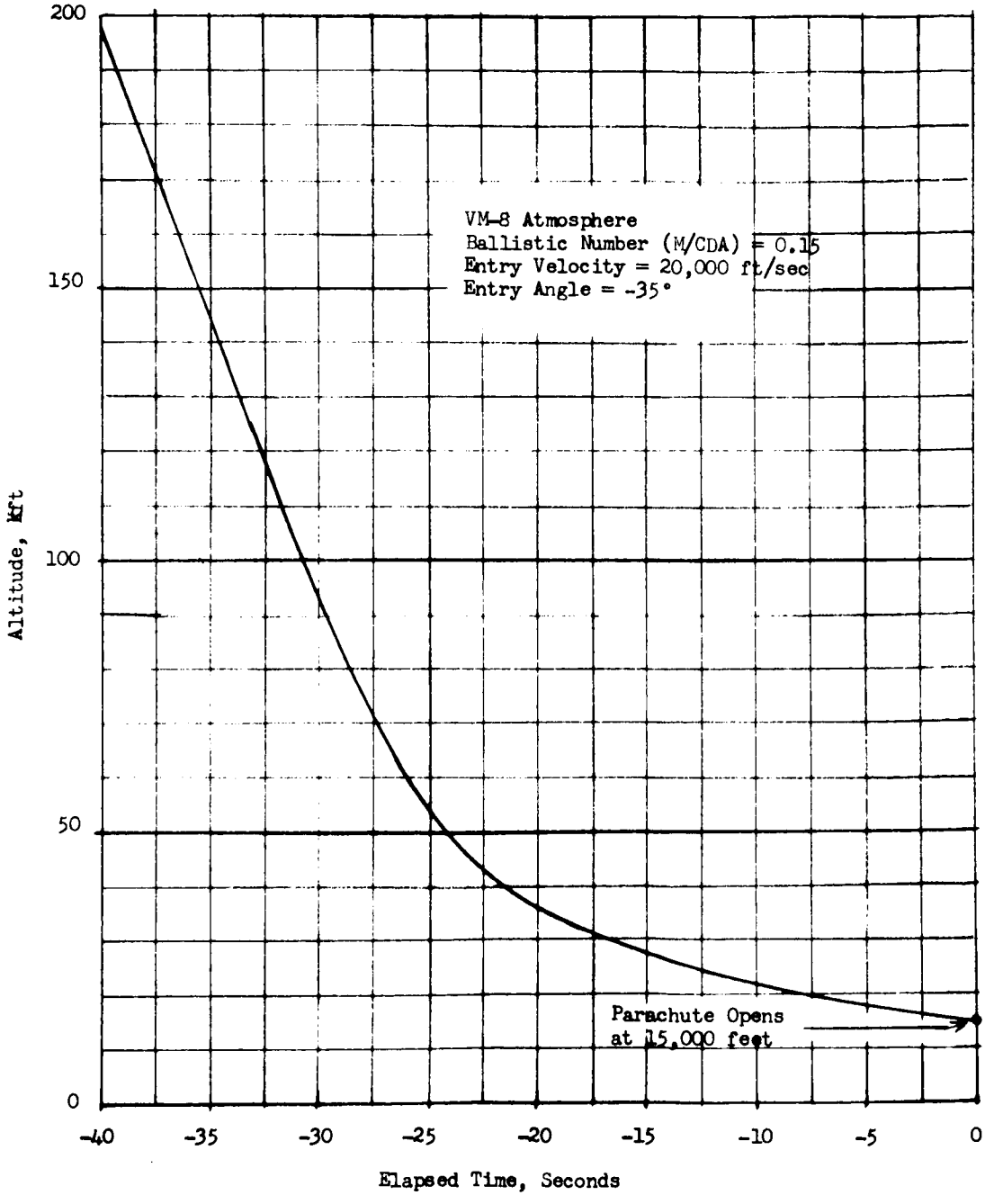

FIGURE 1. - FREE-FALL DESCENT (INITIAL PHASE)

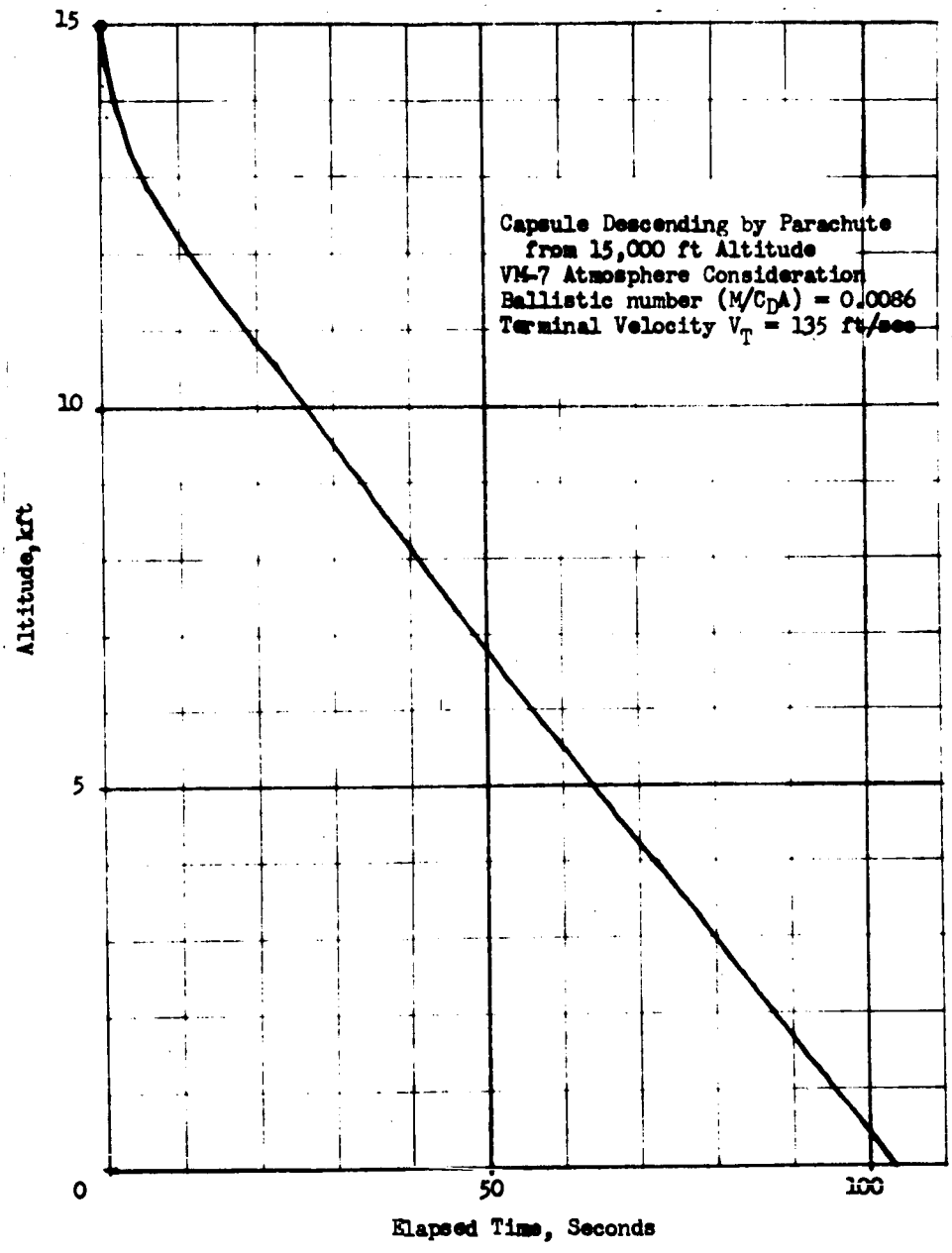

FIGURE 2. - PARACHUTE DESCENT (TERMINAL PHASE)

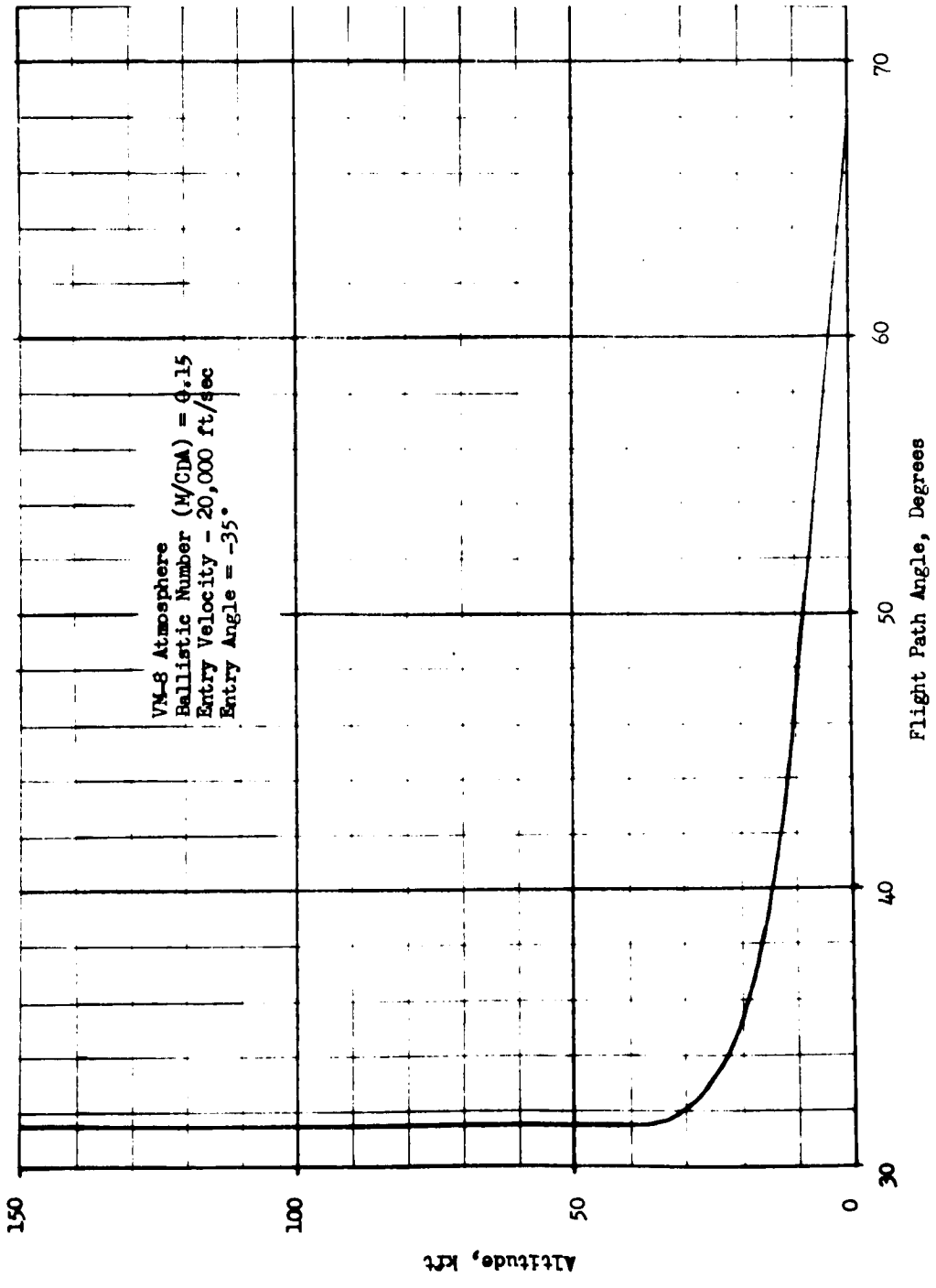

FIGURE 3. - ALTITUDE VS FLIGHT PATH ANGLE

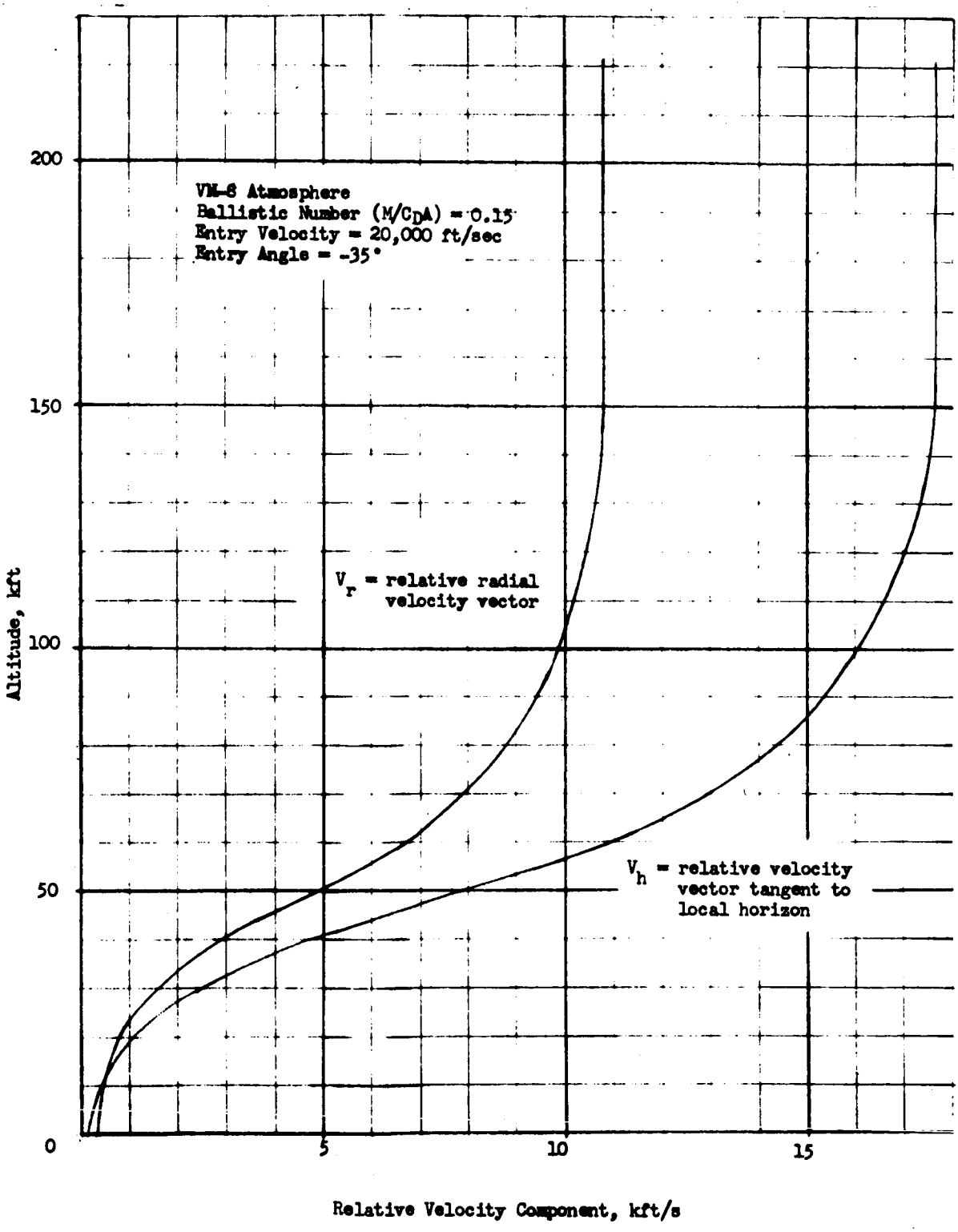

FIGURE 4. - OVERALL VELOCITY PROFILE

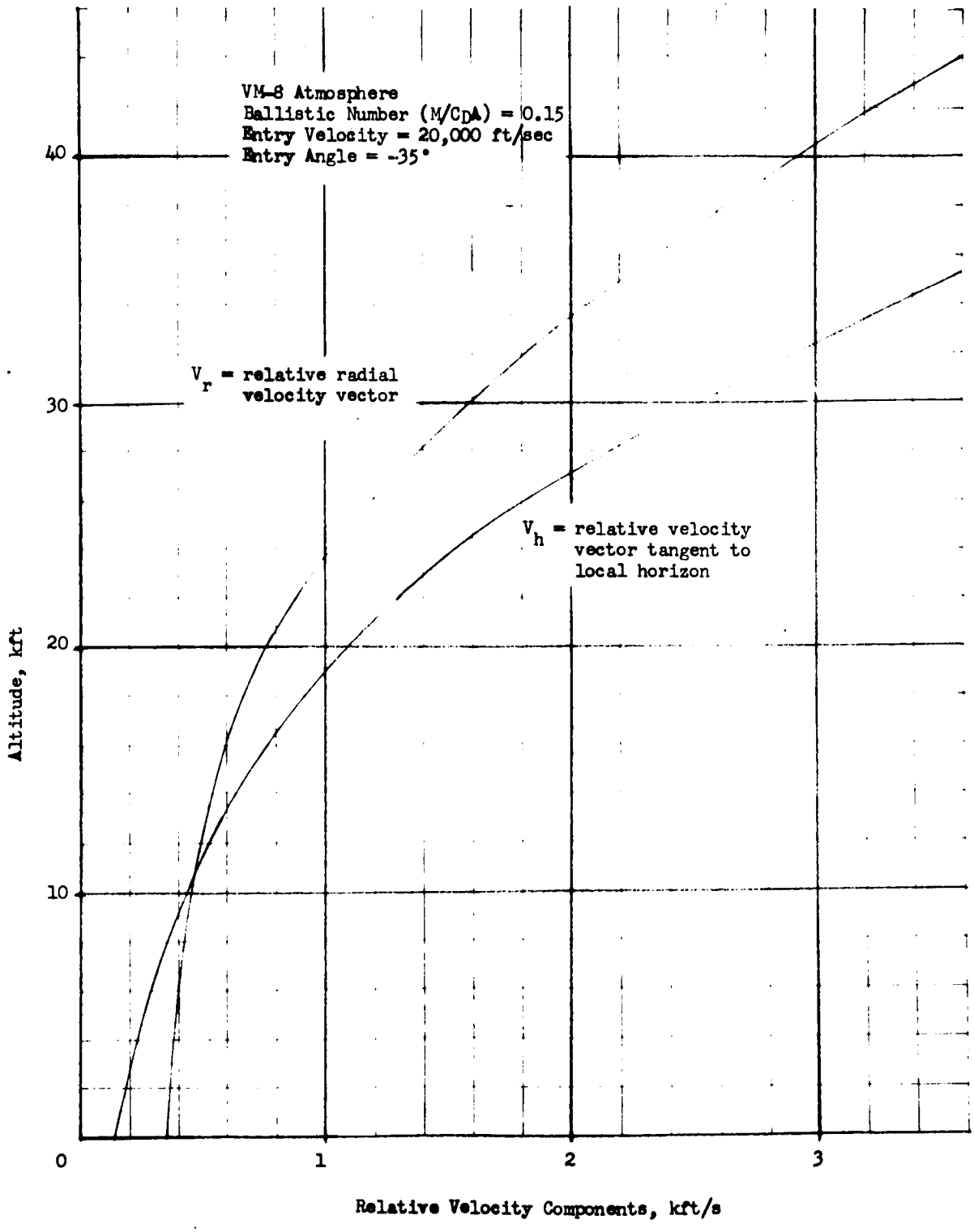

FIGURE 5. - VELOCITY PROFILE NEAR SURFACE

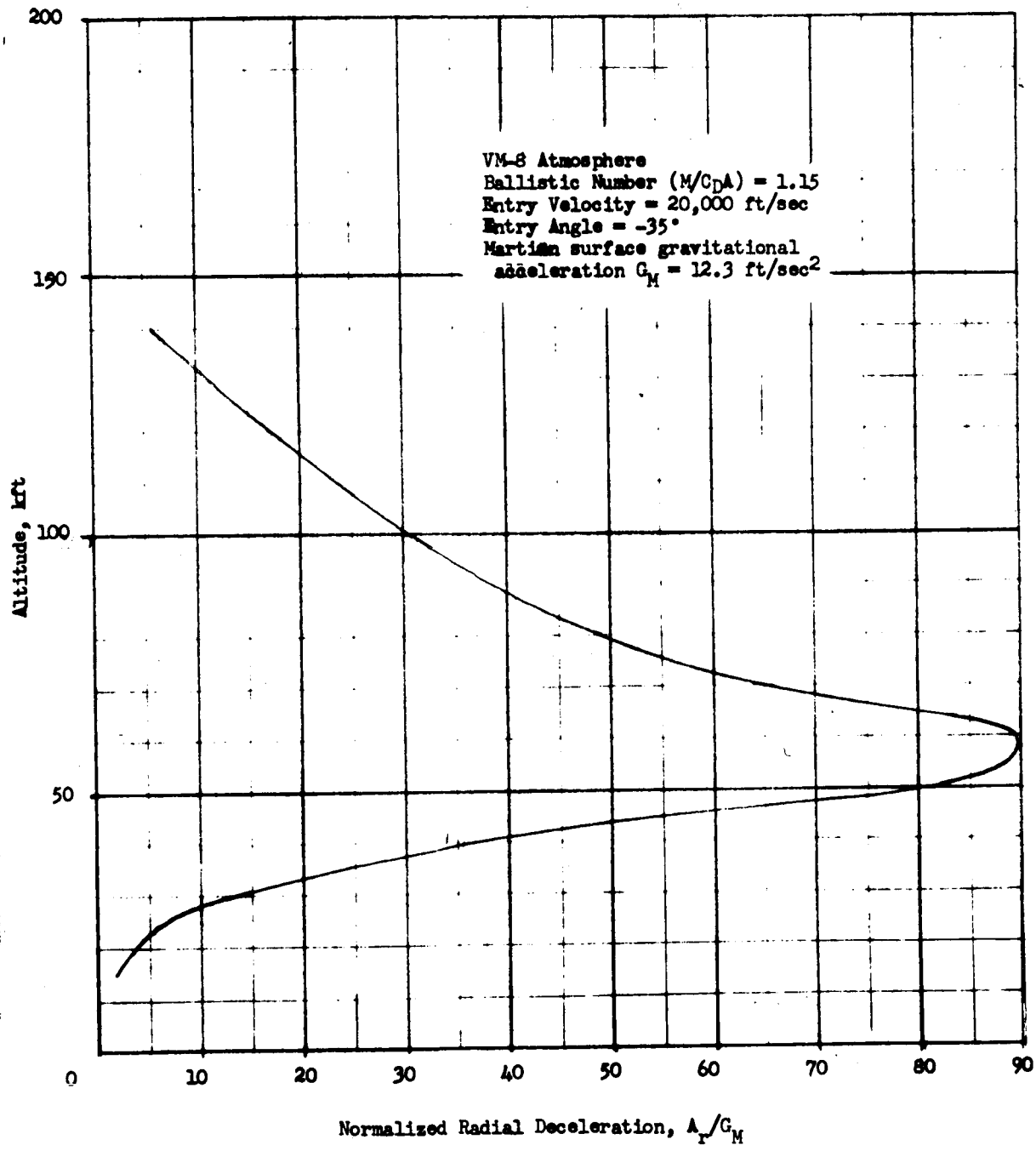

FIGURE 6. RADIAL DECELERATION PROFILE

This trajectory is based on the entry of a blunted cone into the Martian atmosphere and gravitational field. Aerodynamic braking slows the vehicle to a speed at which parachute deployment is possible. Terminal descent is therefore by parachute.

Of course the space probe altimeter might well be used in a vehicle having a different configuration and/or descent mechanism. However, the postulated trajectory is representative and is quite adequate for technique comparison purposes. Performance of the ultimate design will not be unduly influenced by substantial departures from this trajectory.

Angular Coverage

One of the most critical requirements influencing size and weight is angular coverage. It is particularly difficult to establish a firm requirement without very specific definition of the entry vehicle, its trajectory, and its flight angle. However we may assume that the lander will be unstabilized in roll (or, at best, only roughly stabilized); also that it will pitch through a considerable range of angles. Therefore reasonably large angular coverages in both axes are necessary. As a basis for design, Westinghouse has established a required angular coverage of $\pm 60°$ in two axes. This requirement will be covered in the detailed design. However, it need not be considered in comparing generic radar system types since the antenna problem will be shared by all systems (except that some systems require two antennas).

Doppler Shift

One of the key factors influencing altimeter selection is the doppler frequency shift and doppler smearing of the returned signal. These are determined as follows.

Assume the lander capsule is traveling at velocity V and flight angle θ as shown in Figure 7. Further assume an antenna of beamwidth β is directed along the vertical. Assuming generally diffuse scattering, the radar echo will be noiselike with a frequency distribution determined by the velocity of the vehicle with respect to the incremental scatterers illuminated by the antenna and the antenna beam shape.

Within the antenna half-power beamwidth, β, the frequency spread of the significant portion of the return is approximately

$$\Delta f = \frac{2V \cos \theta}{\lambda} (2 \sin \beta/2) \qquad (1)$$

where $V \cos \theta$ = horizontal velocity
λ = RF wavelength

Since β will be reasonably small, $\sin \beta/2 \approx \beta/2$, and

$$\Delta f \approx \frac{2V \cos \theta}{\lambda} \beta \qquad (2)$$

as long as $\theta < (90 - \beta/2)$. When the velocity vector approaches vertical, equation (2) is no longer a good approximation. On the other hand the doppler spread is of most concern at high altitude, where the flight angle is shallow.

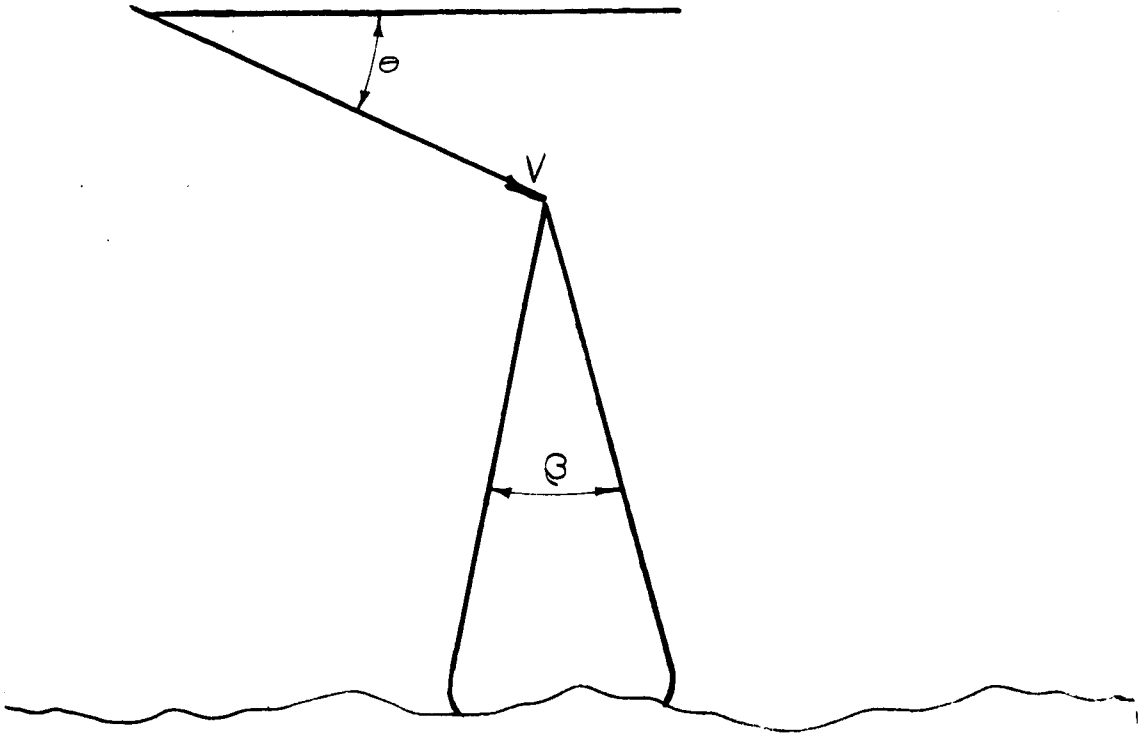

FIGURE 7. - DOPPLER GEOMETRY

The antenna beamwidth is approximately $\beta = \lambda/d$, where d = aperture diameter. Therefore

$$\Delta f = \frac{2V \cos \theta}{\lambda} \cdot \frac{\lambda}{d} = \frac{2V \cos \theta}{d} \qquad (3)$$

The approximate doppler spread is plotted in Figure 8 as a function of horizontal velocity for a 6-inch and 24-inch aperture. These curves are based upon the assumption that the aperture is normal to vertical. For a phased array this condition will not hold, and the doppler spread will be somewhat larger because of beam broadening at large scan angles.

Figure 9 shows the doppler shift of the returned spectrum caused by the vertical velocity component. This doppler shift is

$$f_d = \frac{2V \sin \theta}{\lambda} \qquad (4)$$

where the wavelength is for an RF of 8.0 GHz. Note that, as long as the antenna beamwidth is reasonably small, the doppler spread, Δf, is essentially independent of frequency, being a function of antenna aperture and horizontal velocity only. This, of course, is not true of the doppler shift, f_d.

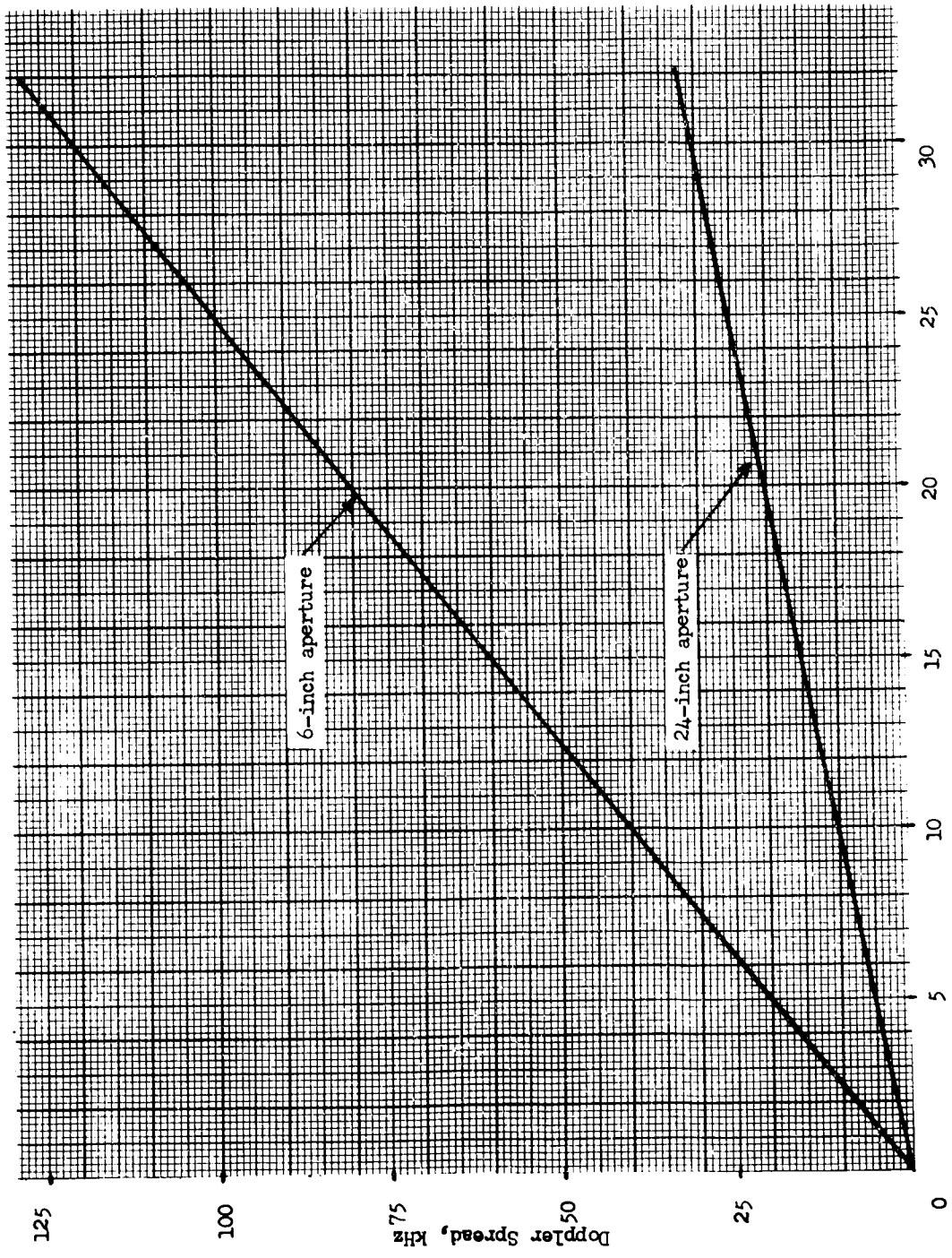

FIGURE 8. - DOPPLER SPREAD

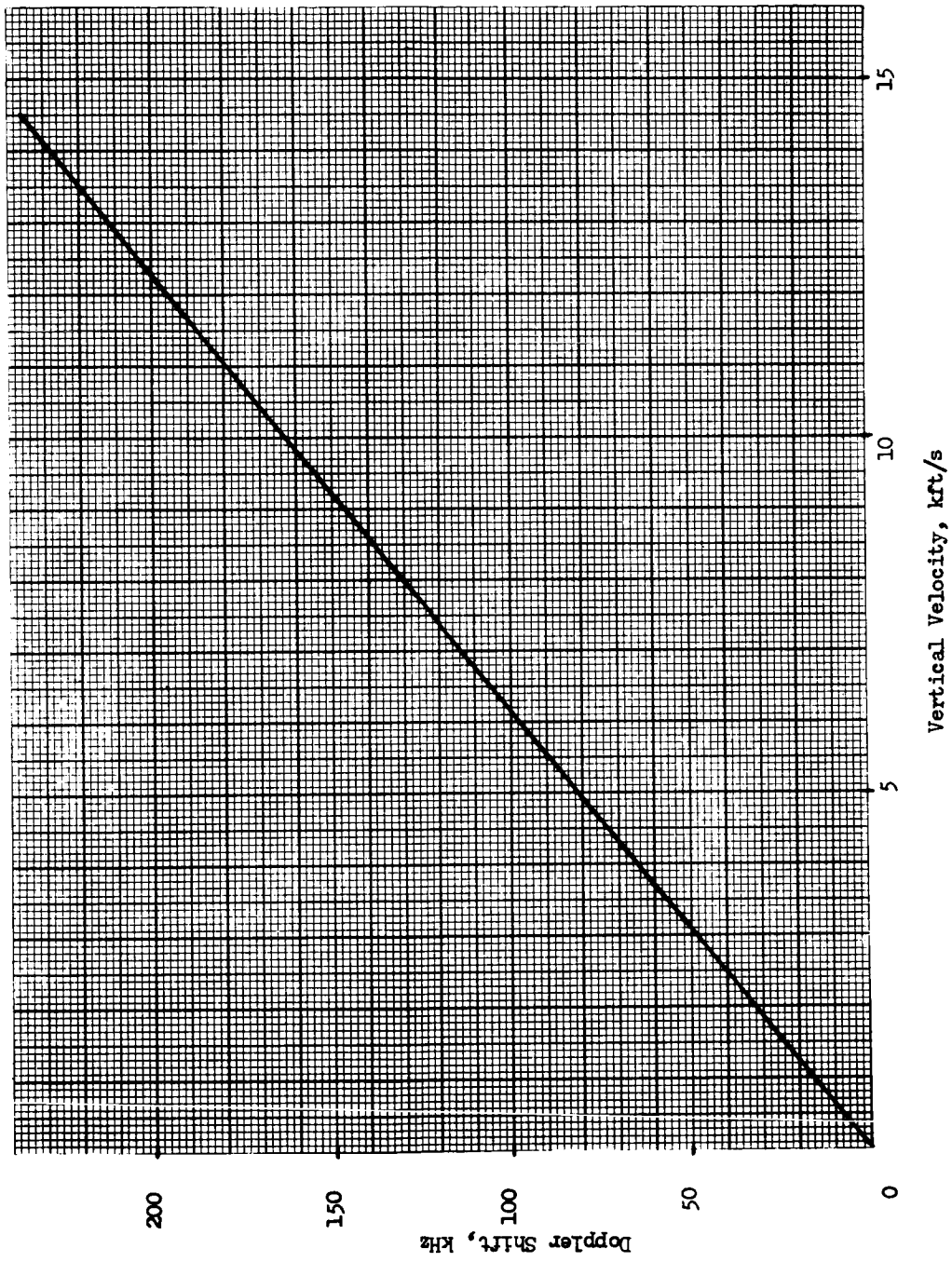

FIGURE 9. - DOPPLER SHIFT

Based on the velocity profile of Figure 4, the doppler shift and spread at maximum altitude (50,000 feet) are approximately 80 kHz and 32 kHz respectively if the antenna aperture is 6 inches. These are representative design values for an altimeter answering the basic requirements. However, keeping in mind the requirement of growth potential for future missions, the basic altimeter technique should be capable of performing at higher altitudes and greater velocities without fundamental difficulty.

Acquisition and Track

The descent history of Figure 1 demonstrates the need for a fairly rapid acquisition capability. A radial velocity of several thousand feet per second is not unlikely. Search times of greater than a few seconds would be excessive. Also, the high velocity and high acceleration influence the performance of the altitude tracking system.

COMPARISON OF ALTIMETER GENERIC TYPES

This section discusses possible types of radar altimeters. The different types are FM/CW, ICW (interrupted cw), and pulse radar. The FM/CW actually may take any of three forms: sawtooth, sinusoidal or sidetone. Also, the ICW may use either PRF ranging or high-PRF pulse doppler. The most favorable technique depends, of course, on the specific requirements of the application. In the space probe application there are some unique constraints which are of particular significance.

Basis for Comparison

Generally speaking, the advantages of FM/CW altimeters are low peak power, the ability to measure essentially zero altitude, and (sometimes) simplicity. Low peak power offers the possibility of using a solid-state transmitter. But, even if a transmitter tube is necessary, the required voltage will be low relative to that of a pulse transmitter.

One of the most commonly recognized problems with FM/CW altimeters is transmitter-to-receiver leakage. Leakage is particularly serious in high altitude operations. Consequently separate transmit and receive antennas are almost always necessary. Another limitation in this application results from the very large doppler shifts and doppler smearing of the surface return. As shown subsequently, large dopplers preclude processing the return coherently in a narrow bandwidth. This loss dictates a much larger power requirement than would ordinarily be expected for an FM/CW altimeter.

ICW altimeters avoid the leakage problem, but they are also subject to limitations imposed by the large dopplers expected in this application. High duty cycle, pulsed systems retain the relatively low peak power advantage of FM/CW systems at the expense of somewhat greater complexity. But, again, large doppler spreads deny the full advantage of coherent processing, thus limiting the appeal of this approach.

Both FM/CW and ICW altimeters, if they are able to use low power transmitters, suffer from the inherently low efficiency of low peak power transmitters. Relatively high peak power, low duty cycle pulse transmitters or inarily have greater overall efficiency. Moreover the doppler spread of the return has little influence on the performance of a wideband, noncoherent pulse system.

The following paragraphs describe and compare altimeter techniques. These comparisons involve such common requirements and operating conditions as altitude, lander trajectory, accuracy, frequency, and antenna size. Systems which meet these requirements are compared on the basis of size, weight, power consumption, complexity, and reliability. Because power consumption is critically important, this parameter was investigated first; the highly unfavorable power requirements of some techniques disqualify them on that basis alone. Following analysis and power calculation, other characteristics of the several techniques are compared.

Sawtooth Modulated FM/CW

The simplest FM/CW radars transmit a signal with periodic frequency modulation, mix the received signal with a portion of the transmitted signal, and measure the beat frequency with some type of cycle rate counter. Figure 10 is a block diagram of such a system. While this system uses an analog frequency meter, the following discussion applies as well to systems with any device which measures frequency as a function of zero crossings.

The modulation applied to the transmitted signal consists of triangular frequency modulation with a repetition period, $T_R = 1/f_r$, and a peak frequency deviation ΔF. The frequency of the signal at the output of the receiver mixer is readily deduced from Figure 11; in this figure, f_t is the transmitted frequency, f_r is the received frequency, and the beat frequency is

$$f_d = |4\Delta F\, f_r\, \tau| \tag{5}$$

where τ= two way propagation time = $2R/c$, where R = range.

The result, expressed as equation (5) assumes that the detailed character of the signal in the region about the crossover may be ignored, since this region contributes a negligible portion of the signal. Obviously, equation (5) is not strictly valid, since a periodic system must produce a periodic difference frequency, and a line spectrum exists in this case. However, the approximation is adequate as long as the modulating frequency is low compared with the frequencies of interest in the difference spectrum.

Derivation of parameters. - The geometry of Figure 11 shows that the number of zeros in the difference wave is independent of the waveform of the modulation as long as the latter is monotonic and the limits of deviation are fixed. Hence, it is legitimate for some analytical purposes to substitute a sinusoid for the sawtooth waveform. Using this latter expedient, assume the transmitted signal amplitude is

$$e_t = E_t \sin [\omega_o t + \mu \sin \omega_r t] \tag{6}$$

where $\mu = \Delta F/f_r$ = modulation index and $\omega_o = 2\pi f_o$ = RF center angular frequency. The received signal is then

$$e_r = E_r \sin [\omega_o (t-\tau) + \mu \sin \omega_r (t-\tau) + \phi_R] \tag{7}$$

where ϕ_R = phase shift at the surface. The detected signal becomes

$$e_d = E_d \sin \phi, \text{ where} \tag{8}$$

$$\begin{aligned} \phi &= \omega_o \tau + \mu [\sin \omega_r t - \sin \omega_r (t-\tau)] - \phi_R \\ &= \omega_o \tau + 2\mu \sin \omega_r \tau/2 \cos \omega_r (t-\tau/2) - \phi_R \\ &\approx \omega_o \tau + \mu \omega_r \tau \cos \omega_r (t-\tau/2) - \phi_R \end{aligned} \tag{9}$$

if $\omega_r \tau/2 \ll 1$, which is true for all ranges of interest.

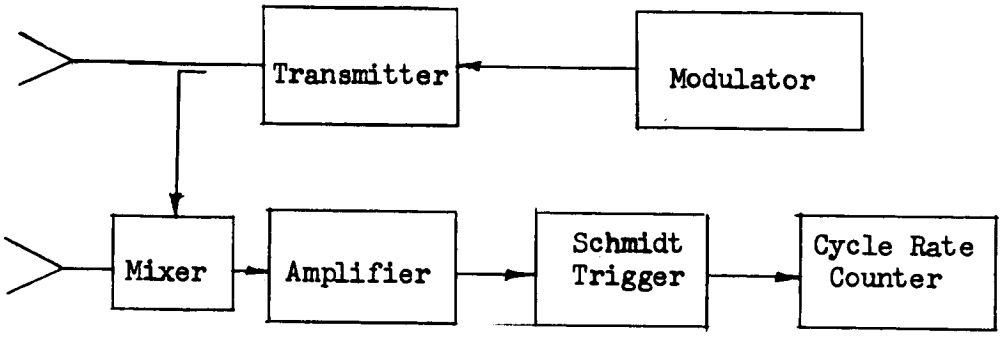

FIGURE 10. - SAWTOOTH FM/CW ALTIMETER

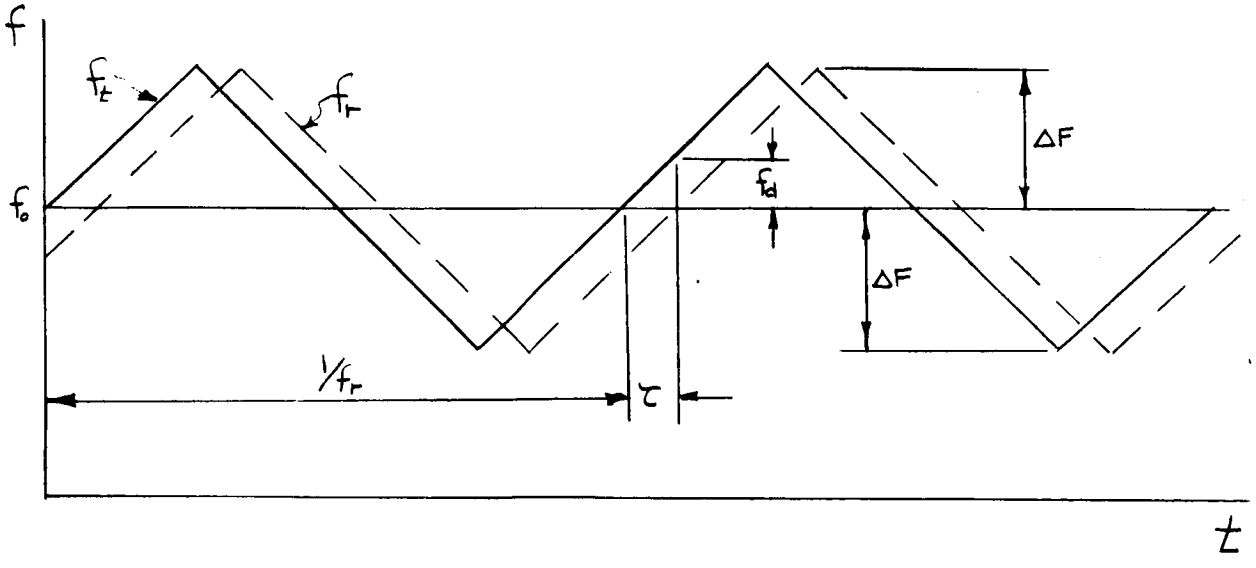

FIGURE 11. - MODULATION WAVEFORM

The quantity in equation (9) which is a measure of range is

$$\gamma = \omega_r \tau = 2\pi \Delta F \tau \qquad (10)$$

The frequency meter merely recognizes positive-going zero crossings. Therefore it is capable of registering only frequencies which are integral multiples of the modulating frequency, as can be seen from equation (9). Hence the range reading will be quantized in steps corresponding to the frequency of modulation, i.e.,

$$d_c = \frac{c}{8\ \Delta F}, \text{ where } c = \text{velocity of propagation} \qquad (11)$$

Equation (11) is an expression for the familiar step or fixed error of sawtooth-modulated cw homodyne radars. The peak frequency deviation must be selected such that the fixed error does not exceed the maximum allowable error at low altitude.

A further constraint in selecting the modulation parameters is that the period of modulation, T_R, should be large compared to the altitude delay, τ. Thus the error introduced during the turn-around of the sawtooth waveform will be small.

Note that unless the ranging frequency, equation (5), is larger than the doppler shift, the doppler frequency rather than the ranging frequency will be measured. Thus the ranging frequency should be made larger than expected doppler shifts. If this requirement is met, the doppler shift will be averaged to near zero over a reasonably long integration time.

Another factor to be considered is the doppler spread of the return. The noiselike doppler dispersion will introduce random error. This error can also be smoothed, but the ranging frequency must be large with respect to the smoothed rms doppler dispersion.

From the foregoing we can derive typical values of ΔF and f_r in order to estimate the altimeter bandwidth and subsequently its transmitted power.

First, the fixed error should be at worst equal to the maximum error at low altitude. From equation (11),

$$30 \text{ feet} = \frac{c}{8\ \Delta F}$$

or $\Delta F = 4$ MHz.

Turning to the second requirement, the modulation period, T_R, should be sufficiently large so that the turn-around error is small. Rather than rigorously defining the minimum T_R (maximum f_r) it will suffice to pick a typical maximum value of about 100 Hz. The modulation period will then be 100 times the maximum altitude delay (about 100 μsec and 50,000 feet) which should result in negligible error due to modulation turn-around.

With $\Delta F = 4$ MHz and $f_r = 100$ Hz, the ranging frequency at maximum altitude will be

$$f_d = 4\ \Delta F\ f_r\ \tau \approx 4 \times 4 \times 10^6 \times 100 \times 100 \times 10^{-6} = 160 \text{ kHz}$$

A lower value would be preferred in order to lower the noise bandwidth. Moreover the expected doppler shift and dispersion will allow a lower ranging frequency, as will be shown subsequently.

If the doppler shift is to be effectively canceled over a period of the sawtooth modulation, the ranging frequency must be greater than the largest doppler shift of the significant portion of the returned signal spectrum. As was pointed out in discussing trajectories, the mean doppler shift due to the vertical velocity component may be as large as 80 kHz. The doppler dispersion of the return from the surface illuminated by the antenna half-power beamwidth will be about 32 kHz. If the antenna beam is perfectly aligned with vertical, the largest doppler frequency of the significant portion of the return will be about $80 + 32/2 = 96$ kHz. Based on this criterion, the ranging frequency at 50,000 feet should be not less than 100 kHz.

The final consideration in establishing the ranging frequency is the error due to the doppler frequency noise. If the bandwidth of the doppler dispersion is Δf, the correlation time of the frequency error is approximately $1/\Delta f$. With an output noise bandwidth of β_n, the number of samples smoothed is approximately $\Delta f/\beta_n$. The doppler smear is reduced by the square root of the number of samples smoothed, leaving an rms doppler dispersion of

$$\Delta f' = \Delta f/\sqrt{\Delta F/\beta_n} = \sqrt{\Delta f\ \beta_n} \qquad (12)$$

A typical value of β_n is 5 Hz. Substituting $\Delta f = 32$ kHz and $\beta_n = 5$ Hz,

$$\Delta f' = \sqrt{32 \times 10^3 \times 5} = 400 \text{ Hz}.$$

With a ranging frequency of 100 kHz, the residual error after smoothing will be about $(400 \text{ Hz}/100 \text{ kHz}) \times 100 = 0.4\%$. Since this is a reasonably small error, the previously derived ranging frequency of 100 kHz is large enough.

Noise error. - The foregoing suggests that the maximum ranging frequency be on the order of 100 kHz. Therefore the receiver bandwidth also will be about 100 kHz. To calculate the transmitted power we must determine the signal-to-noise ratio (S/N) in this bandwidth necessary for the desired accuracy. An estimate of the required S/N is determined as follows.

As mentioned previously, the sawtooth-modulated altimeter measures the ranging frequency by counting the number of zero crossings of the signal in a fixed time period. This can be done digitally or with an analog device such as a cycle rate counter. Either way, the number of zero crossings of the signal plus noise are measured over the system integration

time. The mean error in frequency measurement due to noise can be estimated using an expression relating required S/N to desired accuracy. This relationship (see Appendix A for derivation) appears in equations (13) and (14).

$$S/N = \frac{3\left[1 - (.01)(\Delta\%)\right]^2 - (BW/f_o)^2}{6\left[(.01)(\Delta\%)\right]^2 - 3\left[(.01)(\Delta\%)\right]^2}, \quad \frac{BW}{f_o} \leq \sqrt{3} \qquad (13)$$

and

$$S/N = \frac{-3\left[1 + (.01)(\Delta\%)\right]^2 + (BW/f_o)^2}{6\left[(.01)(\Delta\%) + 3\left[(.01)(\Delta\%)\right]^2}, \quad \frac{BW}{f_o} \geq \sqrt{3} \qquad (14)$$

where $\Delta\%$ = percent error in frequency measurement
BW = low pass bandwidth of noise process
f_o = signal frequency

These expressions are plotted in Figure 12 for two values of frequency error.

As Figure 12 shows, the S/N requirement for a given accuracy grows as the square of the bandwidth-to-frequency ratio (20 dB per frequency decade) except for low BW/f_o ratios. Thus, as altitude (and the ranging frequency) decreases, an increased S/N is required to maintain a given percent accuracy. As will be shown subsequently, for beamwidth-limited altimeter operation, the available S/N is inversely proportional to the square of altitude. Therefore essentially constant accuracy would be expected as a function of altitude.

The exception is the case where the ranging frequency is in the upper portion of the receiver bandwidth (i.e., $BW/f_o < 3$). Here the S/N required does not follow the frequency-squared law. The most stringent requirement is at $BW/f_o = 1$, where the ranging frequency is maximum and equal to the bandwidth. If the power is based upon this S/N and altitude, more than adequate S/N will be available at all other altitudes. However, a somewhat lower power can be used if the receive bandwidth is made larger than the maximum ranging frequency. If the bandwidth is 1.73 times the maximum ranging frequency, the mean noise error will be negligible at maximum altitude and the power requirement will be set at lower altitudes.

Specifically, let the receiver noise bandwidth be 173 kHz (1.73 times the 100 kHz ranging frequency at 50,000 feet altitude). Then at 5,000 feet altitude, where the ranging frequency has decreased to 10 kHz, BW/f_o = 17.3 and the S/N required for 1% mean error due to noise is 37 dB. At 500 feet the S/N requirement will increase to 57 dB.

Thus if we permit 1% error due to this one of several error sources, the power requirement can be calculated using a noise bandwidth of 173 kHz, S/N = 37 dB, and altitude = 5,000 feet. This power will then be adequate for all other altitudes.

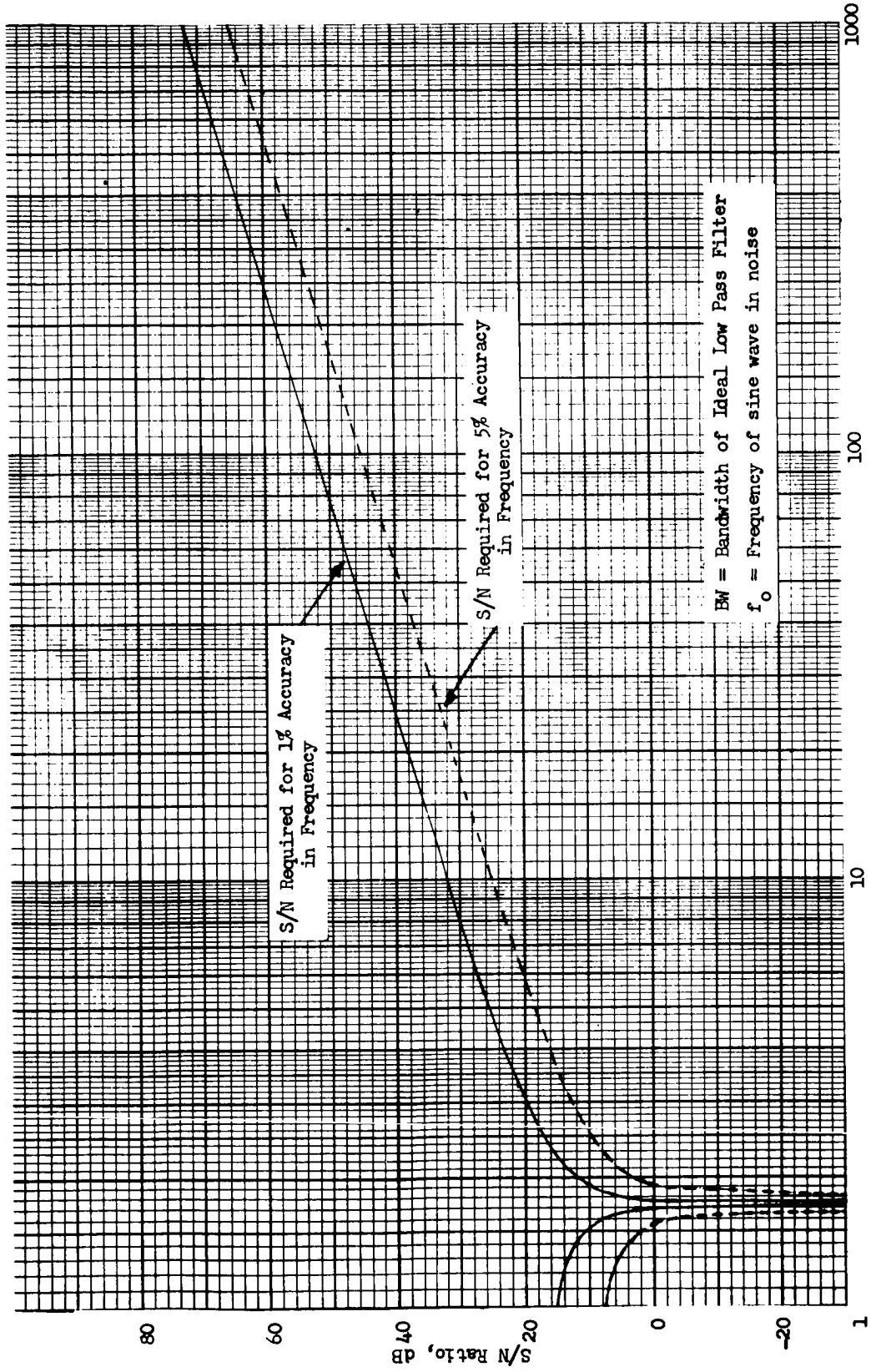

FIGURE 12. - REQUIRED S/N RATIO FOR SPECIFIED FREQUENCY-COUNT ACCURACY

Before calculating the power, observe that the noise error developed above is the mean noise error. Determining the random error is a much more complex problem. However the power required to reduce the mean noise error alone is unreasonably high, so the random error is not considered here.

Transmitted power. - An estimate of the transmitted power requirement is calculable via the standard radar range equation:

$$P = \frac{(4\pi)^3 h^4 KT \overline{NF} BL S/N}{G^2 \lambda^2 A \sigma_o} \qquad (15)$$

where
- P = transmitted power
- h = altitude
- K = Boltzmann's constant = 1.37×10^{-22} joule/°Kelvin
- T = noise temperature = 290° Kelvin
- $\overline{NF}$ = receiver noise figure
- B = noise bandwidth
- L = miscellaneous RF losses
- G = antenna gain
- λ = RF wavelength
- A = reflecting area
- σ_o = reflectivity

Equation (15) can be simplified by substituting the following relationships:

$A = \pi (h\theta/2)^2$, where θ = antenna half-power beamwidth
$\theta = \lambda/d$, where d = circular antenna aperture diameter
$G = (\pi d/\lambda)^2$

and the required power can be expressed as

$$P = \frac{256 h^2 KT \overline{NF} BL (S/N)}{\pi^2 d^2 \sigma_o} \qquad (16)$$

The simplified expressions for antenna beamwidth and gain assume an ideal antenna with circular aperture, d, parallel to a flat, uniformly diffuse reflecting surface. These assumptions are adequate for the purpose of preliminary techniques comparison, but they must be refined in the final analysis.

Values for the parameters in equation (16) are:

$\overline{NF}$ = 9 dB
L = 5 dB
d = 6 inches
σ_o = -30 dB

As stated in the foregoing section, the bandwidth, S/N, and altitude to be used for calculating power are 173 kHz, 37 dB and 5,000 feet respectively. Using these parameters, the power is found to be 220 watts. Clearly this is out of the question. Even with great effort to trim every possible dB from the power requirement, this type of altimeter could not be made competitive.

Sinusoidal FM/CW

A more efficient FM/CW technique uses sinusoidal FM and a superheterodyne receiver (Figure 13). The local oscillator signal is provided by offsetting a portion of the transmitted signal by the intermediate frequency. The peak deviation of the first mixer product is then a function of altitude. This is shown as follows.

The transmitted signal amplitude is

$$e_r = E_T \sin (\omega_o t + m \cos \omega_m t) \tag{17}$$

where ω_o = RF angular frequency
m = transmit modulation index = $\Delta F/f_m$
ΔF = transmit peak deviation
f_m = modulation frequency

The reference for the first mixer is

$$e_L = E_L \sin [(\omega_o + \omega_1)t + m \cos \omega_m t] \tag{18}$$

where ω_1 = intermediate angular frequency

The return signal, delayed by τ seconds, is

$$e_R = E_R \sin [\omega_o (t-\tau) + m \cos \omega_m (t-\tau)] \tag{19}$$

When mixed with the reference signal, e_L, the product of interest is

$$\begin{aligned} e_R e_L &= E_o \sin [\omega_1 t + \omega_o \tau + m \cos \omega_m t - m \cos \omega_m (t-\tau)] \\ &= E_o \sin [\omega_1 t + \omega_o \tau - u \sin (\omega_m t - \omega_m \tau/2)] \end{aligned} \tag{20}$$

where $u = 2 m \sin \omega_m \tau/2$ is a measure of altitude.

The FM signal described by equation (20) is demodulated with a discriminator. The peak amplitude of the demodulated signal will be proportional to u, which in turn is a function of range.

A frequency tracking loop around the discriminator centers the doppler-shifted return signal spectrum in the discriminator. Thus, unlike the sawtooth modulated system, the predetection bandwidth need only encompass the doppler-smeared signal spectrum.

Customarily, the peak deviation of the transmitted signal is increased as altitude is decreased in order to maintain a constant ranging voltage out of the discriminator. This prevents the magnitude of the ranging sidebands from decreasing with delay, τ, as predicted by equation (20) for small values of the argument of the sine function in the modulation index, u. It also offers the advantage of reducing the adverse effect of discriminator nonlinearity on accuracy.

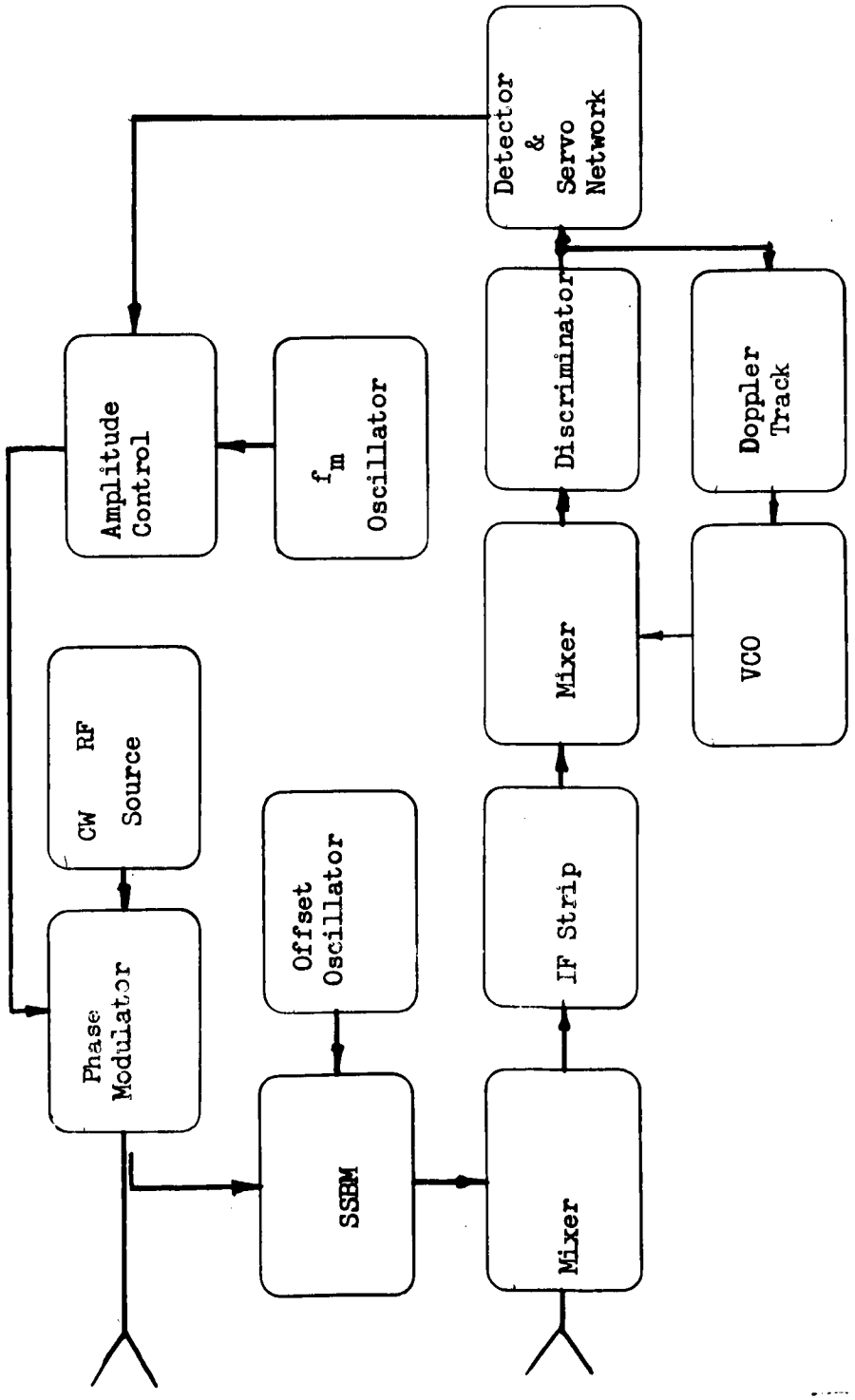

FIGURE 13. SINUSOIDAL FM/CW ALTIMETER

Derivation of parameters. - To make an unambiguous determination of altitude the modulating frequency must be low enough so that the ranging voltage does not cycle with altitude. In other words, $\omega_m\tau/2$ should be less than $\pi/2$ so that sin $\omega_m\tau/2$ will range between 0 and 1. For example, at a maximum altitude of 50,000 feet, τ is approximately 100 μs. With $f_m = \omega_m/2\pi$ = 5 kHz, $\omega_m\tau/2 = \pi/2$ at maximum altitude, and the ranging signal amplitude will decrease monotonically. In general, the doppler spread of the return signal will be substantially greater than the significant portion of a nondoppler-smeared return. Consequently the discriminator bandwidth must be larger than ordinarily would be expected. In this case, the doppler spread will exceed 30 kHz.

The peak deviation of the ranging signal (equation 20) must be large relative to frequency noise caused by the doppler smearing. When the signal is demodulated the discriminator output will be a sine wave with amplitude fluctuations caused by doppler dispersion. Smoothing reduces the doppler noise, but the remaining fluctuations will cause errors just as will system thermal noise.

Assuming an output bandwidth of 5 Hz, the number of independent samples of signal smoothed is approximately 30 kHz/5 Hz = 6000. Thus the effective reduction of doppler noise is by a factor of $\sqrt{6000} = 77$. Referred to the input signal, the doppler is reduced to 30 kHz/77 = 390 Hz. For this doppler noise to cause less than 1% error the peak deviation must be greater than 100 x 390 Hz = 39 kHz. A good value for illustrative purposes is 50 kHz.

Thus, for purposes of preliminary systems comparison, a modulating frequency of 5 kHz and a received peak deviation of 50 kHz may be assumed. The IF or discriminator bandwidth required to accommodate this signal is on the order of 100 kHz.

Noise error.- An estimate of the required S/N follows. Altitude is in effect measured as a function of the amplitude of the detected ranging sine wave. Therefore the ratio of rms noise to the sine wave peak amplitude is approximately equal to the per-unit error. If a $\pm$2% maximum error is desired, the 1σ noise voltage should be 2/3% of the sine wave amplitude. Thus $1/\sqrt{S/N} = 0.006$, or S/N = 44 dB.

As mentioned earlier a reasonable output bandwidth is 5 Hz. Therefore the available S/N in a 5-Hz postdiscriminator bandwidth should be about 44 dB. This bandwidth will be the bandwidth of the servo loop which controls transmitted peak deviation to keep the demodulated signal amplitude constant. The low pass filter immediately following the discriminator should be on the order of 20 kHz to encompass the entire doppler-smeared 5 kHz modulating signal. The S/N ratio in this bandwidth should then be about 20 kHz/5 Hz = 4000 $\sim$ 36 dB lower than the 40 dB required in 5 Hz. Discriminator output S/N will then be about +8 dB.

Middleton[1] has analyzed the noise behavior of FM receivers. From his analysis with an input-to-output bandwidth ratio of 5 (= 100 kHz/20 kHz) and an output S/N of 8 dB, the input S/N will be about +2 dB. Therefore at maximum altitude a S/N of 2 dB in a 100 kHz bandwidth is the approximate requirement.

Power Calculation. - We now substitute into equation (16) the parameters h = 50,000 feet, S/N = 2 dB, and B= 100 kHz; also the remaining values used in the sawtooth example. The required transmitted power is then calculated to be 4 watts. While this is considerably superior to the sawtooth modulated system, it is much too high when transmitter efficiency is taken into account. Besides, optimistic parameter values were used in calculating required power. A more refined analysis would almost certainly reveal that more power is necessary.

Sidetone FM/CW

A third type of FM/CW altimeter measures altitude as a function of phase shift on one of the modulation sidebands. It also incorporates a sideband squaring feature which reduces detrimental effects of doppler dispersion of the returned signal.

The transmitted, received, and IF signals are the same as those of the sinusoidal frequency deviation system (see equations 17,18,19 and 20). Signal processing is different, however. As shown in figure 14, the IF strip includes a notch filter at the intermediate frequency, $f_1 = \omega_1/2\pi$. This filter eliminates most of the direct leak-through signal from the transmitter. The time delay, τ, associated with the leakage will be very small so that the modulation index, μ, of the leakage signal in the IF will likewise be small. Thus, most of the leakage energy will be concentrated in the carrier, ω_1. This is more readily shown by expanding equation 20 into its spectral components:

$$e_p\, e_L = E_o \Big\{ J_o(\mu) \sin(\omega_1 t + \omega_o\tau) + J_1(\mu) \Big[\sin\Big(\omega_1 t + \omega_o\tau + \omega_m t - \frac{\omega_m\tau}{2}\Big) - \sin\Big(\omega_1 t + \omega_o\tau - \omega_m t + \frac{\omega_m\tau}{2}\Big)\Big] + J_2(\mu) \Big[\sin(\omega_1 t + \omega_o\tau + 2\omega_m t - \omega_m\tau) + \sin(\omega_1 t + \omega_o\tau - 2\omega_m t + \omega_m\tau)\Big] + \ldots \Big\} \qquad (21)$$

where $J_n(\mu)$ is the Bessel function of order n and argument μ. Since the $\mu = 2\,m \sin \omega_m\tau/2$ associated with the leakage will be small, the Bessel functions of order greater than zero will also be small. By notching out most of the leakage signal, it may be possible to use a single antenna, which is not the case with the other types of FM/CW systems.

1. David Middleton, "On Theoretical Signal-to-Noise Ratios in FM Receivers: A Comparison with Amplitude Modulation," Journal of Applied Physics; April 1949, pp 334-351.

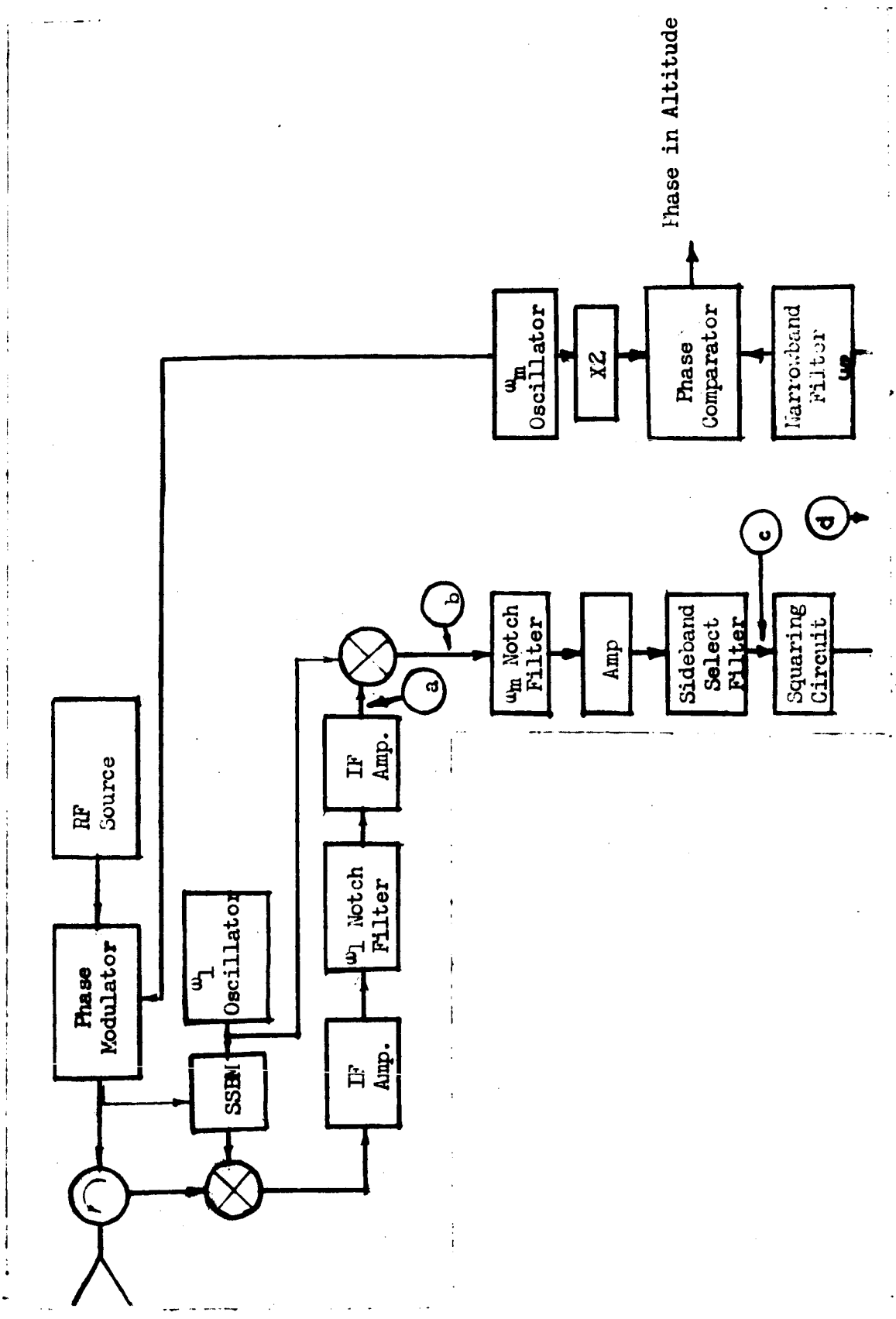

FIGURE 14. - SIDETONE RANGING ALTIMETER

Following the notching operation and amplification, the signal spectrum is folded about the IF carrier, ω_1. The spectrum before and after folding is shown in Figure 15. After folding, the doppler-shifted and smeared sidebands are symmetrically located about the modulating frequency, ω_m. At this point, a notch filter at ω_m attenuates the first order leakage sideband, providing further immunity from leakage. The doppler shift of the return signal permits this operation.

The spectral components of interest are the upper and lower first sidebands of the return signal spectrum. These are filtered out by the sideband select filter, leaving only the two doppler-smeared sidebands shown in Figure 15c. Squaring these sidebands results in a signal at twice the modulating frequency,

$$E_o^2 J_1^2 (\mu) \left[\cos (2\omega_m t - \omega_m \tau)\right] \qquad (22)$$

This process removes the doppler shift and smear, leaving a clean signal whose phase shift relative to that of the modulating frequency is proportional to altitude. Other spectral components, also produced by squaring, are shown in Figure 15d.

Thus the sidetone altimeter offers superior performance with respect to leakage rejection and has a mechanism for eliminating doppler smear and shift. The doppler effects, however, influence the selection of modulating frequency, as shown in the following section.

Derivation of parameters. - To measure altitude unambiguously, the modulating frequency, f_m, must be sufficiently low for the phase shift, $\omega_m \tau$, to be less than 2π radians. On the other hand, ω_m must be high enough with respect to the doppler shift so that the proper sidebands can be uniquely selected for squaring. In this application, the high doppler shift precludes the use of an unambiguous modulating frequency.

Aside from complexity, the disadvantage of using two ambiguous modulating frequencies is the creation of blind spots or "altitude holes" as the modulation index, μ, cycles through zero. This problem can be circumvented at the cost of additional complexity. For example, more than two (or variable) modulating frequencies could be used. To determine the power requirement, it will suffice to derive a nominal value for the modulating frequency.

The minimum value of $f_m = \frac{\omega_m}{2\pi}$ is twice the doppler shift plus the doppler spread if overlapping of the sidebands in the folded spectrum is to be avoided. With a doppler shift of 80 kHz and a doppler smear of 33 kHz, the minimum f_m is about 200 kHz. This, also, is the minimum presquaring bandwidth.

Noise error. - The accuracy and S/N required for ambiguity resolution is determined as follows: If there are M ambiguities, the difference between the phases measured with the two modulating frequencies must be known to within $\frac{2\pi}{M}$ radians. Since there are two measurements perturbed by

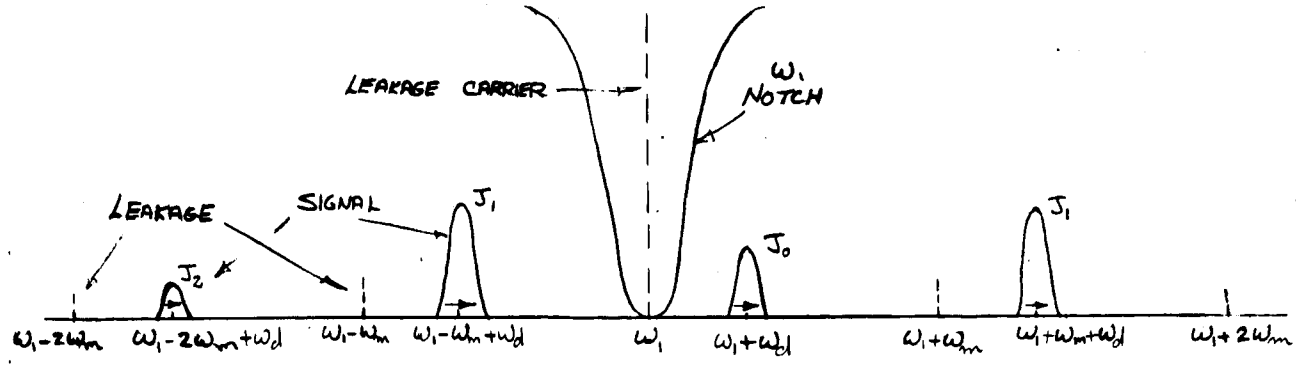

a - Before Folding

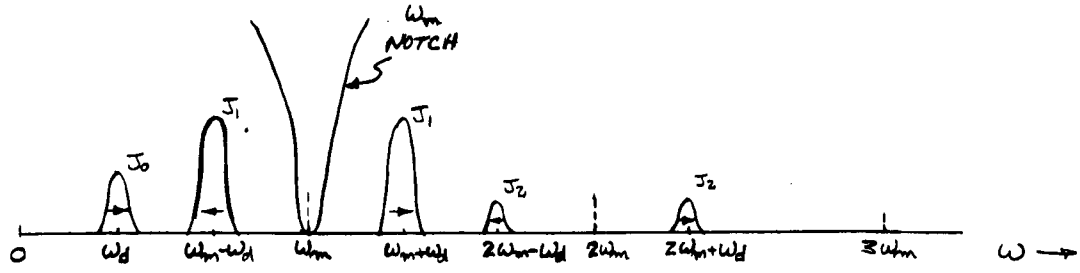

b - After Folding

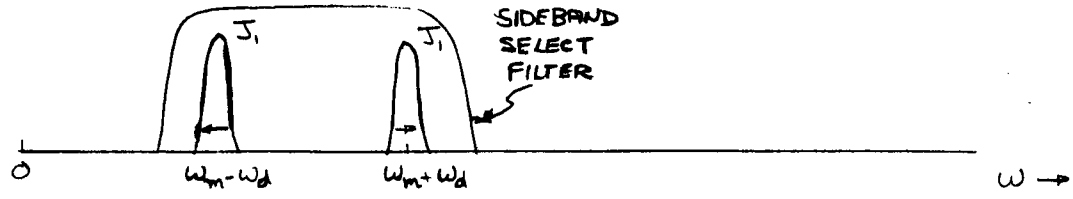

c - Before Squaring

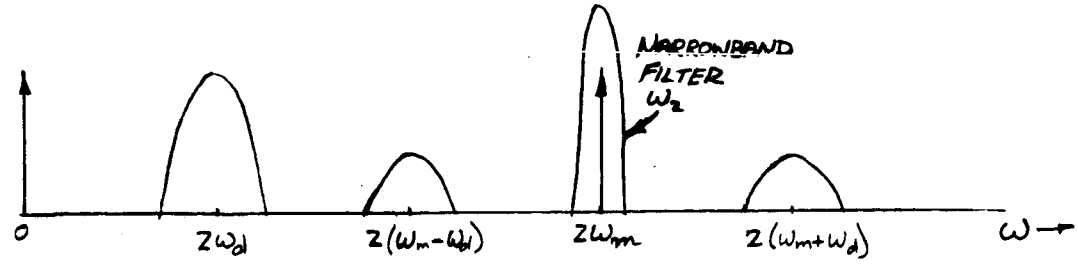

d - After Squaring

FIGURE 15. - FREQUENCY SPECTRA

independent noise, each must be measured with an accuracy of $\pm \frac{2\pi}{2\sqrt{2M}}$ radians.

With noise having a Gaussian amplitude distribution, the one-sigma error in phase measurement is[1]

$$\sigma = \frac{1}{\sqrt{2}\ S/N} \text{ radian} \tag{23}$$

Since $3\sigma = \frac{2\pi}{2\sqrt{2}\ M}$, the minimum S/N required for ambiguity resolution is

$$(S/N)_{min} = \frac{9M^2}{\pi^2} \tag{24}$$

With a 200 kHz modulating frequency, the maximum unambiguous time delay is 5 μs. There are 20 ambiguities in measuring an altitude of 50,000 feet, so

$$(S/N)_{min} = \frac{9(20)^2}{\pi^2} \approx 400 \text{ or } 26 \text{ dB} \tag{25}$$

Substituting (25) into (23), the error in measuring the phase of the 200 kHz signal is 0.036 radian. This corresponds to an rms time error of 0.18 μs which indicates an altitude error of about ±0.5%. Thus ambiguity resolution requirements are more demanding than are accuracy requirements in establishing the minimum S/N.

Appendix B of this volume analyses the noise properties of the sideband squaring signal processing system. It shows that the S/N in a filter of bandwidth B centered at $2\omega_m$ after the square law device is

$$(S/N)_o = (S/N)^2_{in} \cdot \frac{2W}{B\left[\frac{1}{2}(S/N)_{in} + 1 - B/8W\right]} \tag{26}$$

Here, $(S/N)_{in}$ is the signal power in one of the sidebands of interest divided by the total noise power in the presquaring bandwidth 2W. Figure 16 shows this relationship for two values of W/B. With 2 W = 200 kHz, B = 5 Hz (a typical value), and an output S/N of 26 dB, the required S/N in the 200 kHz bandwidth is -10 dB.

Required power. - If the transmitted modulation index is selected such that the first-order sidebands are maximized (by making $\mu \approx 1.8$), the sideband will be smaller than the carrier by $J_1^2(\mu) = J_1^2(1.8) \approx (0.58)^2$ or -4.7 dB. But, because $\mu = 2\ m \sin \omega_m \tau/2$ will cycle between $\pm 2m$ as altitude changes, it is not possible to maintain an optimum received modulation index, μ. By making programed changes in m and ω_m as a function of altitude, the average sideband level can be kept reasonably high, however. An average level of -6 dB with respect to the unmodulated carrier is probably the maximum average which can be assumed.

1. M. I. Skolnik, "Introduction to Radar Systems," McGraw Hill Book Company, 1962; Chapter 10.

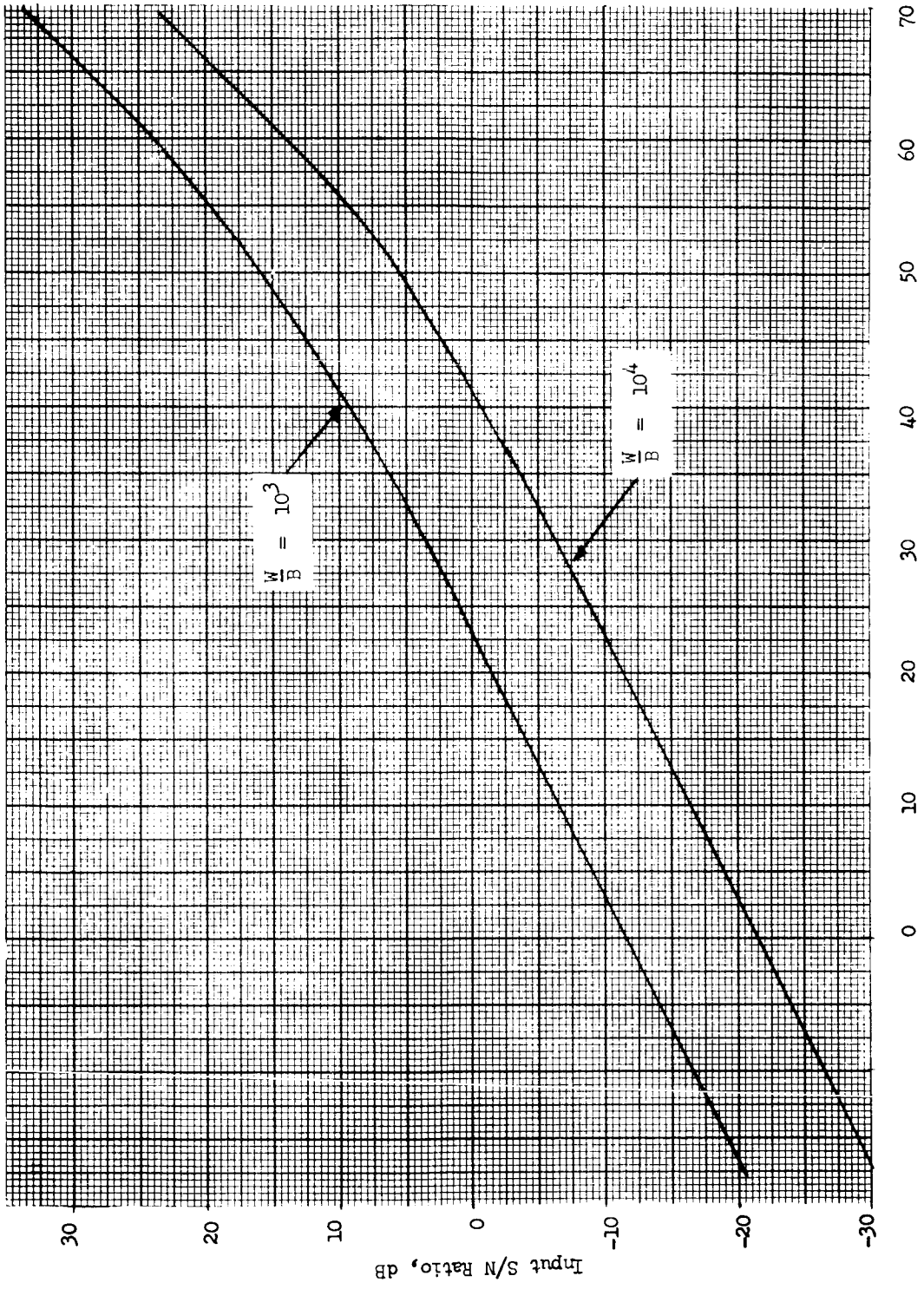

FIGURE 16. S/N PROPERTIES FOR SIDEBAND SQUARING

Using this (optimistic) value, the required carrier-to-noise ratio referred to a 200 kHz bandwidth is -4 dB. Scaling from previous calculations, this translates to a transmitted power requirement of 2 watts.

Power levels on this order can be obtained from varactor multiplier sources. However, the efficiency of these devices is at best about 2% today. Even if a (difficult to justify) 5% efficiency were assumed for the near future, the transmitter would need 20 watts of prime power, a considerable requirement. The efficiency of microwave tubes at this power level is not favorable either. Thus it can be concluded that this technique offers little hope of meeting the power consumption goal.

Interrupted CW

Interrupted cw (ICW) systems can use a variety of modulation schemes for altitude measurement, but they have the common characteristic of relatively low peak power, high duty cycle, pulse transmission. As previously stated, coherent processing in a narrow bandwidth is generally required to recover the signal from noise. But, as in the case of FM/CW systems, ICW cannot take full advantage of coherent processing because of the large doppler spread experienced in this application.

The only advantage of the ICW approach over FM/CW is the elimination of leakage. This, of course, can be a commanding advantage in some cases; however, it is gained at the expense of higher peak power. Average power will be comparable, but peak power will increase roughly as the reciprocal of the duty cycle. This virtually precludes the use of a solid state transmitter.

An additional disadvantage is the complexity of modulation. Multiple ambiguous PRFs might be used as linear FM combined with high duty cycle pulse modulation. PRF ranging is another possibility. However, the complexity required in these systems cannot be justified when simpler alternatives are available.

Pulse Modulation

The simplest and most straightforward of all candidate techniques is a conventional pulse, range tracking radar. Large doppler shifts and dispersions which complicate other types of altimeters have little effect on inherently wideband pulse altimeters.

Figure 17 shows the principal functional blocks of a pulse altimeter. A relatively narrow, high peak-power pulse is transmitted. The received pulse is detected in a bandwidth approximately matched to the pulsewidth (much larger than combined dopper spread and dispersion) and tracked with a type II range tracker.

Derivation of parameters. - In order to obtain an estimate of the power required by a pulse altimeter, typical values of the pertinent parameters are derived here. The parameters of interest are those appearing in equation (15),

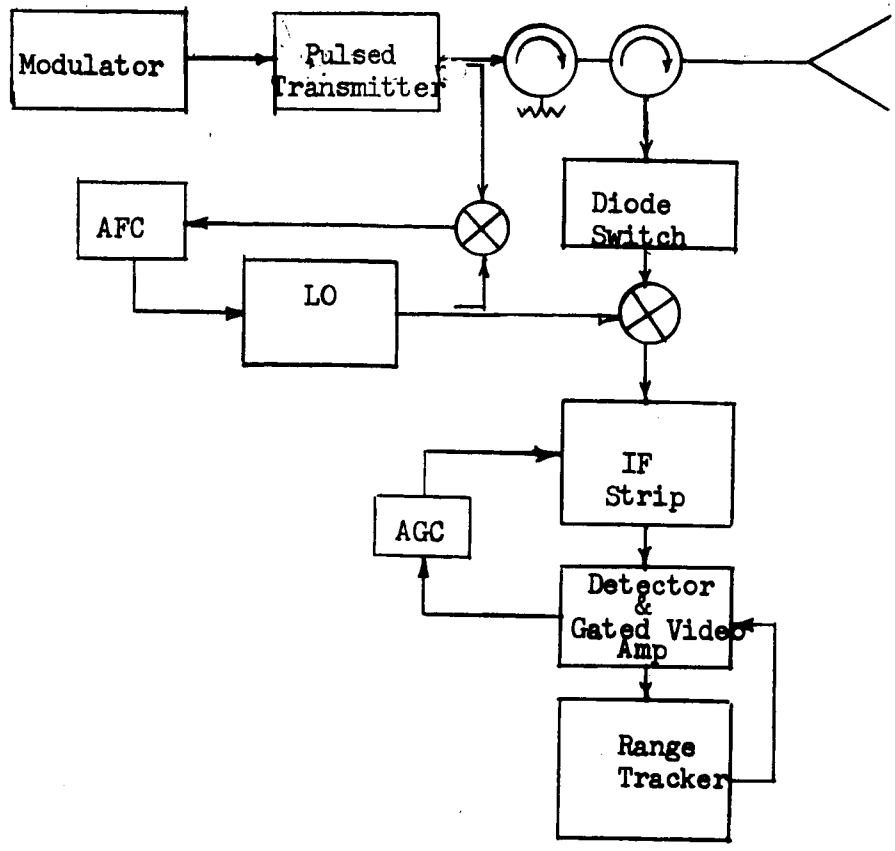

FIGURE 17. - PULSE ALTIMETER

$$P = \frac{(4\pi)^3 h^4 KT \overline{NF} B L S/N}{G^2 \lambda^2 A \sigma_o}$$

Some of these parameters may be assigned values identical to those used in calculating FM/CW power requirements. Specifically,

$\overline{NF}$ = 9 dB
L = 5 dB
$G = (\pi d/\lambda)^2$ = 22 dB, where λ= 0.123 ft and d = 6 inches
σ_o = -30 dB
h = 50,000 feet (15.5 km)
KT = -204 dBW

The IF bandwidth, B, should be approximately equal to the reciprocal of the pulsewidth, τ, for optimum predetection S/N ratio. The pulsewidth is limited by the minimum altitude requirement (300 m) if a dual-mode system is to be avoided. Also, $1/\tau$ should be large with respect to the combined doppler shift and dispersion in order to avoid appreciable signal loss due to mismatch of the signal spectrum and the IF filter. Another factor favoring a short pulse is the inherently higher accuracy associated with a wideband system.

Of course, a wide bandwidth implies greater competing noise power, so it is undesirable to make the pulsewidth shorter than necessary. For the present we shall adopt a pulsewidth of 1 μs matched to a 1 MHz IF bandwidth. This choice results in an eclipsed region of about 500 feet, allowing adequate time for transients to subside prior to the return of signals from minimum altitude (about 1000 feet). The one-MHz bandwidth is large enough relative to doppler shifts to prevent significant degradation due to the latter effect.

S/N ratio. - The S/N requirement is influenced by two factors: detection performance and accuracy. The former is more demanding. For illustration we may assume a 90% detection probability, 4 pulses integrated (using video integration), and a false alarm number of 10^3. (Here, false alarm number is defined as the number of opportunities for a false alarm during the time in which the probability of a false alarm is 50%). For this case, the required S/N is 6.4 dB. Choosing a PRF of 250 Hz, the 100 range cells in the 50,000-foot altitude interval will be searched through in 400 times the interpulse interval, or 1.6 seconds. This is a reasonably short search time. Moreover, the 250 Hz PRF allows for an unambiguous range much larger than required, while at the same time providing a sample rate large enough for any imaginable tracking requirements.

With a S/N of 6.4 dB, the 3σ range error due to noise is calculated to be approximately 28 feet at maximum altitude. Error is calculated using the equation[1]

$$\sigma = \frac{\tau}{2.5\sqrt{2\ S/N}}\sqrt{\frac{B_n}{f_r}} \text{ seconds,} \qquad (27)$$

1. D.K. Barton, "Radar System Analysis", Prentice Hall, 1964; Chapter 11.

where σ = one-sigma error
τ = pulsewidth = 1 μs
S/N = signal-to-noise power ratio = 6.4 dB
θ_n = tracking loop noise bandwidth = 5 Hz
f_r = sample rate = 250 Hz.

This accuracy far exceeds the requirement, so that detection performance sets the S/N requirement. A S/N of 6.4 dB will be used for system comparison purposes, since it offers adequate detection probability.

The final parameter to establish is the reflecting area, A. Reflecting area may be limited by the antenna beamwidth (as it is with cw systems), or by the transmitted pulsewidth. The beamwidth-limited area is simply

$$A_L = \pi\left(\frac{h\theta}{2}\right)^2 \qquad (28)$$

where θ = antenna half-power beamwidth $\approx \lambda/d$.

Pulsewidth-limited area is derived from Figure 18. The reflected signal builds up to a maximum at the time the trailing edge of the two-way pulse packet reaches the surface. The area contributing to the first τ seconds of return signal is π times the square of the radius of the circular area illuminated by a single pulse packet. This radius is

$$r = \sqrt{(h + \frac{c\tau}{2})^2 - h^2} = \sqrt{hc\tau + (\frac{c\tau}{2})^2} \approx \sqrt{hc\tau}$$

Thus the pulsewidth-limited area is

$$A_p = \pi hc\tau \qquad (29)$$

The crossover altitude above which the area becomes pulsewidth limited is determined by equating (28) and (29):

$$\pi\left(\frac{h\theta}{2}\right)^2 = \pi hc\tau$$

$$h_c = \frac{4c\tau}{\theta^2} \qquad (30)$$

Substituting τ= 1 μs and $\theta = \lambda/d = 0.25$ radian into (30), h_c is calculated to be approximately 64,000 feet. Therefore the reflecting area is limited by the antenna beamwidth and is equal to approximately 1.23×10^8 square feet.

Required power. - Using equation (15), the peak power requirement is calculated to be slightly over 100 watts. Average power is therefore $P_{PK} \cdot f_R \tau$, or 100 watts x 250 Hz x 1 μs = 25 milliwatts. Obviously the pulse system is vastly superior to any of the other available techniques in terms of power consumption requirements. Heater power for the transmitter tube will exceed the beam power.

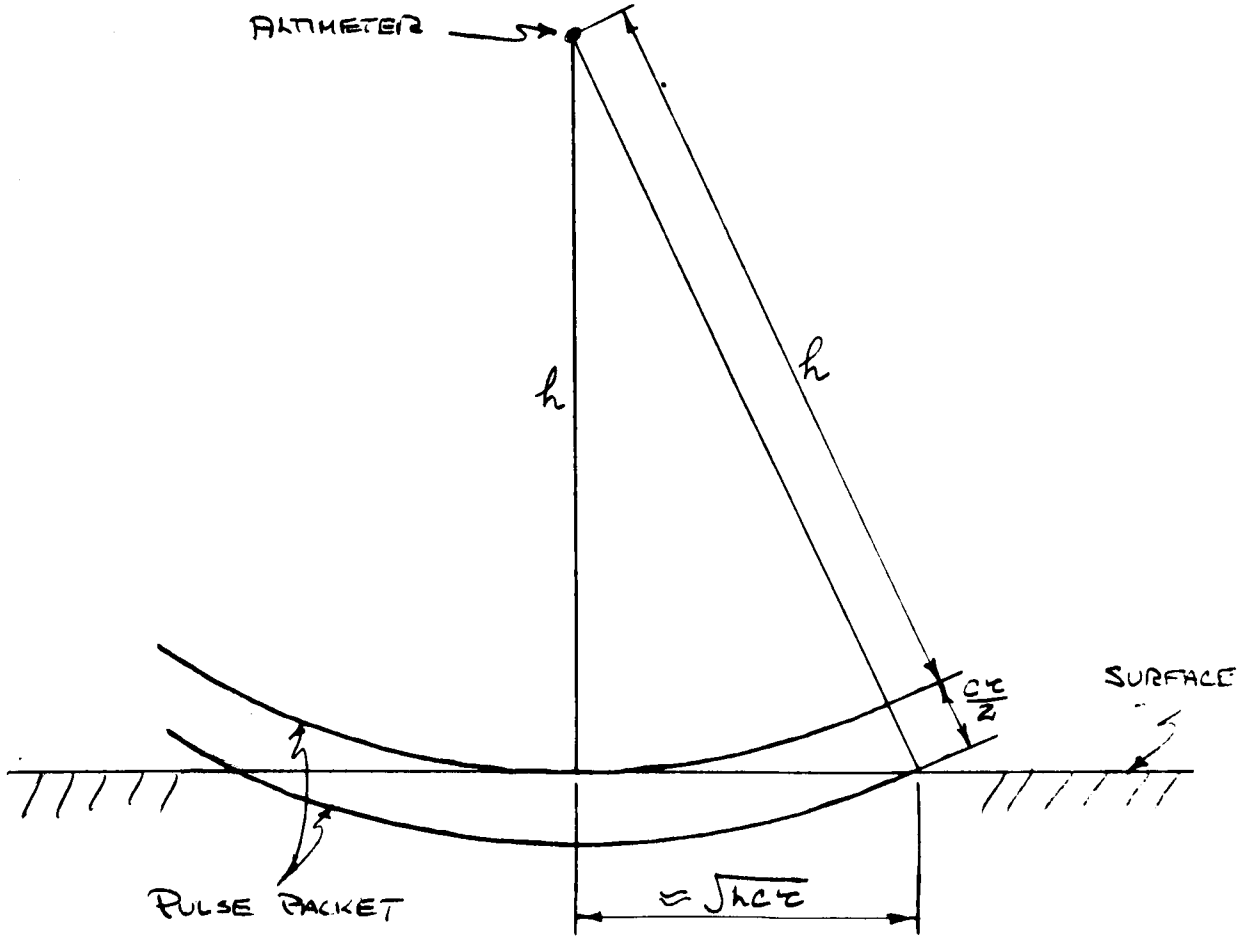

FIGURE 18. - PULSEWIDTH - LIMITED AREA GEOMETRY

Comparison and Conclusion

As an aid in comparing the candidate altimeter systems, we evaluate each and assign them relative ratings for power consumption, complexity, size and weight, and reliability. These ratings are shown in Table II.

TABLE II - RATINGS OF CANDIDATE TECHNIQUES

Technique	Power	Complexity	Size & Weight	Reliability
FM/CW				
Sawtooth Modulated	5	1	5	4
Sinusoidal Frequency Deviation	4	3	2	3
Side Tone Ranging	2	5	4	2
ICW				
PRF Ranging	3	4	3	4
High PRF PD	2	5	4	4
Pulse	1	2	1	1

NOTE: A ranking of number 1 indicates, as appropriate, lowest power, least complex, lowest size and weight, and highest reliability.

The sawtooth-modulated FM/CW altimeter is the simplest, conceptually. But its unreasonable power requirement, together with the fact that it requires separate transmit and receive antennas, makes it the largest and heaviest as well as one of the most unreliable of the candidate techniques.

Power required for the sinusoidally modulated system is substantially less, but is still too much to permit the use of a solid-state transmitter. It is not unduly complex or heavy, but both power and complexity are greater than the pulse system. These factors are also reflected in its reliability ranking.

The sidetone ranging system goes a long way toward overcoming the doppler-induced problems which afflict the other cw systems. Although it is marginal, a solid-state transmitter might possibly be used with this technique. However the complexity is considerable. Also, a solid state transmitter, if used, would be driven to its maximum ratings. These factors make the technique less reliable than a pulse radar. In addition, size and weight are not favorable, again because of complexity and the inefficiency of solid state transmitters.

The ICW systems are closely matched, but require considerably more power than the pulse radar. Because they are fundamentally ill-suited to this kind of signal environment, considerable complexity is involved in implementing a satisfactory modulation scheme.

The pulse radar is without question the best suited for the SPRA application. It is inherently accurate, requires much less power than other techniques, and its simplicity, together with the low power requirement, make it the most reliable. Accompanying its low power and simplicity is a size and weight advantage. Perhaps the biggest disadvantage is the high voltage required for a high peak-power transmitter. But this is regarded as an area requiring careful design, not a fundamental problem.

PULSE RADAR DESIGN

This section presents the recommended pulse radar system and subassembly electrical and mechanical designs. System parameters are first developed and followed by a mechanization description. Other topics discussed are magnetic cleanliness, thermal analysis, reliability prediction, performance, and growth potential.

Parameter Optimization

The optimization of overall radar altimeter parameters was an iterative process during which system parameters (e.g., power, antenna gain, pulsewidth) were adjusted in an attempt to arrive at the smallest, lightest system capable of specified performance. A discussion of the final set of parameters and overall specifications is given here.

Requirements.-In developing these parameters, certain basic requirements were given in the contract work statement (see earlier discussion of requirements). Some additional requirements associated with detection and acquisition have also been established as follows.

A starting assumption is a detection probability of 90% when searching the altitude interval once. A search time of not more than several seconds is desirable since vertical velocity may be quite high. Maximum altitude capability should be substantially greater than the specified 15.5 km to permit early acquisition should the reflected signal strength be great enough. A maximum altitude on the order of 20 km will allow several seconds of search before reaching 15.5 km even if the trajectory is steep. Finally, it is necessary that correct tracking of the surface return be firmly established prior to output of a lockup indication. This tracking is to prevent noise false alarms from initiating erroneous altitude information which would be fed to external subsystems.

Some of the system parameters can be specified without the need for a tradeoff process. Others evolved as discussed below.

Noise Figure, $\overline{NF}$.-Because of the relatively low transmitted power level a low noise RF amplifier front end will not yield a net savings in size and weight. Using a conventional crystal mixer, a noise figure of 8.5 dB can be expected.

Reflectivity, σ_o.-In the absence of anything but very coarse measurements, it is appropriate to make a conservative estimate of σ_o. The contract work statement suggested values between -20 and -30 dB. Allowing for safety margin, Westinghouse has chosen a value of -30 dB.

Wavelength, λ.-An X-band frequency of from 8 to 10 GHz was specified. The exact choice has little effect on altimeter design. But, in order to minimize doppler shift, 8.0GHz(λ = 0.123 foot) was selected.

RF losses, L.-Based on the state of the art in miniature microwave hardware, allowing for approximately 3 feet of transmission line between transmitter and antenna, and considering radome losses, the total RF losses will be 5.1 dB. The breakdown is as follows:

Transmit Losses:	
Circulator	0.6 dB
Transmission line	0.75
Radome	1.00
	2.35 dB
Receive Losses:	
Radome	1.00 dB
Transmission line	0.75
Circulator	0.30
Diode TR switch	0.70
	2.75 dB
TOTAL	5.1 dB

Antenna parameters.-One tradeoff is between antenna gain/beamwidth and transmitted power to minimize the overall size, weight, and prime power. The conclusion was that there should be maximum use of the available antenna aperture. Of course, antenna size and weight increase considerably with a small beamwidth and high gain. However, antenna weight does not increase as rapidly as the weight associated with higher power needed to offset a less-than-maximum antenna gain.

Specifically, required power varies inversely with the square of antenna aperture under beamwidth—limited operation. When the antenna beamwidth is sufficiently large that the reflecting area is pulsewidth limited, required power varies inversely with the fourth power of antenna aperture (or as the square of antenna gain). Therefore a modest savings in antenna size results in a large increase in required power. This increase has a significant impact, not only on the weight of the transmitting tube itself, but also on the power supply and prime power source. Furthermore, higher voltages associated with higher peak powers require greater protection from arcing, and such devices increase weight.

Therefore, the full available 6-inch aperture will be used. As will be shown subsequently, antenna gain will be 19 dB at broadside, and 16 dB at a scan angle of 60° off broadside. Beamwidth is approximately 15° broadside increasing to over 20° at 60° off broadside.

Pulsewidth, τ.-For reasons discussed earlier, a pulsewidth of approximately 1 μs is a good value. This width will allow ranging to the minimum altitude without an auxiliary short range mode. It will also restrict the extent of the pulsewidth-limited reflecting area under those conditions of scan angle

and altitude which do result in pulsewidth-limiting. Such restriction prevents the introduction of significant error due to terrain averaging.

Mechanization convenience has resulted in an actual pulsewidth of 1.067 μs. The matched IF bandwidth is 1 MHz.

Reflecting area.-For most altitudes, the reflecting area will be beamwidth-limited. However, at maximum altitude it is likely that the antenna scan angle will be at or near its 60° extreme. It is then that the beamwidth is sufficiently broad that the reflecting area is pulsewidth limited. As was shown by the geometry of Figure 18 and the derivation of equation (29), the area at maximum altitude is

$$Ap = \pi hc\tau \approx 1.6 \times 10^8 \text{ square feet}$$

where $h = 15.5 \text{ km} \approx 50{,}000 \text{ feet}$
$c =$ speed of light
$\tau = 1.067 \ \mu s$

S/N ratio and acquisition time.-As pointed out previously, the S/N requirement is determined by detection and acquisition requirements rather than by accuracy considerations. Detection probability, acquisition time, pulsewidth, false alarm time, and PRF are interrelated parameters which together determine S/N. Some of the considerations in arriving at these parameters are discussed below.

Pre-acquisition search is accomplished by stepping a range gate in pulsewidth increments through the altitude interval. The number of pulses integrated in each range gate position is limited because of the likelihood of a rapid descent which would cause the surface return to coast out of the range gate. It is, however, desirable to integrate several pulses in order to keep the peak power low. On the other hand, the PRF should be reasonably low to keep average power as low as practical and to avoid second time around echo (STAE) which might be troublesome if the reflection coefficient is unexpectedly large.

A combination of parameters which satisfy these restrictions has been generated. In so doing we have allowed some margin for a more severe trajectory than the model previously presented. Exact parameters values have been selected for compatibility with a digital range tracker which will be described subsequently.

Maximum range tracker altitude is $(2^{11}-1)$ X 10 meters = 20.47 km, where 10 m is the basic altitude quantization in the range tracker. The 1.067 μs pulsewidth corresponds to a distance of 160 meters. Range search is accomplished by stepping the range gate in 160-meter steps through 20.47/0.160 = 128 positions.

Two PRFs have been selected, one for search and one for track. During search the PRF is 457.4 Hz and during track it is 228.7 Hz. In the search PRF the interpulse interval is 2.19 ms, and ten pulses are integrated in each

range interval. This takes 10 X 2.19 ms = 21.9 during which time altitude may change as much as 21.9 ms X 3 km/s = 66 meters, where 3 km/s is the radial velocity. Since the range gate is 160 meters, the surface return will not move enough out of the range gate position to be harmful.

Range sweep time is 128 X 21.9 m = 2.8 seconds. The detection probability is 90%. With a 2.2 dB S/N, the false alarm time is approximately 3 seconds. When a detection is made, altitude information is not output, but the range tracker is committed and the PRF is reduced to 228.7 Hz. Then, as the return is tracked, 64 pulses are integrated in an acquisition channel operating in parallel with the detection channel. The threshold in the acquisition channel is set for a false alarm number of 10^{10} and a 99.99% detection probability. Since tracking has begun, there is no problem of the signal leaving the range gate. After the acquisition threshold has been exceeded, altitude information is output. Since the false alarm probability is virtually nil at the acquisition threshold, there is negligible chance for erroneous altitude outputs.

Power required for a 2.2 dB S/N at 15.5 km, assuming the return is through the low gain (16 dB) antenna pattern at large scan angles. This is calculated via the range equation,

$$S/N = \frac{P G^2 \lambda^2 A \sigma_o}{(4\pi)^3 h^4 KT \overline{NF} BL} \qquad (31)$$

where altitude is 15.5 km and other parameters are as listed in Table III. Accuracy, as shown in a later section, is more than adequate even with the low PRF during track.

Mechanization

Block diagram.-Overall altimeter electrical design is illustrated by the block diagram of Figure 19. As shown, the transmitter is a master oscillator power amplifier system using a TWT. The microwave circuitry enclosed by dotted lines is integrated into a stripline package. The local oscillator is controlled by a conventional AFC, and a digital range tracker performs closed-loop altitude tracking. The antenna is an electronically steerable array controlled by digital logic.

Packaging.-The altimeter is designed into two separate packages, the antenna and the electronics. Since the detailed configuration of the spacecraft is not firmly fixed at this time, the two-package arrangement allows maximum versatility in subsystem placement within the spacecraft. Functionally the subsystem will operate perfectly satisfactorily with a cable interconnection, provided the separation distance is less than three feet. If, when the spacecraft is better defined, it is determined that there is a volume utilization advantage in having the antenna and the altimeter packaged together, this consolidation could be easily accomplished.

TABLE III.- ALTIMETER PARAMETERS

Frequency	8 GHz
Peak Power	500 watts
Average Power:	
Search	0.244 watt
Track	0.122 watt
Pulsewidth	1.067 μs
PRF	
Search	457.4 Hz
Track	228.7 Hz
Antenna Gain	
Broadside	19 db
At 60°	16 db
Antenna Coverage	±60°, 2 axes
Antenna Steering	Discrete - 64 steps
Maximum Altitude	20.47 km
IF Noise Bandwidth	1 MHz
Noise Figure	8.5 dB
Reflection Coefficient	-30 dB
RF Losses	5.1 dB
Minimum S/N at 15.5 km	2.2 dB
Pulses Integrated	
Detection Threshold	10
Acquisition Threshold	64
Range Sweep Time	2.8 sec
Acquisition Probability	90%
False Alarm Time - Detection Threshold	3 sec
False Alarm Number - Acquisition Threshold	10^{10}
Altitude Noise Error	±0.3%
Altitude Quantization	10 meters

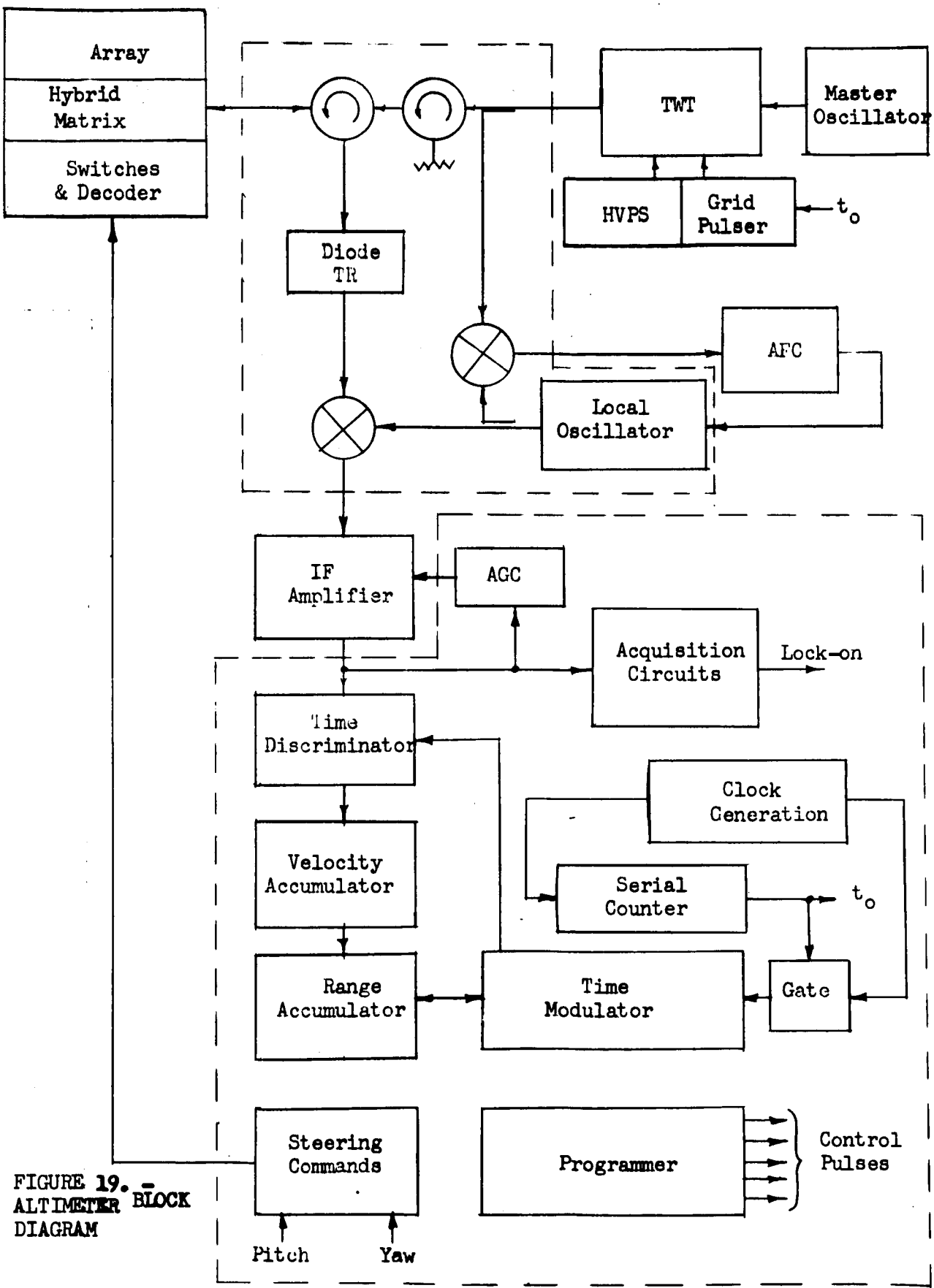

FIGURE 19. - ALTIMETER BLOCK DIAGRAM

Sub-units.-Two basic considerations were followed in the design of the altimeter. The first was that the use of connectors between various subunits be held to the very minimum. This was accomplished through soldering or welding all interconnections except for the high frequency coax line connectors. The other consideration was that the various sub-circuits be fabricated as separate functional, testable, replaceable modules. This concept of course allows these sub-units to be tested prior to final assembly, and also permits their repair during the assembly and test period.

Functional divisions.-The altimeter divides into seven major functional areas; antenna, transmitter, microwave circuitry, IF strip, AFC, range tracker, and power supply. Electrical and mechanical designs of each of these are discussed in the following paragraphs.

Antenna

Introduction.-Mission and system configuration give rise to the following general requirements for the altimeter antenna system.

Coverage	120° cone
Aperture size	6 inches
Configuration	Flush mounted
Frequency	8 GHz
Power	0.5 to 1.0 kW peak, 0.5 W average
Polarization	Linear
Gain	Maximized
Weight and volume	Minimum

In addition, the antenna system must be capable of withstanding sterilization and decontamination, and must be designed for maximum reliability under mission environment. A numberof antenna types were considered for this application; these will be briefly discussed here emphasizing the traits leading to the selection of the recommended antenna system.

Candidate antenna designs.-The following paragraphs discuss the several possible antenna designs from which the SPRA antenna was selected.

(a) Dual-axis mechanically gimbaled reflector.-This antenna type consists of a vertex-fed or Cassegrain reflector gimbaled about orthogonal axes and driven by small servo motors. Because of the scanning motion of the reflector, a relatively large swept volume must be allotted, although the weight is not excessive. The gimbaled reflector does not lend itself to flush mounting since the actual aperture must be several inches behind the radome. In addition, the gimbaling and drive assembly requires the use of bearings, gears, servo motors, etc.—devices which would degrade antenna system reliability.

(b) Electronically scanned line source.-This type of antenna can be either a combination power divider and phase shifters feeding a row of radiating elements (one phase shifter per element), or a linear Butler matrix and beam

switching network. In either case, the radiated pattern is essentially a fan beam having a 120° beamwidth in one plane and a narrow (approximately 16°) beamwidth in the scanned plane. Among the advantages of this antenna type are light weight, low scanning drive power, small volume, and simple (and therefore reliable) design. Its major disadvantage is low gain (about 13 dB) which essentially precludes its use. This gain could be increased to 16 dB by increasing the array length to 12 inches, but it would still fall short in view of other system parameters. Further increasing the array length would nullify the major advantages mentioned above.

(NOTE: Should vehicle characteristics be revised such that a narrower antenna beamwidth could be tolerated in the roll plane, we might use a planar array of elements, scanned in one plane by one of the methods mentioned above. It would provide most of the advantages of the linear array and, in addition, have adequate gain.)

(c) Combination mechanically/electronically scanned planar array.-This antenna type consists of a planar array of radiating elements, electronically scanned in one plane using a phase shifting manifold, and mechanically scanned about an axis normal to the aperture, thus providing the required 120° conical coverage. This configuration fulfills most of the antenna requirements although it requires the use of bearings, a motor, and other moving parts. However, its mechanical complexity is not as great as that of the dual-gimbaled reflector.

(d) Electronically scanned planar array using digital phase shifters.-This antenna consists of a planar array of radiating elements fed through a corporate power-dividing network with a digital phase shifter for each element. Such an antenna is completely versatile, affording good gain and agile beam pointing. However, several properties keep it from being ideally suited for this application. Principal among these is the weight and complexity of the digital phase shifters. Despite the tremendous strides made recently in the development of these devices, their cumulative weight is still prohibitive for space systems when a two-dimensional matrix of reasonable size is considered. For example, a reciprocal ferrite phase shifter weighing four ounces would appear to be a remarkably light weight device. However, when an array incorporates a matrix of 50 to 60 of these, 12 to 15 pounds of antenna weight are attributable to phase shifters alone. In addition, the complexity and power requirements of the drive circuitry become prohibitive when this type of antenna is considered for spaceborne systems.

(e) Electronically scanned, Butler beam forming matrix.-The final approach uses an 8 X 8 element array fed by a network of microwave transmission lines and hybrid junctions. There are a variety of configurations which could be used for the beam forming and beam selection network. These offer advantages over the other techniques under the conditions of two ground rules: (1) increased passive circuitry complexity and loss are acceptable providing they result in decreased active electronic complexity and hence improve reliability; and (2) size and weight are of paramount importance.

Under the present state of the art, both ground rules preclude variable ferrite phase-shifter beam forming techniques. On the other hand, Butler matrices* (Figure 20) are competitive for beam forming, using semiconductor switches for beam selection.

Selected antenna approach.-On the basis of the foregoing considerations, the Butler matrix is the obvious choice for the altimeter application. It remains to decide what form of switching should be used to select the beams; also, how to best organize the composite beam-forming and selecting networks.

Since the particular array is 8 X 8 elements and beams, most imaginable solutions will find 8-throw switches both necessary and sufficient. An ideal switch would be a 9-port junction with series diodes in 8 legs; such devices have been fabricated at S-band. Realization of such a device at X-band should be possible but will require considerable development. The major problem is that of mounting the various semiconductor chips to yield tolerable parasitic reactances.

Two alternatives are three cascaded double-throw switches, and the image hybrid matrix switch** (see Figure 21). The cascaded switches are quite inferior to the matrix because losses are higher and individual diodes must handle more power. The switch matrix is similar to the Butler matrix and indeed can be derived by first connecting two Butler matrices back-to-back via 8 switchable phase shifters, then collapsing the network to remove extraneous elements and finally folding the network to be reflective rather than transmissive. The folding requires the addition of a circulator in one port to realize an entry port. This poses a problem in that the direction of circulation must be reversed if input and output are to be interchanged. Alternatively, the device can be used as a 7-throw switch and the circulator eliminated.

With a little manipulation the networks of Figures 20 and 21 can be combined to produce the combined switching and beam forming network of Figure 22. Actually, many such configurations are possible; the one shown has fewer crossovers than most.

A conceptual layout of the total array is shown in Figure 23. This array can be formed from a 64-element radiator, 9 or 10 matrices as per Figure 22, and an additional auxiliary switch. The radiator elements are taken 8 at a time in the vertical direction and combined with the matrix of Figure 22. This arrangement provides eight 8-beam "super elements" which are then further arrayed with an additional matrix to provide 64 beams.

---

* Butler and Lowe, "Beam-Forming Matrix Simplifies Design of Electronically Scanned Antennas," Electronic Design; April 12, 1961.

** H.E. Schrank, W.P. Hooper, R.D. Grove, "A Study of Array Beam Switching Techniques," Final Report, Contract AF30(602)3394-FSC-A082 with Rome Air Development Center; July 1965.

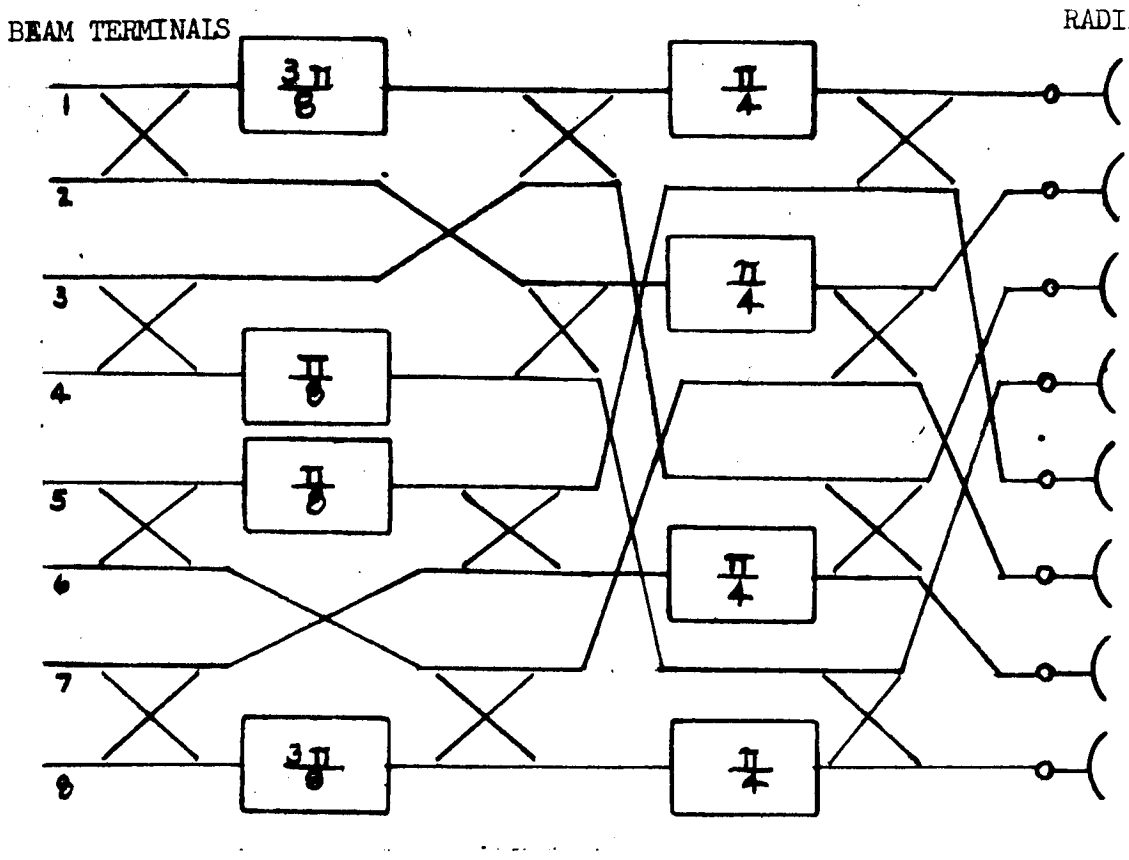

FIXED PHASE SHIFTERS
(All other lines between groups of elements to be of equal lengths)

FIGURE 20. - 8 ELEMENT BUTLER MATRIX

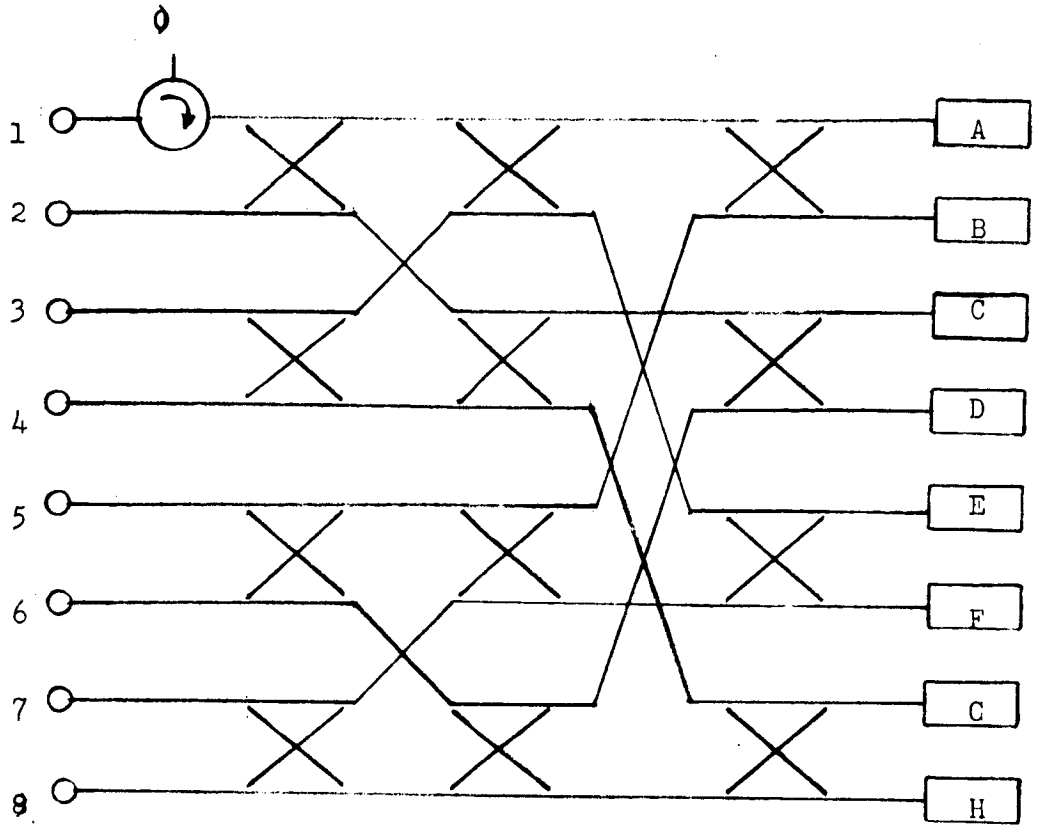

180° Ø Shift Reactive Termination

Input 0
Output

	1	2	3	4	5	6	7	8
A	0	180	180	180	180	180	180	0
B	180	0	0	0	180	180	180	0
C	180	180	0	180	0	180	0	0
D	0	0	180	0	0	180	0	0
E	180	0	180	180	0	0	180	0
F	0	180	0	0	0	0	180	0
G	0	0	0	180	180	0	0	0
H	180	180	180	0	180	0	0	0

FIGURE 21. - SP8T HYBRID MATRIX SWITCH

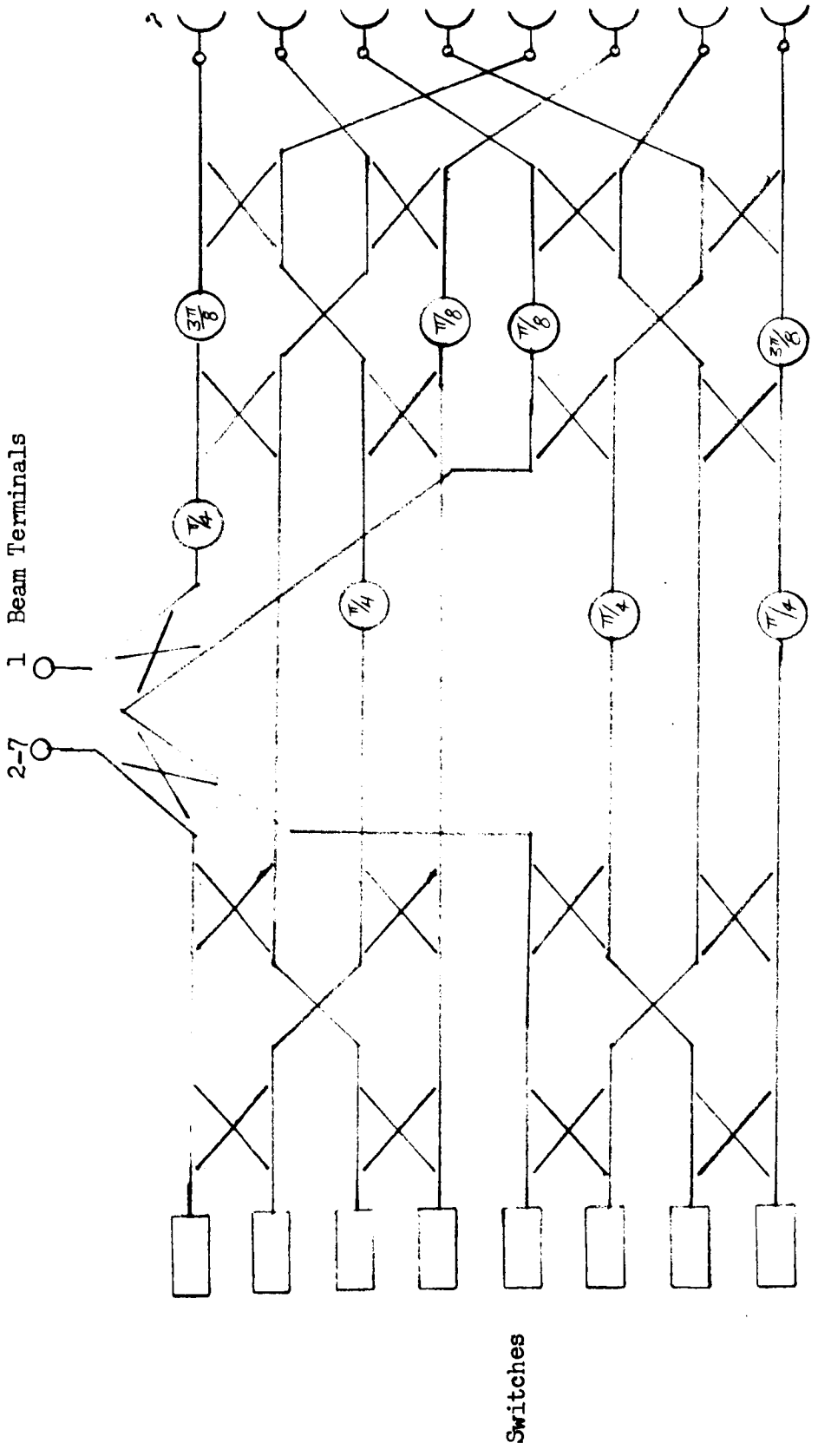

FIGURE 22. - COMBINED SWITCHING AND BEAM FORMING NETWORK

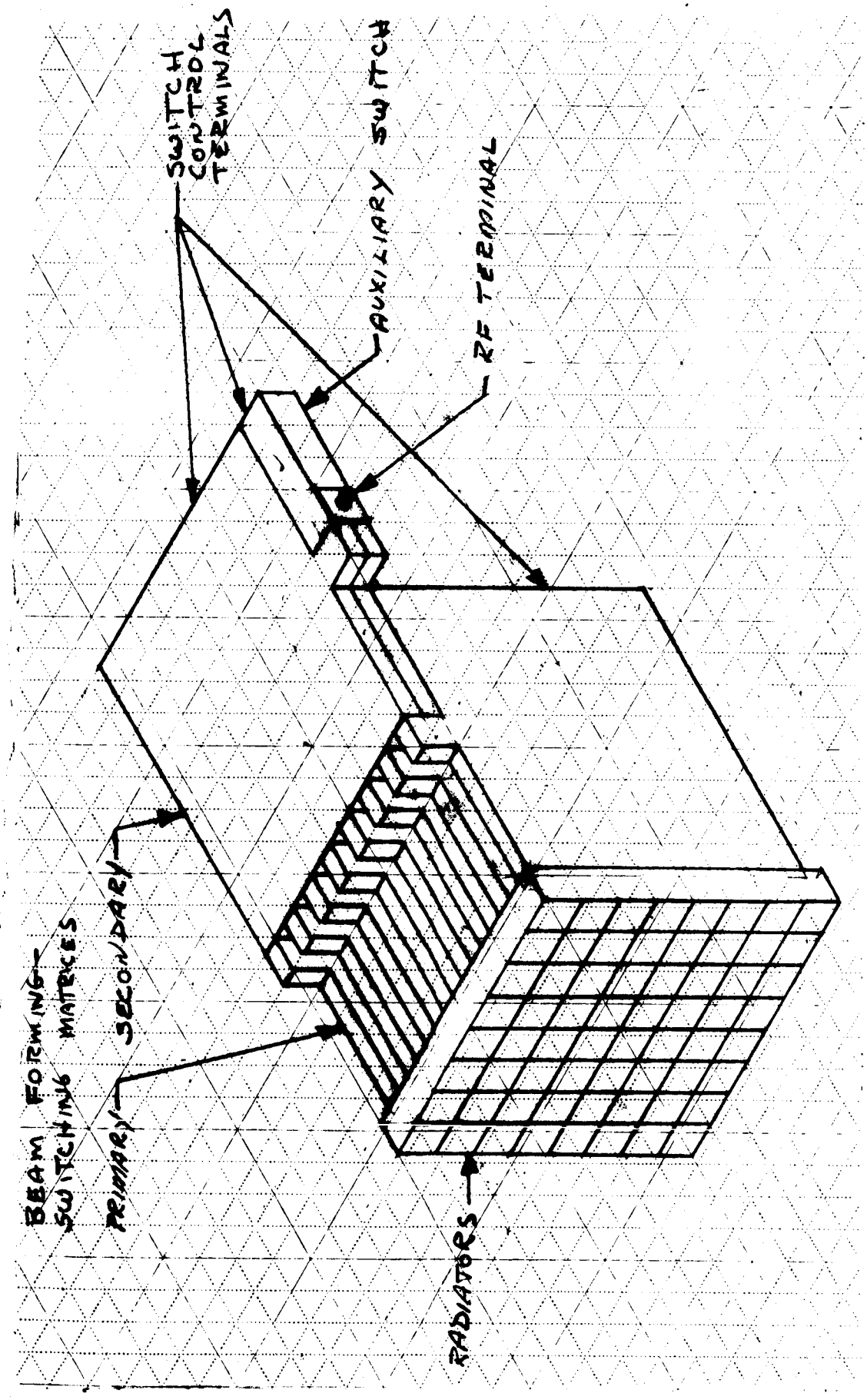

FIGURE 23. - CONCEPTUAL LAYOUT, TOTAL ANTENNA ARRAY

If all 64 beams are desired, two secondary matrices are used, one connected to the terminal labeled 1 in Figure 22, and the other connected to the terminal labeled 2-7. If we were willing to discard a row of eight beams, the 10th network is not required. With the particular network values shown, the missing beams would be closest to broadside. If desired, another set may be chosen by modification of fixed phase shift values and/or rearrangement of the matrix connections.

The same situation repeats at the terminals of the secondary matrices. If all 64 beams are required, we must select between four RF terminals. A 4-throw switch can be added for this purpose.

There then exist four possible solutions to the switch-matrix entry problem. These provide beam arrangements of 8X8, 7X8, 7X7 or 8X8 less one. The last solution obtains if the auxiliary switch is a 4-throw version of the image hybrid matrix switch and used as a 3-throw in the manner that the 8-throw is used as a 7-throw.

The 7X7 (49 beam) operation is attractive since it completely deletes one matrix board and the auxiliary switch. Full 8X8 operation involves the greatest network loss, and the greatest number of active elements. The other cases are intermediate, increased numbers of beams being realized at the cost of loss and complexity.

Because of circuit complexity and performance the utility of the 7X7 beam set should be examined carefully. It is possible to arrange it such that the 15 lost beams are pairs of 1/2 beams, at maximum angular shift from broadside. This results in the useful beams being symmetrical about broadside. Angular coverage is, however, reduced by 7/8.

The SPRA antenna requirements are best satisfied by the electronically scanned array with the Butler matrix beam-forming network providing 64 beams in a 120° X 120° field of view. Beamwidths are approximately 15° and peak gain is 19 dB. Table IV summarizes the characteristics of the several types of antennas considered.

Matrix design by stripline techniques.-The compact size of microwave stripline encourages its use in applications such as Butler matrices where a large number of low power elements is required. Systems are usually built with a 50-ohm characteristic impedance. Using recently available materials, systems are operable in the temperature range from -270°F to +375°F. For these materials, the loss of 50-ohm stripline is typically 0.1 dB per inch.

Butler matrices require the use of hybrids, phase shifters, and crossing elements. The phase shifters are made by accurately controlling line lengths. Hybrid designs are available with phase shift accurate to within 1° and power split to within 0.5 dB over a reasonable bandwidth. At X-band frequencies, 20 dB isolation is feasible. The circuitry is fabricated by photo-etching, permitting accurate production and repeatability.

Table of Symbols

All symbols are defined in the body of the report as they are used. For reference a listing of symbols is given in the order in which they appear.

P = transmitted power
h = altitude
k = Boltzmann's constant = 1.37×10^{-22} joule/°Kelvin
T = noise temperature in degrees Kelvin
NF = receiver noise figure
B = noise bandwidth
L = RF losses
G = antenna gain
λ = RF wavelength
A = reflecting area
σ_o = reflectivity
d = antenna diameter
θ = antenna half power beamwidth
S/N or SNR = signal-to-noise ratio
C = velocity of light
f_r = pulse repetition frequency
τ = pulsewidth
B_n = tracking loop noise bandwidth
fm = modulation frequency
fd = doppler shift frequency
ω_o = RF angular frequency
m = transmit modulation index = $\Delta F/fm$
ΔF = transmit peak deviation
Jn(u) = Bessal function of order n and argument u
fs = sample frequency
G(z) = open loop gain
ω_o = undamped natural resonant frequency
ζ = damping factor
H(jv) = closed loop gain
$\Delta\tau$ = differential gate position
Hz = cycle per second
W = watts
A = ampere
V = volt
LO = local oscillator
AFC = automatic frequency control
HVPS = high voltage power supply

List of References

David Middleton, "On Theoretical Signal-to-Noise Ratios in FM Receivers: A Comparison with Amplitude Modulation," Journal of Applied Physics; April 1949, pp 334-351.

M. I. Skolnik, "Introduction to Radar Systems," McGraw Hill Book Companry, 1962; Chapter 10.

D. K. Barton, "Radar System Analysis," Prentice Hall, 1964; Chapter 11.

Butler and Lowe, "Beam-Forming Matrix Simplifies Design of Electronically Scanned Antennas," Electronic Design; April 12, 1961.

H. E. Schrank, W. P. Hooper, R. D. Grove, "A Study of Array Beam Switching Techniques," Final Report, Contract AF30(602)3394-FSC-A082 with Rome Air Development Center; July 1965.

J. S. Bendat, "Principles and Applications of Random Noise Theory," John Wiley and Sons, Incorporated, New York; 1958.

Povejsil, Raven, and Waterman, "Airborne Radar," D. Van, Nostrand Companry, Inc., 1961; page 254.

op. cit., page 248

TABLE IV.-COMPARISON OF ANTENNA SYSTEMS

	Weight	Gain (Excluding Radome Losses)	Scanning Drive Power Required	Complexity (In Order Of Increasing Over All Complex.)	Volume	Reliability	Remarks
Mechanically Gimbaled Reflector	3.4 lb	19.5 dB	4	3	5	5	Not suited to flush mounting
Electronically Scanned Line Source	1.2 lb	13.0 dB	1 (least)	1 (least)	1 (least)	1 (Most Reliable)	
Combination Mechanical/ Electronic Scan	1.8 lb	20.0 dB	3	2	2	4	
Electronic Scan Ditital Phase Shift	17 lb	19.5 B	5	5	3	3	
Electronic Scan Butler Matrix & Diode Switch	3.35 lb	19.0 dB	2	4	4	2	

Semiconductor switches.-The semiconductor switching devices may be of several types. In the primary matrix switches each switch has incident 1/64 of the total transmitted power. For 1 kW total peak, about 15 watts peak is delivered to the switch. This is about the present state-of-the-art limit for varactor switches. PIN diodes can easily handle this much power but at increased loss. PIN diodes would definitely be required for all switches.

Integrated RF Unit

Description.-For economy in size and weight and to enhance reliability by eliminating RF interconnections, the microwave components are integrated into one package. The unit, shown functionally in Figure 24, is a composite structure consisting of stripline, coaxial lines, and bulk resistor elements. The mixers, circulator, isolator, and couplings are fabricated in stripline circuits. The bulk resistor material serves as terminations, and coaxial lines are used for the diode switch.

All of this circuitry is located in the lower portion of the unit (see Figure 25). In the upper portion is the local oscillator, a solid state device in which the X-band signal is generated by a frequency multiplier driven by a voltage-controlled solid-state oscillator.

Specification.-Table V lists the principal specifications of the components in the integrated RF unit.

Transmitter

Choice.-Two candidate transmitters for the radar altimeter are the pulsed oscillator (magnetron) and the master oscillator/power amplifier (MOPA). The latter would use a solid state driver and either a traveling wave tube (TWT) or klystron output amplifier. The magnetron transmitter is the simplest and smallest, although it does require over two pounds of magnetic shielding material to prevent magnetometer interference. The most favorable MOPA configuration is one using a high-gain TWT.

The TWT transmitter is somewhat larger than a magnetron transmitter because of the tube size, the additional RF source, and a larger high-voltage power supply (HVPS) and modulator. But the size and weight advantage of a magnetron transmitter is outweighed by the vastly superior reliability of the TWT transmitter. This, coupled with magnetic cleanliness considerations, led to the selection of the TWT configuration.

Description.-Figure 26 is a conceptual schematic of the chosen transmitter. The X-band signal is derived by multiplying the output of a UHF oscillator to 8 GHz. The TWT requires a minimum input signal level of 5 milliwatts.

The TWT is a grid-pulsed, conduction-cooled device of metal ceramic construction. Table VI summarizes the TWT specifications.

HVPS/Modulator.-The HVPS/modulator consists of a transistor amplifier operated as an emitter follower, an oscillator for the power supply driver, a power amplifier for the high voltage ac, and a high-voltage bridge rectifier with the necessary filter capacitors.

A pulse (12 V @ 100 mA) from the synchronizer drives a 4:1 step-down transformer to provide 400 mA initial drive to the base of an MHT-5002 connected as an emitter follower. The transistor is kept out of storage by a diode zener anti-storage circuit.

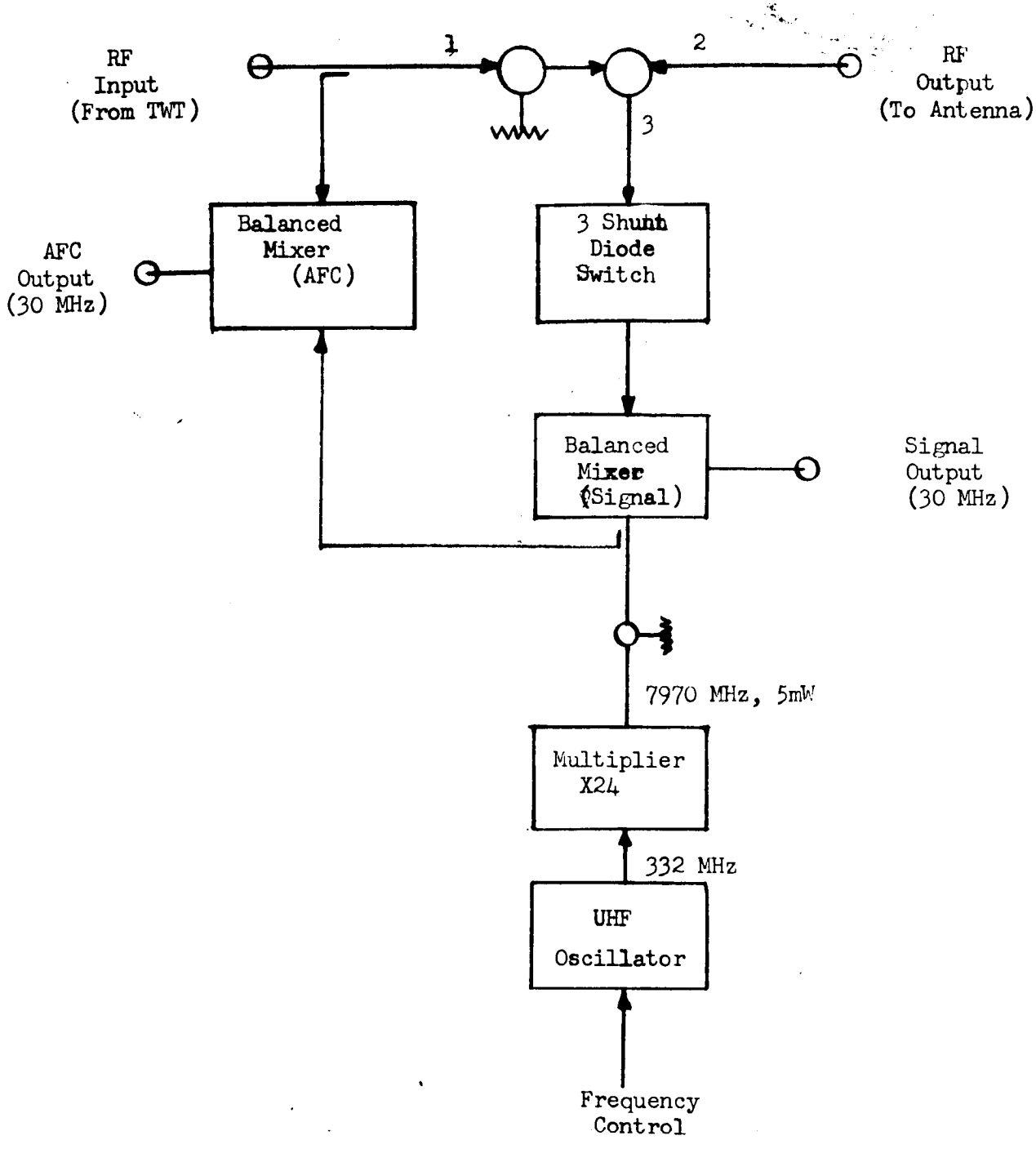

FIGURE 24.- INTEGRATED RF UNIT, BLOCK DIAGRAM

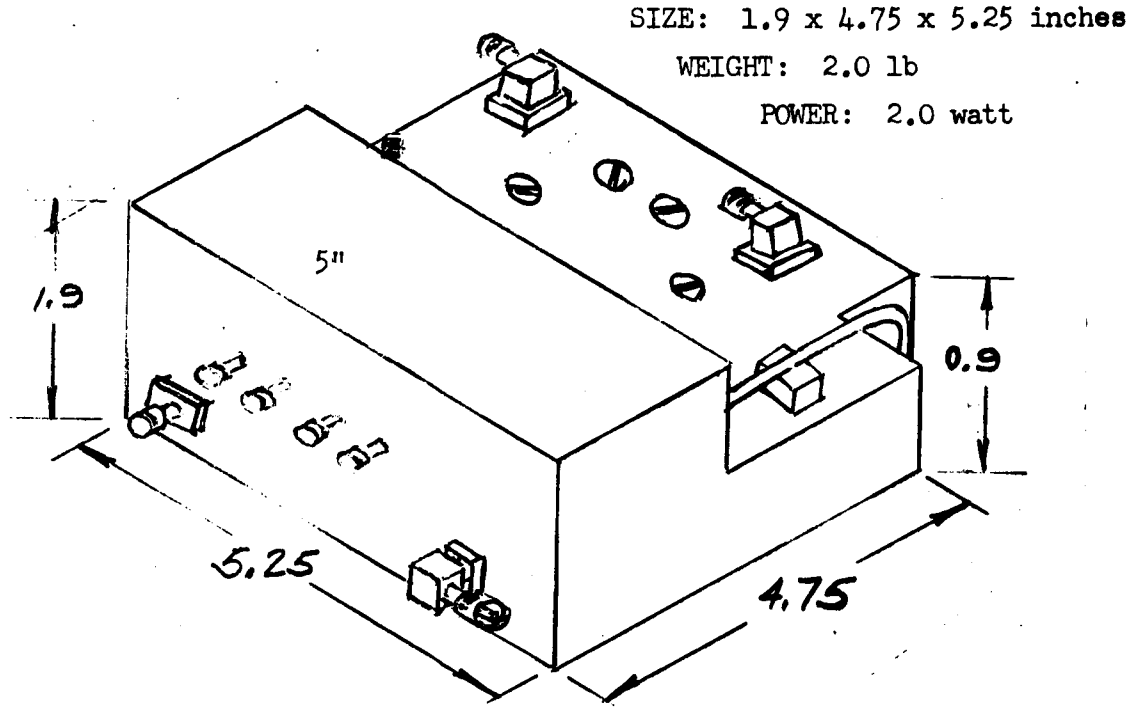

FIGURE 25.- INTEGRATED UNIT, PHYSICAL APPEARANCE

TABLE V.- SPECIFICATIONS INTEGRATED RF UNIT

Four-Port Circulator:	
Center frequency	8.00 GHz
Bandwidth	20 MHz (min)
Peak power rating	5 kW
Average power rating	1 W
Insertion loss	
1-2	0.6 dB
2-3	0.3 dB
Isolation	
1-3	20 dB
2-1	40 dB
Diode Switch:	
Center frequency	8.0 GHz
Bandwidth	20 MHz (min)
Switching time (10%-90%)	20 ns
Insertion loss	0.7 dB
Isolation	55 dB
Configuration	shunt, coaxial
Mixer (Signal):	
Signal frequency	8.0 GHz
Bandwidth	20 MHz (min)
Noise figure	8.5 dB (with 2.0 dB IF noise figure)
Intermediate frequency	30 MHz
Mixer (AFC):	
Signal frequency	7.970 GHz
Bandwidth	20 MHz (min)
Noise figure	8.5 dB (with 2.0 dB IF noise figure)
Intermediate frequency	30 MHz

(TABLE V.- Continued)

Isolator:	
Center frequency	7.970 GHz
Bandwidth	30 MHz (min)
Peak power rating	10 W
Average power rating	1 W
Insertion loss	0.3 dB
Isolation	20 dB
Voltage-Controlled Oscillator:	
Center frequency	7.970 GHz
Tuning range	$\pm$10 MHz
Power	5 mW
Stability	1 part in 10^4

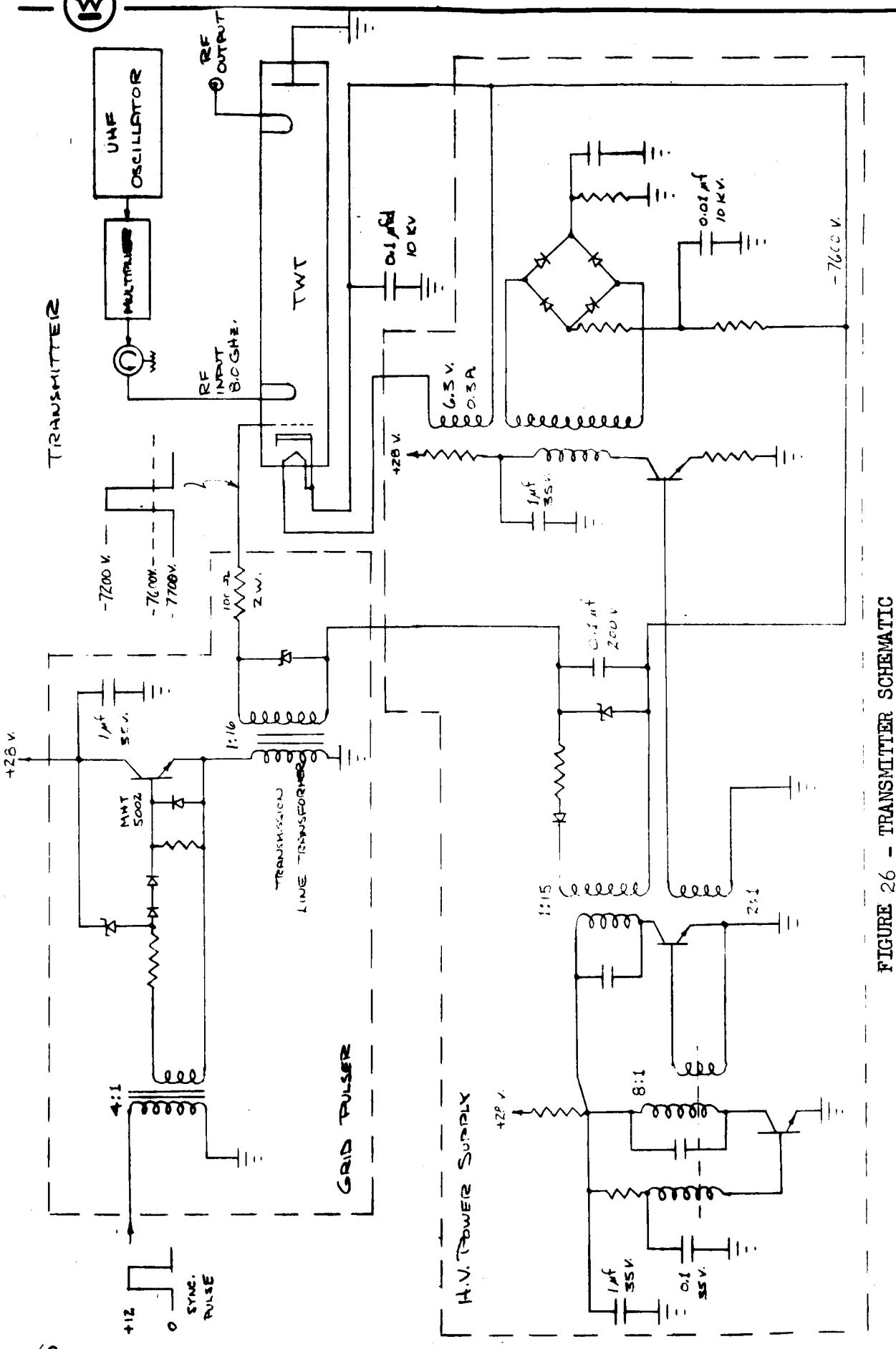

FIGURE 26 - TRANSMITTER SCHEMATIC

TABLE VI.- TWT SPECIFICATIONS

Parameters	
Frequency	8.0 GHz
Bandwidth	20 MHz (min)
Duty cycle	0.001 (min)
Peak power	500 W
Pulse width	2 μs (min)
Power gain	50 dB
Efficiency	20% minimum
Filament power	2 W
Filament voltage	6.3 V
Filament current	0.3 V
Beam voltage	7600 V
Peak beam current	0.33 A, peak
Peak collector current	0.310 A, peak
Grid bias	-100 V dc
Grid pulse voltage	+400 V
Grid peak current	+0.04 A
Grid leakage current	200 μA
Grid capacitance	15 pF
Weight	2.5 lb
Outline	11 X 1 X 1 inches
Focusing	PPM (platinum cobolt magnets)
Environment	
Heat sink temperature	0°C to +70°C
Vibration	20-200 Hz, 20 g (3 axes) (non-operating)
Shock	2-5 m s, 50 g (non-operating)
Acceleration	100 g for one minute (operating)

A transmission line transformer (TLT) is connected in the emitter of the transistor to provide the necessary 1:16 step-up ratio to generate a 500 volt pulse for the TWT grid. TWT grid bias is applied via the TLT secondary.

The bias, high voltage, and filament supply are derived from a 5-kHz ac source. The 5 Hz oscillator frequency allows the use of a small, low-weight power transformer. The solid state oscillator drives a solid state amplifier with two outputs. One is rectified to provide bias for the TWT, the second output drives a power amplifier.

A step-up transformer in the collector of the power amplifier provides 7.6 kV ac to the bridge rectifier. RC filtering can be used because the current is small. The TWT filament connects to a winding on the high voltage transformer.

Packaging.-The packaging of the several transmitter parts will be discussed next. As shown in Figure 27, the master oscillator is essentially a metallic shielding case containing solid-state components and an integral isolator. Figure 28 shows the outline dimensions for the TWT. This item is a ceramic vacuum tube which has circular focussing magnets situated along its length; the magnets are made of platinum-cabalt for minimum size and weight. The whole unit is potted and enclosed in a metallic case for rigidity and protection against shock.

The high voltage power supply and modulator will be packaged into one assembly as shown in Figure 29. In this design there are approximately 15 relatively large components, including 3 toroidal transformers which operate at 7.6 kV. This voltage level can present problems at lower atmospheric pressures. As the pressure decreases, the dielectric strength of air decreases until it reaches a minimum at a pressure equivalent to an altitude of about 150,000 feet above the earth. As the pressure decreases further, the dielectric strength of air increases again.

Since the altimeter will operate during the descent phase of the mission, and since present indications are that surface Mars pressure is equal to approximately 150,000 feet earth pressure, the altimeter will be operating in the most critical pressure range. The loss of dielectric strength of course applies to air. Therefore the way to prevent breakdown at high voltages and critical pressures is to ensure that leads and component are completely surrounded with proper insulative material to the exclusion of air. To be particularly avoided are air bubbles and inproperly bonded interfaces between two surfaces which provide an uninsulated path to ground.

In the HVPS/modulator, the breakdown will be prevented by mounting all the high voltage components in a relatively open board type construction on the lower section of the case. Although it is purchased outside, the TWT will be designed in close cooperation with the supplier in such a manner that it can be attached to and made an integral part of the HVPS/modulator case. When these two units have been joined, and the high voltage interconnections made, the completed assembly will be potted in silicone insulating material

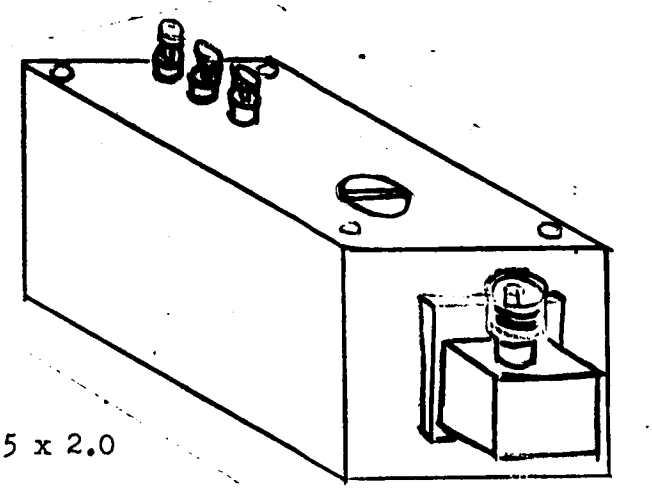

SIZE: 1.5 x 1.5 x 2.0
WEIGHT: .15 lb
POWER: 2.0 watt

FIGURE 27.- MASTER OSCILLATOR APPEARANCE

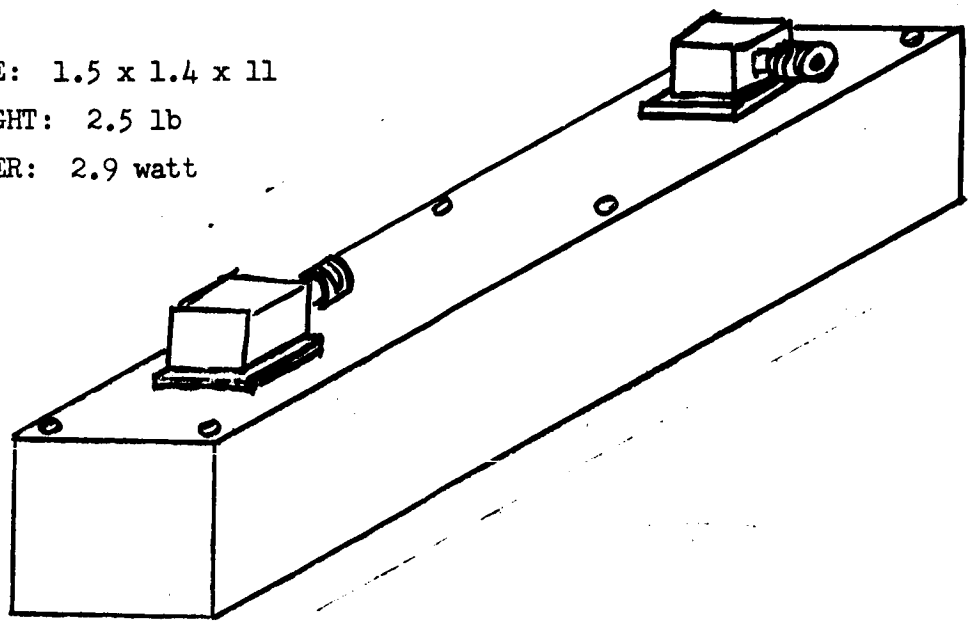

SIZE: 1.5 x 1.4 x 11
WEIGHT: 2.5 lb
POWER: 2.9 watt

FIGURE 28.- TWT APPEARANCE

SIZE: 3.5 x 4.0 x 2
WEIGHT: 1.75 lb
POWER: .52 watt

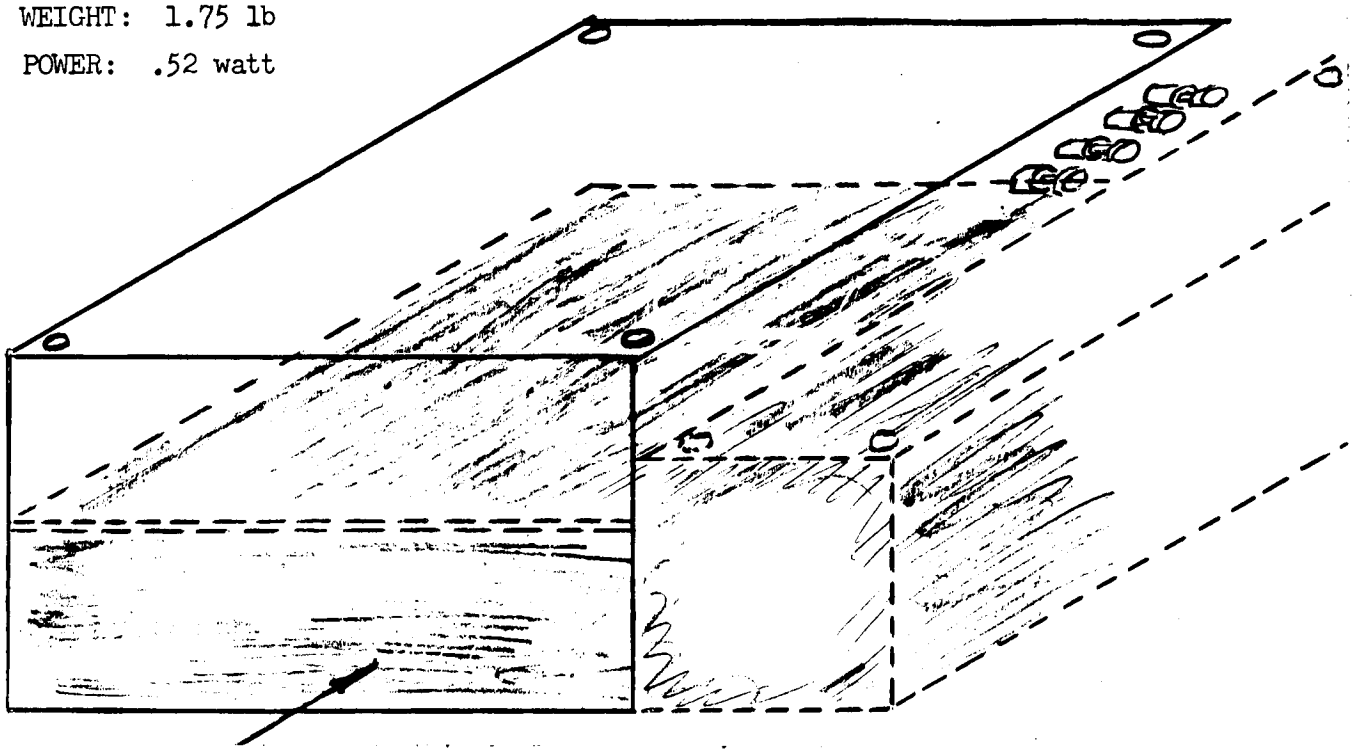

Lower Section Potted Integrally with TWT for Arcing Protection at 7.6 KV.

Upper Section Contains Lower Voltage Components, Unpotted.

FIGURE 29.- HVPS/MODULATOR APPEARANCE

which covers all paths to ground potential. This of course includes all components on the lower section of the HVPS/modulator case. The 30 lower-voltage components in open board construction will be mounted into the upper section of the case. No potting is planned there because the cover needed shielding also protects the contents.

IF Amplifier

Block diagram.-A block diagram of the IF amplifier mechanization appears in Figure 30. The amplifier has an overall operating voltage gain of 113 dB, a noise figure of 2 dB, a power requirement of 275 mW, and an AGC range of 70 dB. Semiconductor components in the amplifier include 7 monolithic integrated circuits, 1 multichip integrated circuit, 1 transistor, and 5 diodes. A discussion of the amplifier operation follows, starting from the input of Q1 in the block diagram.

Circuit description.-Transistor Q1 (2N3571) was selected for its low noise figure and high power-gain capabilities as a common emitter stage. A high power-gain to the input of the second amplifier stage is required to reduce the effect of noise contributions of latter stages. A noise figure of approximately 2 dB is expected with this circuit.

CR1 (1N3066) is a low-capacity diode which is back-biased during small signal operation. Accordingly, it acts as a shunt resistor whose resistance decreases with forward bias supplied by the AGC when signal level increases. Diode CR1 provides signal attenuation of 20 dB and limits to 15 mV rms the maximum signal applied to the following stage.

The initial bandwidth of the circuit between Q1 and Z1 is approximately 10 MHz so that capacity changes in CR1 with increasing AGC have a negligible effect on the overall IF bandwidth. The interstage bandwidth increases with AGC.

Z1a, Z1b and Z2 are Motorola MC-1935 monolithic integrated circuits used as amplifiers to which AGC voltage is applied. Z1a and Z1b are connected as a balanced push-pull amplifier stage that acts as an attenuator during the transmit time. Reduction of the transmitter leakage signal is required in order to detect minimum altitude return. The MC-1935 becomes nonlinear at an input signal level of approximately 30 mV rms but this level is not a function of the AGC voltage applied. The input and output impedances of the MC-1935 vary only slightly with AGC level. With AGC applied, most known semiconductor devices have large variations in input and output impedances and their signal input capability decreases with increasing AGC voltage. The maximum signal level applied to any of the MC-1935 units occurs at the input to Z1 and this level is limited to 15 mV rms which corresponds to a system input signal level of -38 dBm. The per-stage voltage gains of Z1 and Z2 are approximately 16 dB.

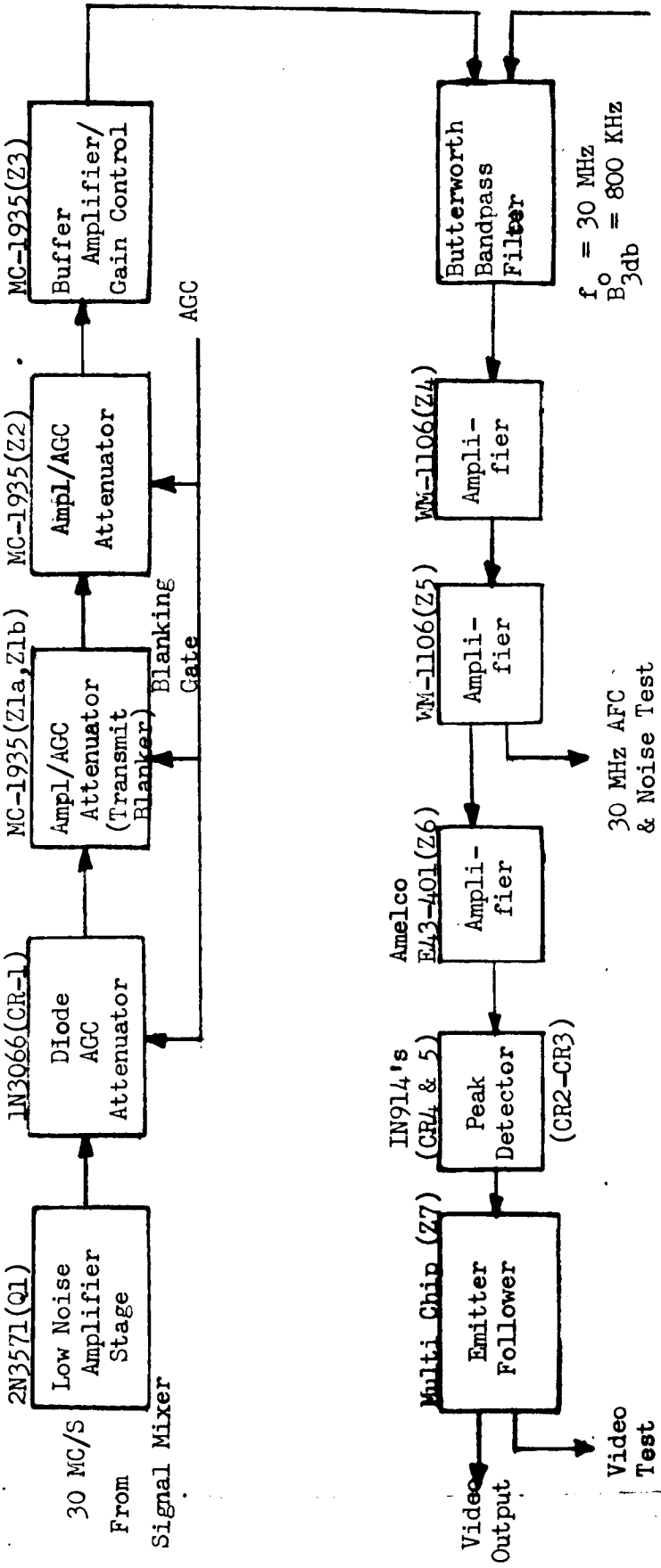

FIGURE 30.- IF AMPLIFIER BLOCK DIAGRAM

Z3 is also an MC-1935 integrated circuit used as a variable-gain amplifier and buffer for the bandpass filter following Z3. The gain of Z3 is varied manually (over a 12 dB range) by setting the initial gain-adjust potentiometer, R12. R12 compensates for component gain variations in different amplifiers, and adjustments of the gain have a negligible effect on the overall IF bandwidth. R12 is adjusted to obtain an overall voltage gain of 10 dB above 113 dB, where the 10 dB is a "reserve gain" normally removed by the noise AGC. Thus 10 dB of system noise output variation is allowed before the noise AGC would no longer regulate. This compensates for system gain variations versus environment.

Following Z3 is a 3-pole, 30 MHz, LC, Butterworth bandpass filter with an 800-KHz 3-dB bandwidth and a minimum attenuation of 60 dB at frequencies $\pm$10 MHz from 30 MHz. Even though there are 5 other tuned circuits in the amplifier, this filter basically determines the IF response since the narrowest of the other circuits has a 7-MHz 3-dB bandwidth.

Z4 and Z5 are Westinghouse WM-1106 monolithic integrated circuits used as high fixed gain amplifiers. Z6 is an Amelco E43-401 monolithic integrated circuit with higher power capabilities than the WM-1106. The interstage between Z5 and Z6 is untuned and provides the AFC and an IF test output for measuring the overall IF noise figure. The output of Z6 is a 30 MHz tuned circuit with a 3 dB bandwidth of approximately 3.5 MHz. This bandwidth is determined partially by the output resistance of Z5 and the dynamic load resistance appearing at the input of the following peak detector. The combined gain of Z5 and Z6 is approximately 80 dB.

The peak detector consists of CR4 and CR5 (1N914 diodes) along with the required filter components. The 3 dB video bandwidth is approximately 1 MHz with the detector load and filter component values shown on the schematic. With this value of load resistance the voltage doubler circuit was chosen since its input impedance is low enough to allow stable operation of the driver stage, Z6. CR2 and CR3 are 1N914 diodes that forward-bias the detector diodes to increase the detector linearity for small signal levels. The forward bias current is a compromise since overbiasing will cause the diodes to conduct on both positive and negative excursions of the IF signal so that detection does not actually exist at low signal levels. Forward biasing of the detector also partially compensates for the shift in the E-I characteristic of the detector diodes with temperature.

Z7 is a multichip integrated circuit acting as an emitter follower. It normally supplies a 1.2 volt pulse to a 1,000 ohm load.

Packaging.-Construction of the IF strip is as shown in Figure 31. IF amplifier active components (principally molecular circuits) are packaged in flat packs. These, together with miniature conventional components, are formed into small cordwood modules which represent the various stages. These modules are placed into the isolation cells of a compartmented structure. This structure is made of thin sections chemically milled and then brazed to form the completed box. After test, potting of the completed assembly provides environmental protection. Side plates are attached for total isolation.

Size: .75 X .75 X 4.3

Weight: .25 lb

Power: .40 watt

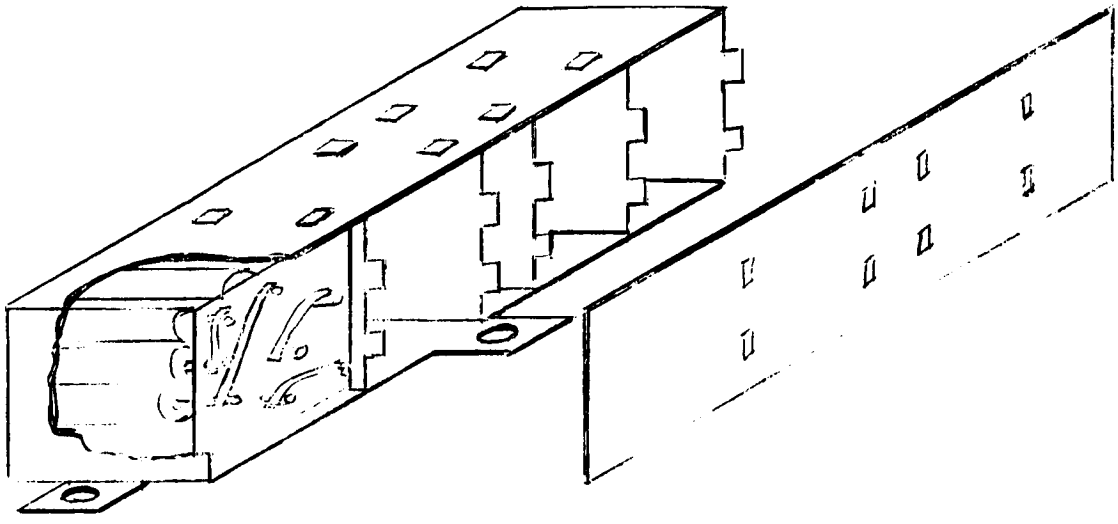

FIGURE 31. - IF AMPLIFIER APPEARANCE

Automatic Frequency Control

Block diagram.-A block diagram of the AFC amplifier and sweep circuitry appears in Figure 32. Basically this AFC scheme is a sampled-data feedback system with the application of pulse stretching to reduce the loop gain requirements.

Circuit description.-The local oscillator (LO) frequency is kept at a 30-MHz difference from the transmitter frequency. This offset is accomplished by sensing the error signal from a 30-MHz frequency discriminator that is designed to generate zero error signal at its center frequency. A peak-to-peak frequency separation of approximately 1.5 MHz simplifies the tracking requirements (environmental) between the center frequency of the main IF amplifier and the crossover frequency of the discriminator.

The relatively narrowband discriminator requires that the LO be swept in frequency to increase the AFC pull-in range to ± 10 MHz from the discriminator center frequency. The sweep will stop and hold when the transmit sample is within the high-gain portion of the discriminator frequency response. This sweep and lock circuitry is an integrated circuit version of a scheme employed in the Gemini Rendezvous Radar System.

Packaging.-The AFC, illustrated in Figure 33, contains 5 integrated circuits, 2 transistors, 9 diodes, and 50 passive components packaged as a cordwood module. Outputs are via solder terminals and the module is potted for environmental protection.

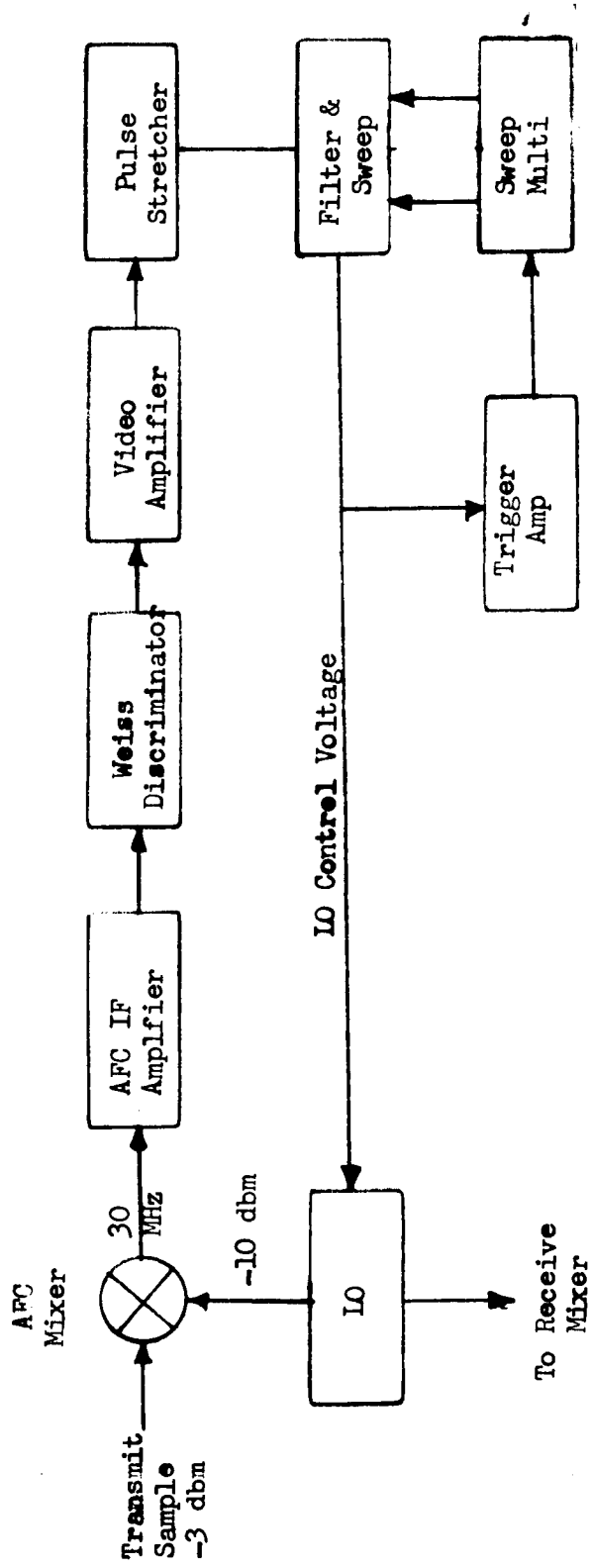

FIGURE 32. - AFC BLOCK DIAGRAM

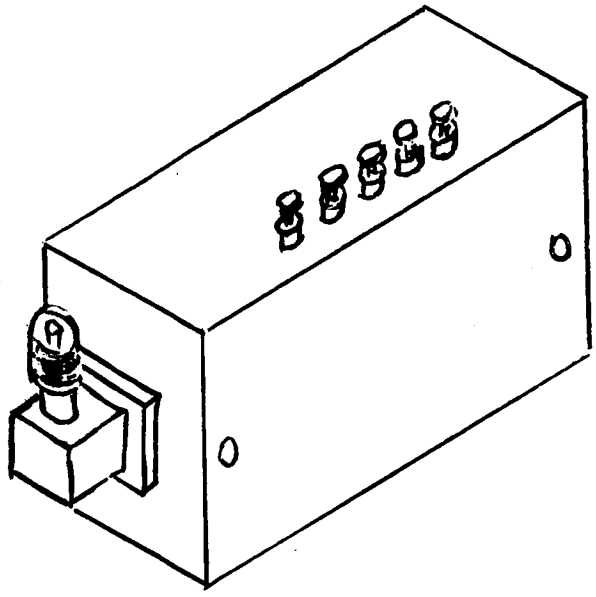

Size: 2.6 X 1.3 X 0.75

Weight: 0.14 lb

Power: 0.3 watt

FIGURE 33 - AFC

Digital Range Tracker - Electronics Package

Introduction.-Functionally, the range track sub-system in a pulse radar serves to search for, automatically acquire, and track a received target echo. The accuracy with which target range and relative range rate can be measured is essentially dependent on the time and environmental stabilities of the processing circuitry. With the advent of integrated circuit components, the digital mechanization of previously analog circuits has become entirely feasible in terms of weight, size, and power dissipation. As such, the deleterious effects of analog parameter instability and thermal drifts, which formerly plagued designers of analog equipments, can now be obviated by design in a digital processor. However, because of the nature of the received signal, the derivation of range error must be performed using analog circuit elements. In an effort to minimize the limiting effects of the error detector, the system described below embodies a significant departure from conventional detector configurations and mode of error extraction.

System description.-The basic range tracker configuration is shown in the simplified block diagram of Figure 34. It is assumed that in this and following discussions that the primary functions of search and acquisition have been performed so that system operation can be described in the track mode.

In the block diagram, note that during track a narrow gate is centroidally partioned over the video return pulse. The position of this

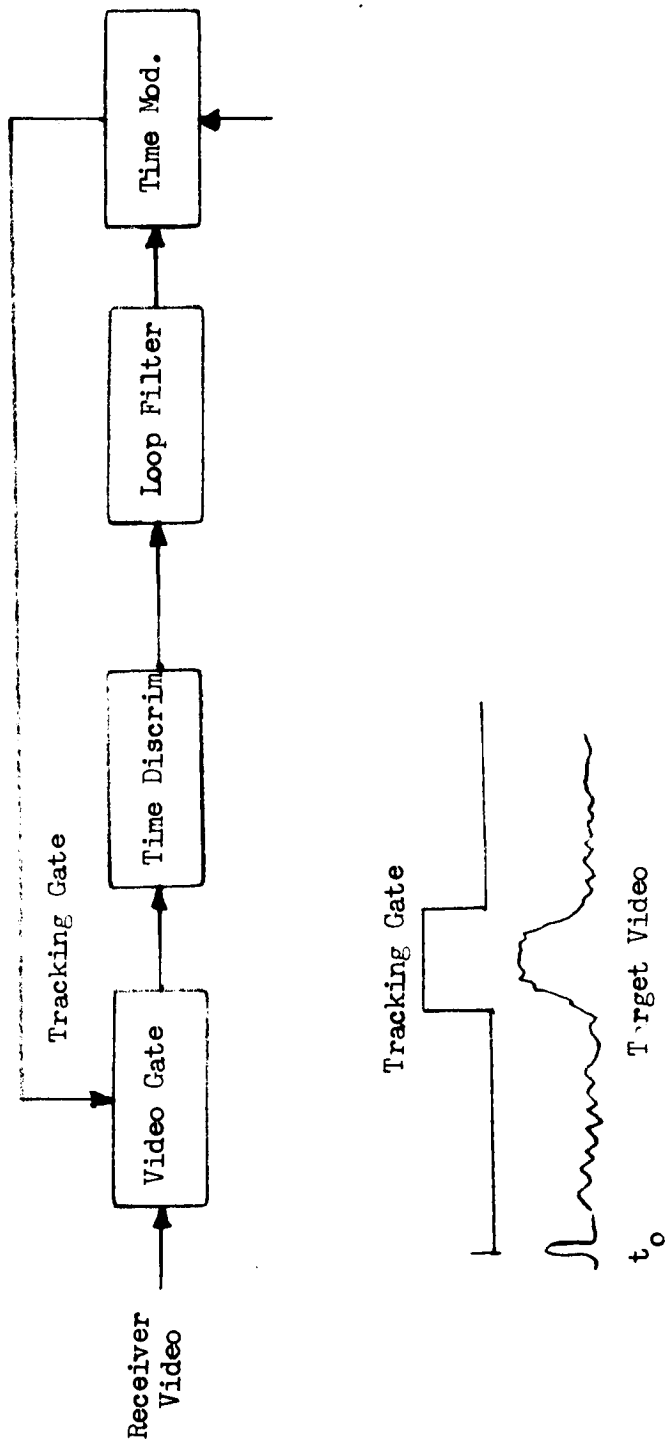

FIGURE 34. - SIMPLIFIED BLOCK DIAGRAM, RANGE TRACKER

pulse relative to the time zero (t_o) reference is determined by a numerical input to the time modulator. Loop error is determined from the relative difference of the centroids of the video and range tracking gate; it is generated as a numerical output at the output of the time discriminator.

The time discriminator output is coupled to the loop filter which, in the design example to be described, is configured so as to produce closed-loop limiting range and range rate errors of zero. The loop damping factor is arbitrarily assigned and the effective loop bandwidth is chosen as a compromise between allowable acceleration error and error due to noise. The loop filter output is coupled to the time modulator input, closing the loop.

The mechanization of the control loop differs mainly in the formation of the clock signal and the extraction of loop error. The mechanizations of the clock and time discriminator are presented below.

In a typical system, the basic quantized interval corresponds to the period of the clock signal. Thus, a coarse measure of target range can be determined by counting the number of clock pulses generated in the time interval beginning at t_o and ending when the target echo returns. Since the target can appear in an interval between two sucessive clock pulses, the range error will be uniformly distributed between values of $-q/2$ to $+q/2$ where q is the quantized range interval equal to the reciprocal of the clock frequency.

The system to be described permits positioning of the tracking gate in increments between any two sucessive clock pulses, and thus reduces the quantization error to a value corresponding to the time difference between each incremental position. The method which accomplishes the vernier range positioning uses two clocks. The frequency of each clock is identical but their relative phase can be altered digitally from zero to 2π radians in increments of $2\pi/2^n$.

The non-phase-shifted or reference-phase clock signal is coupled to an M-stage serial binary counter which divides the clock frequency by 2^M to produce the PRF pulse (t_o time reference). Although the serial counter experiences propagation delays in the division process, the time delay between the leading edge of the clock pulse and the leading edge of the PRF pulse is constant, enabling synchronous decoding, i.e., extraction of a single clock pulse at the PRF rate. The range-tracking gate pulse is generated by an M-stage synchronous counter which counts a specified number of the phase-shifted clock pulses. This counter is analogous to the time modulator in a conventional system, and it produces a time or range delay as a function of a numerical input rather than an analog voltage input.

The synchronous counter can be envisioned as a multi-tap delay line with taps placed at intervals corresponding to the period of the clock. Thus the time or phase displacement of the phase-shifted clock, relative to the t_o reference clock, will be present for any number of counts after the generation of t_o. Since the phase displacement is present in the generation of the tracking pulse, the tracking pulse can be positioned

incrementally anywhere in the interval occupied by two successive reference phase clock pulses (see Figure 35). The generation of two clock signals which can be digitally phase shifted with respect to each other is discussed next (see Figure 36).

Clock pulse generation.-The reference oscillator output (a square wave at frequency w_o) is coupled to an n-stage synchronous counter, synchronous decoder, and the square-wave modulators. The synchronous counter output is a square-wave at frequency $w_1 = w_o/2^n$. The decoder output is also a square-wave at frequency w_1 but with 2^n possible phases relative to the synchronous counter output. That is, the decoder provides a pulse train at a frequency $w_o/2^{n-1} = 2w_1$ which selectively sets or resets a control flip-flop. The pulses are formed by

$$A_{1j} \cdot A_{2j} \cdot A_{3j} \cdots A_{n-1j}$$

Where $A_{10} = \overline{A_{11}}$

The time delay of the first pulse relative to the state

$$A_{10} \cdot A_{20} \cdot A_{30} \cdots A_{n-1,o} \; ; \; \tau(A_{io}) = 0$$

is given by

$$\tau = \sum_{i=1}^{n-1} A_{i1} \left(\frac{2\pi}{w_o}\right) = i-1$$

Note that $w_1 \, A_{n1} \left(\frac{2\pi}{w_o}\right) 2^{n-1} = \frac{2\pi \, w_1}{2w_1} = \pi$ radians = phase shift relative to w_1

That is, the relative phase shift, ϕ_R equals $w_1 \tau$ For clarity, suppose n=4 and the set/reset pulses are formed by

$A_{11} \cdot A_{20} \cdot A_{31}$ with $A_{40} = 0$ indicating set on first pulse, reset on second pulse

$$\tau = \frac{2\pi}{w_o} + \frac{4(2\pi)}{w_o} = \frac{10\pi}{w_o}$$

$$\phi_R = \frac{10\pi}{w_o} \; w_1 \quad \text{but} \quad w_1 = \frac{w_o}{2^4}$$

$$= \frac{10\pi}{w_o} \cdot \frac{w_o}{16} = 5/8 \; \pi \text{ radian}$$

Note further that the phase can be represented by the number

$$\underset{A_4A_3A_2A_1}{0\;1\;0\;1} \equiv 5$$

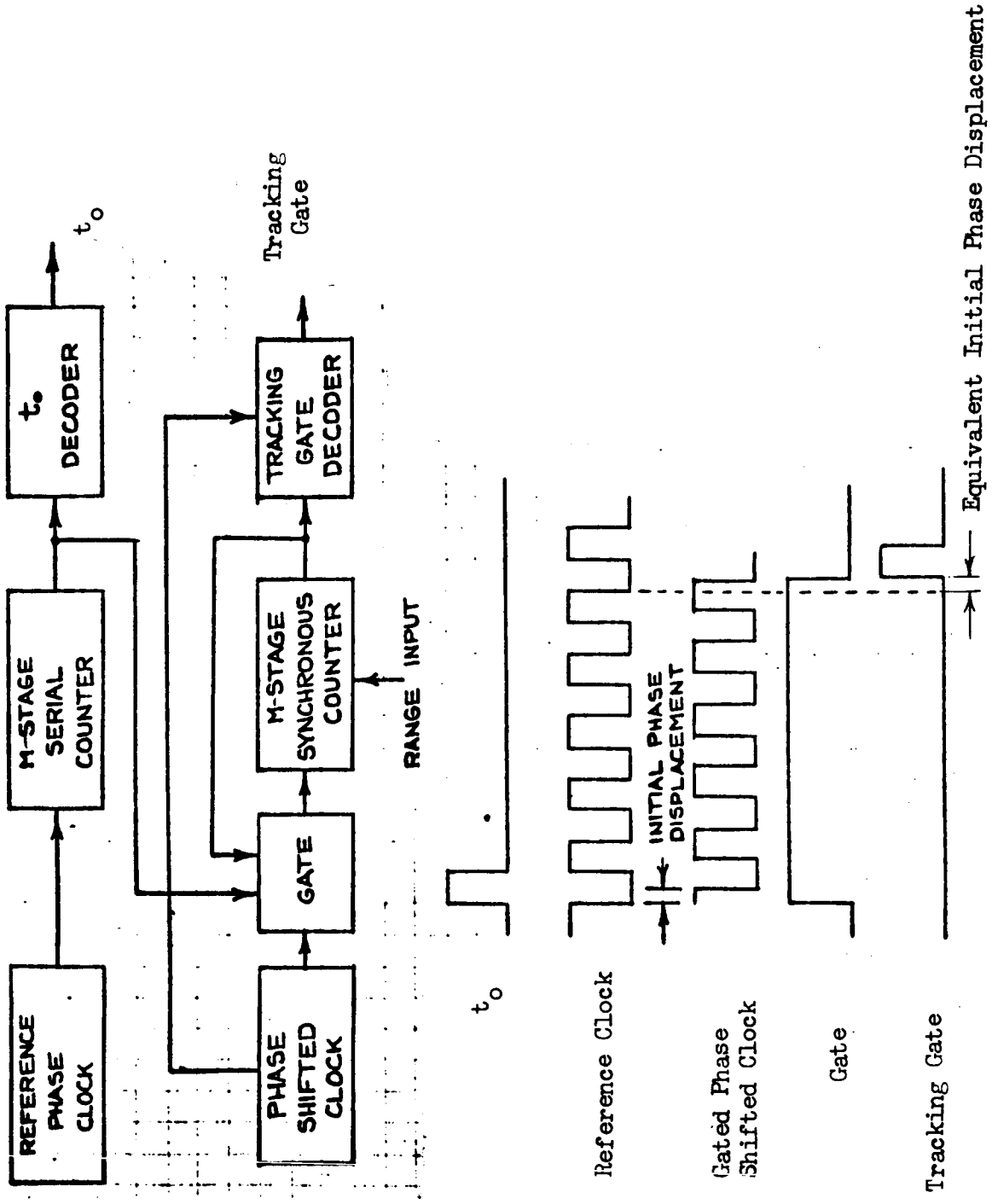

FIGURE 35. - TRACKING GATE AND t_o GENERATOR

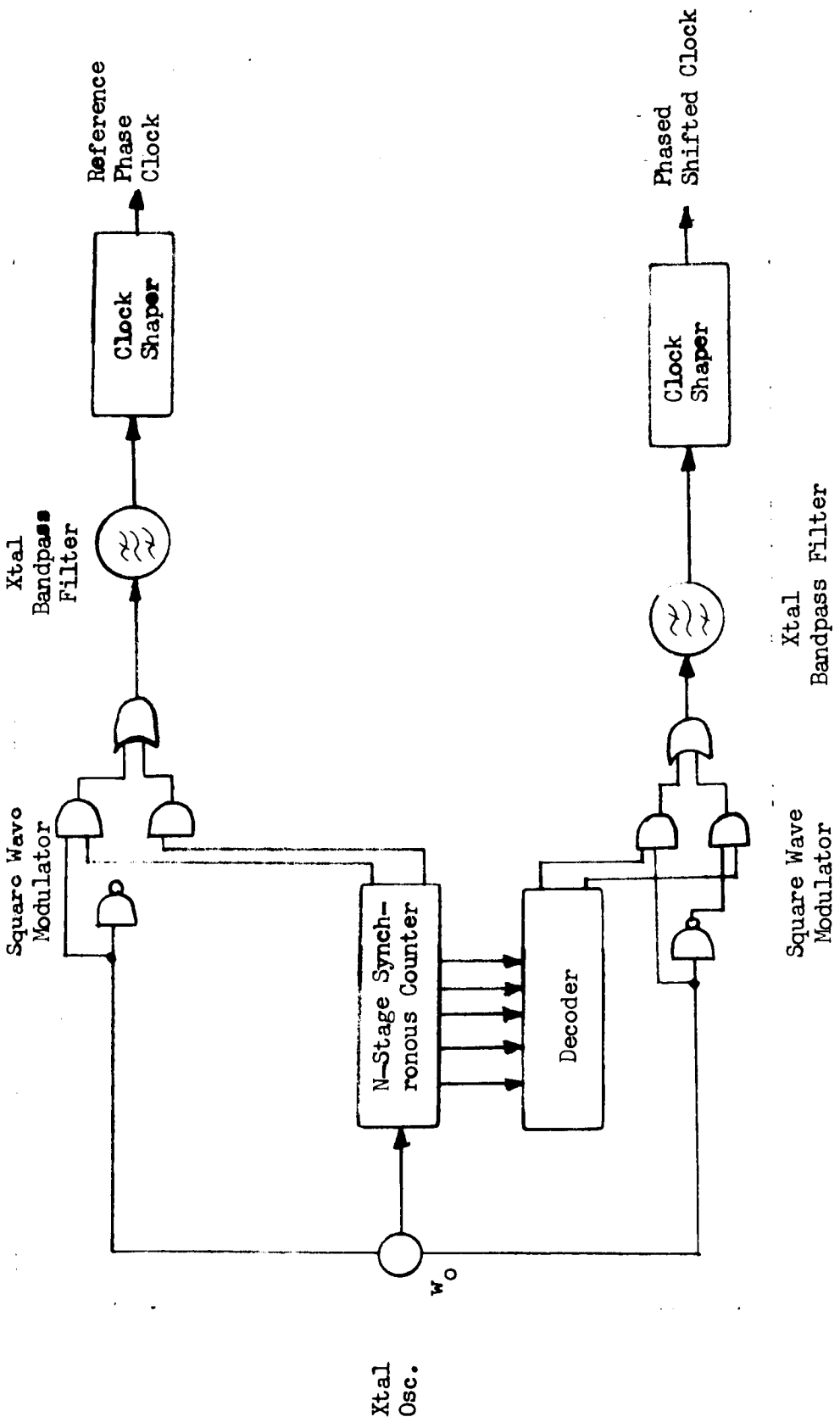

FIGURE 36. - CLOCK GENERATOR

Thus the numerical equivalent of the binary number describing the relative states of the flip-flops in the synchronous counter multiplied by the factor $2\pi/2^n$ will yield the relative phase between the signals generated at frequency w_1.

The square wave modulator output signal is given by:

$$E_m(t) = \left[E_o \; A_1(w_o t) \cdot A_2(w_1 t) + \bar{A}_1(w_o t) \cdot \bar{A}_2(w_1 t)\right]$$

$$A_i + \bar{A}_i = 1$$

The clock is given by (from a Fourier series)

$$A_1(w_o t) = \frac{E_o}{2} + E_o \sum_{n=1}^{\infty} \left[\frac{1 + (-1)^{n-1}}{2}\right] \frac{2}{\pi n} \sin n w_o t$$

The modulating signal is given by

$$A_2(w_1 t) = \tfrac{1}{2} + \sum_{m=1}^{\infty} \left[\frac{1 + (-1)^{m+1}}{2}\right] \sin\left(m w_1 t + \frac{m^k}{2^k} 2\pi\right)$$

(Note that for the reference signal K=0)

Neglecting terms beyond n=1, the modulator output signal is therefore

$$E'_m(t) = \frac{E_o}{2} + E_o \left\{ \sum_{m=1}^{\infty} \frac{4}{m\pi^2} \left[\frac{1 + (-1)^{m+1}}{2}\right] \cos\left[(w_o - m w_1)t - \frac{mk}{2^k} 2\pi\right] \right.$$

$$\left. - \sum_{m=1}^{\infty} \frac{4}{m\pi^2} \left[\frac{1 + (-1)^{n+1}}{2}\right] \cos\left[(w_1 + m w_1) + \frac{mk}{2^k} 2\pi\right] \right\}$$

(Note that carrier cancelation (absence of frequency at w_o) occurs in this process and because of the even division in obtaining w_1 from w_o and the fact that only odd terms occur, there is only one component at frequencies $w_o \pm m w_1$.

Since $w_1 = \frac{w_o}{2^k}$

The upper sideband fundamental component is given by

$$E_1(t) = \frac{4E_o}{\pi 2} \cos \left(\frac{2^k + 1}{2^k}\right) w_o t + \frac{2\pi k}{2^k}$$

$$k=o,1, \ldots(2^k-1)$$

From the above, the minimum resolvable time delay is given by

$$\Delta t = \frac{2\pi}{(2^k+1)w_o}$$

Crystal bandpass filters extract the upper sideband fundamental components from the modulator outputs. The resultant sine waves are shaped by squaring circuits to form the two required clock signals.

Error detection.-Conventionally, the video and tracking gate signals couple to a discriminator circuit which produces a bipolar output whose amplitude is proportional to the time displacement between the centroids of the video and tracking gates. A null output indicates the two signals are perfectly aligned; the polarity of the misalignment error is a measure of whether the tracking gate is at a greater or lesser range than the video signal being tracked. The true null is affected by analog bias errors and, when they occur, the null is dependent on target amplitude. Independent of the processing system following the time discriminator, the ultimate system accuracy is limited to the time and environmental bias errors introduced in the discriminator process. Except for the basic quantization error, no additional errors occur in the remainder of the digital processing system.

The following discusses extraction of a numerical error signal from the analog discriminator output signal. The time discriminator output is coupled to a zero-threshold comparator which produces a unit output for positive errors of any magnitude, and a null output for negative errors of any magnitude. To translate the binary nature of this circuit into a measure at range error, the tracking gate position is swept digitally across the video return pulse, advancing in small increments once each successive interpulse interval.

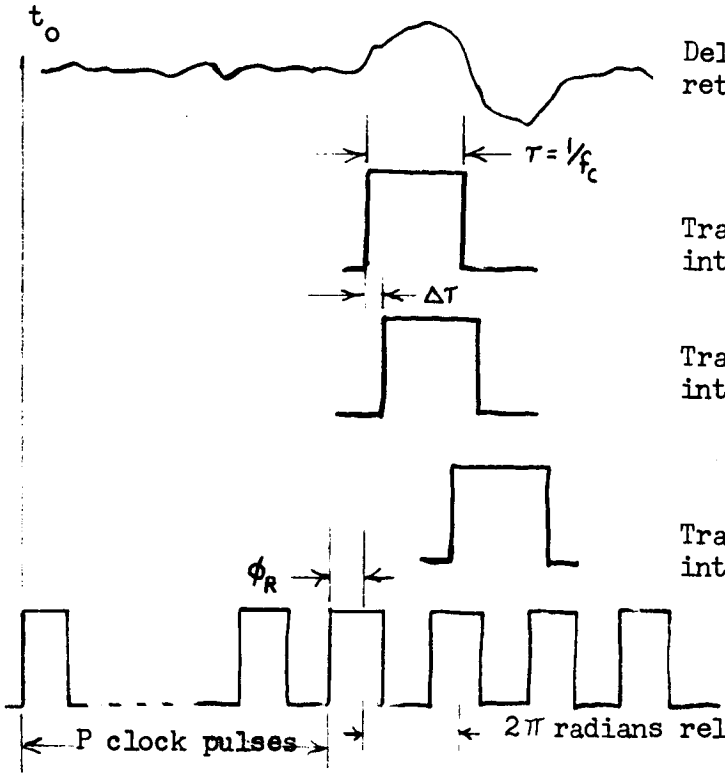

Delay line differentiated video return pulse

Tracking gate position for zeroeth interpulse interval

Tracking gate position for first interpulse interval

Tracking gate position for (2^n-1) interval

Reference clock (freq f_c)

As shown, starting with an initial phase shift, ϕ_R, the digital phase shifter is stepped at the PRF rate resulting in the generation of 2^n error signals when the phase has been advanced through 2π radians. A computation of all the measured discriminator error signals during the one recurrent sweep constitutes a single error measurement so that the effective sample rate becomes $f_{PRF}/2^m = fs$. During the sweep, N of the generated error signals will be positive, M will be negative, and $N+M = 2^m$. The zero threshold comparator output is sampled during each PRF interval giving N counts in the interval 1/fs. Bias value 2^{m-1} is subtracted from N, yielding the error $\mathcal{E}_n$ defined by

$$\mathcal{E}_n = \left| N-2^{m-1} \right| \quad \text{counts}$$

with algebraic sign defined by the sign of $(N-2^{m-1})$. P is the number of clock pulses counted from t_o to the interval just preceding the return of the target echo. The loop clases when P, ϕ_R are such that $N=M=2^{m-1}$.

Since $\phi_R = \frac{m}{2^m}\left(\frac{1}{f_c}\right)$, range R is thus defined as

$$R = \frac{C}{2}\left(P+\frac{m}{2^m}\right)\left(\frac{1}{f_c}\right)$$

Where C = velocity of light in free space

f_c = clock frequency

The minimum resolvable range displacement, ΔR, is given by

$$\Delta R = R_{m+1} - R_m = \frac{C}{2}\Delta\tau = \frac{C}{2}\left(\frac{1}{2^m f_c}\right)$$

The altimeter range tracker uses a clock frequency of 936,852.5 Hz and a PRF of 228.727 Hz. In addition, with a 16-step phase shifter, the effective sample rate is 14.295 Hz and the range quantization is 10 meters.

It is important to note that range resolution in this system is limited to the transmit pulse width although the change of the leading edge (or centroid) of the return pulse position can be measured to the given quantization values. Furthermore, a portion of the effective detected S/N ratio is sacrificed by the given processing method since each return pulse does not result in a complete range error measurement. In a later analysis the rms range error, μ'_R will be shown to be

$$\mu'_R = \frac{\tau}{2\sqrt{2}}\sqrt{\frac{BN}{s}}\;\frac{1}{\sqrt{2S/N}}$$

where τ is the received pulse width

fs is the sample rate

BN is the effective noise bandwidth of the range track loop

S/N is the signal to noise (power) ratio

Figure 37 is an overall block diagram of the range tracker.

Servo loop analysis.-The loop diagram of Figure 38 was developed from the actual range tracker mechanization. It is important to note that the least significant bit of the range accumulator output produces a one-bit change in the output of the error detector, so that the time discriminator in this system has an effective gain of one. Further, the action of the vernier is such that the effective sample rate of the system is equal to the vernier sweep frequency. That is, for incremental positioning of 2^k steps, the sample rate $fs = f_{PRF}/2^k$ where f_{PRF} is the radar pulse repetition frequency.

Numerical computations are performed at the end of a simple period and are therefore delayed by one unit of time. This factor accounts for the insertion of the transport lag in series with the velocity accumulator output. Through time sharing, the delayed velocity accumulator output is added to the range accumulator output after independent multiplication by the scale factors, a and b. Lead compensation is accomplished by subtraction of the delayed velocity accumulator output after an additional delay and multiplication of the scale factor, b. Note that the scale factor a and b are, respectively, $a = 2^{-m}$ and $b = 2^{-n}$. Here, m and n are integers that represent the number of binary stages in the range accumulator existing ahead of the stage representing the least significant range bit

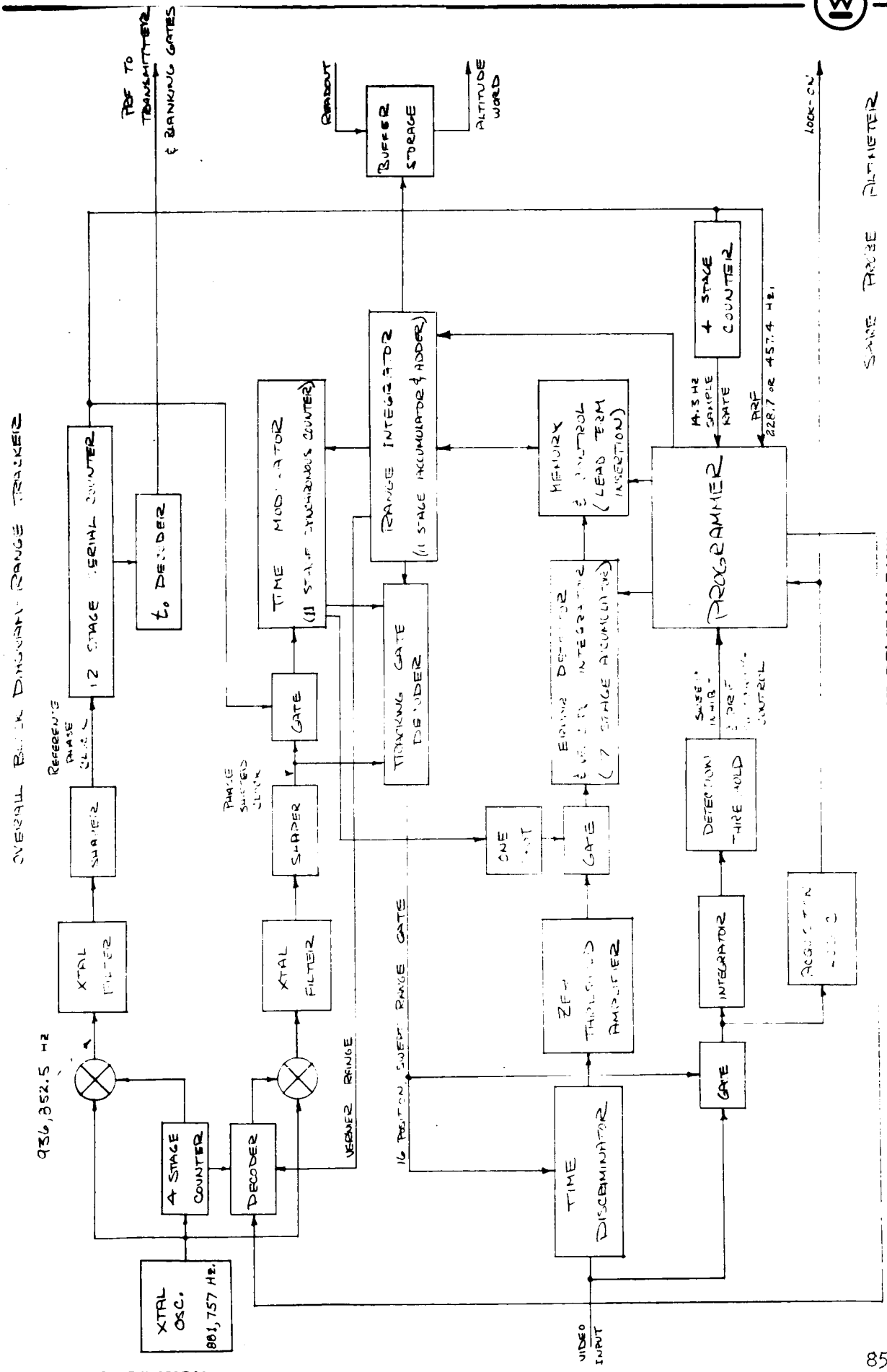

FIGURE 37. - OVERALL BLOCK DIAGRAM RANGE TRACKER

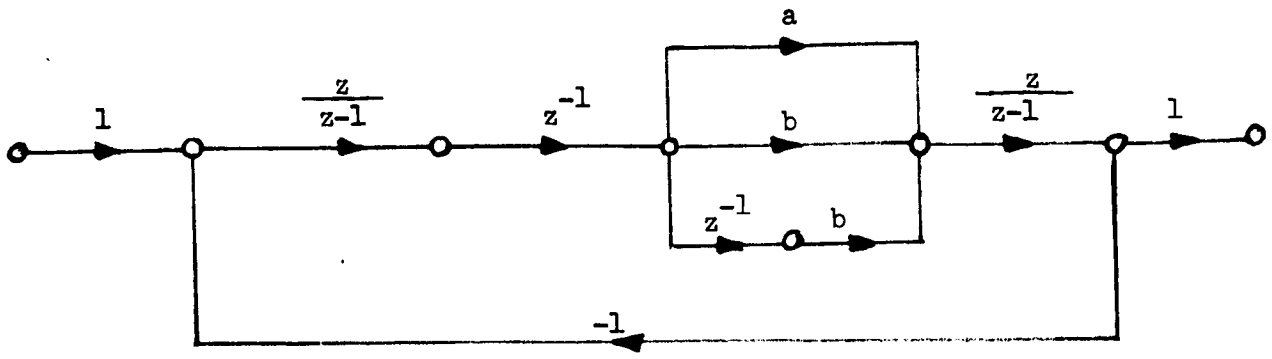

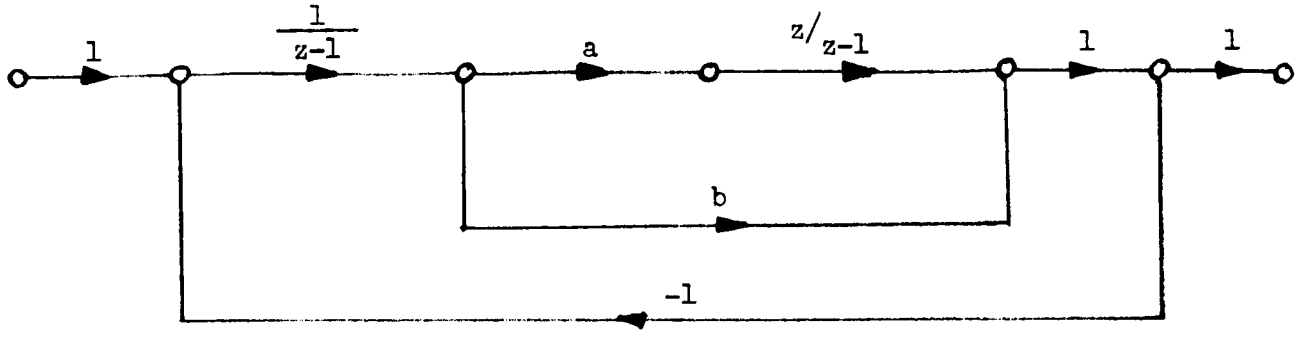

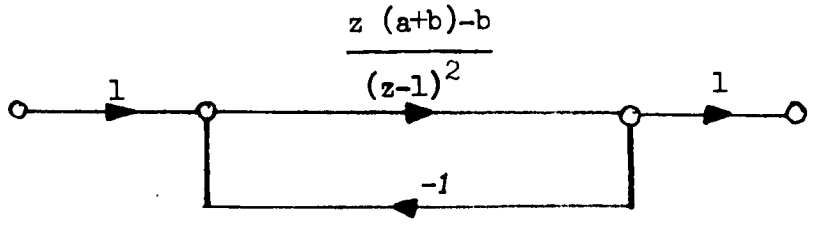

FIGURE 38 - SERVO LOOP DIAGRAM

that are manipulated by a one-bit change in the velocity accumulator output. Noting that the z-transform for an accumulator is given as $A(z)=z/z-1$ as shown in the figure, resultent simplifications of the loop diagram can be performed as in Figure 38.

To permit further analysis through conventional methods, we transform coordinates via the bilinear transformation,

$$z = \frac{1 + W}{1 - W}$$

The open loop transfer function can thus be obtained in terms of the function/G(jv)/wherein we let W=jV and V is a fictitious frequency related to the real frequency W by the relationship $V = \tan \frac{W}{2fs}$. From the loop diagram, the open loop gain G(z) is given by

$$G(z) = \frac{Z(a+b)-b}{(Z-1)^2}$$

from which

$$G(W) = \frac{a}{4W^2} \quad (1-W) \left[1+(1+\frac{2b}{a})\ W\right]$$

$$G(W) = \frac{K(1-W)}{W^2} \left[1+CW\right]$$

where $K = a/4$

and $C = 1+2b/a$

Further, it can be shown that

$$G(jv) = \frac{K\left[1 + CV^2 + j\ (C-1)V\right]}{-V^2}$$

and the open loop phase, $\phi = \tan^{-1}\frac{(C-1)V}{1+CV^2} - \pi$

The closed loop transfer function of the system, H (W), given by

$$H(W) = \frac{G(W)}{1 + G(W)} = \frac{\frac{K}{1-KC}(1-W)\ (1+CW)}{W^2 + \frac{K(C-1)}{1-KC}\ W + \frac{K}{1-KC}}$$

We now apply conventional servo analysis and examine the denominator of this expression. Rewriting we obtain the following characteristic expression,

$$W^2 + 2\zeta W_o W + W_o^2$$

where $W_o = \left(\frac{K}{1-KC}\right)^{\frac{1}{2}}$ = undamped natural resonant frequency of the system

$\mathfrak{J} = \left(\frac{K}{1-KC}\right)^{\frac{1}{2}} \left(\frac{C-1}{2}\right)$ = damping factor

with $m = 2$ and $n = 1$ $(K=1/16,\ C = 5)$

we get $W_o = \frac{1}{3.32}$

and $\mathfrak{J} = 0.603$

The closed loop gain response, $|H(jv)|$ is obtained from H(W) by noting that

$$|H(jv)|^2 = H(W)\, H(-W)\Big|_{W = jv}$$

which in terms of the parameters derived from the characteristic equation is given by

$$|H(jv)|^2 = \frac{W_o^4 (1+V^2)\ 1 + (1 + \frac{2\mathfrak{J}}{W_o})^2 V^2}{(W_o^2 - V^2)^2 + 4\mathfrak{J}^2 W_o^2 V^2}$$

Outputs from the range and velocity accumulators yield quantized target range and range-rate information which is updated at the sample rate fs. Referring to the loop diagram, the closed loop transfer functions (z-domain) for the measurement of range and range rate are, respectively,

$$H_R(z) = \frac{Z(a+b) - b}{Z^2 + Z\,(a+b-2)+1-b}$$

$$H_R^{\bullet}(Z) = \frac{Z-1}{Z^2 + Z\,(a+b-2)+1-b}$$

In addition, the error function,

$$\frac{\mathbf{E}(z)}{Ei(z)} = \frac{1}{1+G(z)}$$

is given by

$$\frac{\mathbf{E}(Z)}{Ei(Z)} = \frac{(Z-1)^2}{Z^2 + \mathbf{Z}\,(a+b-2)+1-b}$$

The input signal to the loop can be represented by

$$Ei(Z) = \frac{RZ}{Z-1} + \frac{\dot{R}}{fs\,(Z-1)^2} + \frac{\ddot{R}Z\,(Z+1)}{2fs^2(Z-1)^3}$$

where R is the quantized range, and the first and second derivatives represent target range rate and acceleration, respectively. Note that $R = \frac{r}{q_R}$ where

$$R \text{ bits} = r \text{ units} \cdot \left(\frac{1}{q_R}\right) \frac{\text{bits}}{\text{unit}}$$

The final value theorem in the Z domain is given by

$$\lim_{n \to \infty} \mathcal{E}(nt) = \lim_{Z \to 1} (Z-1)\,\mathcal{E}(Z)$$

So that

$$\lim_{n \to \infty} \mathcal{E}(nt) = \lim_{Z \to 1} (Z-1)\left[\frac{(Z-1)^2}{Z^2+1\,Z(a+b-2)+1-b} \cdot \frac{Rf_s^2Z(Z-1)^2+\dot{R}f_s(Z-1)+\ddot{R}/2\,Z(Z+1)}{f_s^2(Z-1)^3}\right]$$

$$\lim_{n \to \infty} \mathcal{E}(nT) = \frac{\ddot{R}}{af_s^2}$$

As noted, the final errors for the range and range rate components are zero. The output of the velocity accumulator, $E_{\dot{R}}(Z)$, is given by

$$E_{\dot{R}}(Z) = Ei(Z)H_{\dot{R}}(Z)$$

and, for $Ei(Z) = \frac{\dot{R}}{f_s(Z-1)^2}$, application of the final value theorem yields

$$\lim_{n \to \infty} E_{\dot{R}}(nT) = \frac{\dot{R}}{af_s}$$

From the above, the quantization in range rate, $q_{\dot{R}}$, is thus given by

$$q_{\dot{R}} = af_s q_r$$

Estimation of rms error.-With approximate representative models of the actual processor we can estimate range and range rate errors due to noise. In addition, calculations are based on input signals which exhibit large input S/N ratios and for a vernier which produces a large number of sample values in the control loop sample time.

Under the above assumptions, the probability density function of the time discriminator output signal can be represented by

$$P(x) = \frac{1}{\sqrt{2\pi}\,\sigma} \exp\left[-\left(\frac{x-S_n}{\sqrt{2}\,\sigma}\right)^2\right]$$

where σ^2 = variance of the input noise

S_n = average time discriminator output signal measured in the n^{th} sweep interval

S_n is a function of the relative positions of tracking gate and video return pulse centroids. During tracking the tracking gate is linearly swept in discrete steps about the video return. Therefore S_n is proportional to the peak value of the input video, the relative displacment of the tracking gate from the zero position, and the slope of the discrimator. That is

$$S_n = n \frac{\Delta\tau}{\tau/2} S_o$$

where

S_o = peak input signal

τ = pulse width

$\Delta\tau$ = differential gate position in each sweep interval

n = the sweep interval number; n is an integer; $-M/2$, $-(M/2)+1$, ... 0, ... $M/2$

where M is the total number of sweep intervals in the control loop sample interval

Since $M\,\Delta\tau = \tau_o$ where τ_o is the sweep range,

$$S_n = S_o \frac{\tau_o}{\tau} \frac{2n}{M}$$

Further, let $k_o = \dfrac{2S_o \dfrac{\tau_o}{\tau}}{\sqrt{2}\,m\sigma} = \dfrac{\sqrt{2}}{M}\left(\dfrac{\tau_o}{\tau}\right)(2S/N)^{\frac{1}{2}}$

Where S/N = input signal-to-noise ratio = $\dfrac{S_o^2}{2\sigma^2}$

The time discriminator output signal is coupled to a zero threshold comparator with a characteristic

$$e_o(x) = \begin{cases} 1, & x \geq 0 \\ 0, & x < 0 \end{cases}$$

With the binary threshold circuit employed, the cumulative error is produced by various combinations of individual error probabilities arising from the false interpretation of the discriminator output at a particular tracking gate position. For example, for $S_n>0$, $e_o(x)$ should be 1, so that the probability of exceeding the zero threshold, P_s^+, is given by

$$P_s^+ = \text{probability } (0 \leq x \leq \infty) = \int_0^\infty P(x)\,dx = \frac{1}{\sqrt{2\pi}\,\sigma} \int_0^\infty e^{-\left(\frac{x}{\sqrt{2}\,\sigma} - k_o n\right)^2} dx$$

$$\text{If } u = \frac{\frac{x}{\sqrt{2}\,\sigma} - K_o n}{k_o} \quad \text{then}$$

$$Ps^+ = \frac{ko}{\sqrt{\pi}} \int_{-n}^{\infty} e^{-k_o^2 u^2}\,du$$

Similarly, $S_n < 0$,

$$Ps^- = \int_{-\infty}^{0} P(x)dx = \frac{k_o}{\sqrt{\pi}} \int_{-\infty}^{n} e^{-ko^2 u^2}\,du$$

The error probability distribution, P_ε, is simply $1-P_s$. Thus the error probability density for $S_n > 0$, is

$$P_\varepsilon(n) = \frac{dP_\varepsilon}{dn}\left(1 - \frac{k_o}{\sqrt{\pi}} \int_{-n}^{\infty} e^{-k_o^2 n^2}\,du\right) = \frac{k_o}{\sqrt{\pi}}\, e^{-k_o^2 n^2}$$

The density function for $S_n < 0$ is identical, so that a cumulative probability density function representing the total error can be given by

$$P_\varepsilon(n) = \frac{2k_o}{\sqrt{\pi}} \exp\left(-4k_o^2\,|n|^2\right)$$

$$\mu^2 = \int_{-\infty}^{\infty} n^2\, P_\varepsilon(n)dn = \frac{1}{8K^2_0} = \text{variance of quantized input noise to tracker}$$

The equivalent noise factors at the range and range rate outputs of the tracker can be determined from the following:

For $\Phi(z) = \overline{\mu^2}$ it can be shown that since

$$\overline{\mu_o^2} = \frac{1}{2\pi j} \int_\Gamma H(z)\, H(z^{-1})\, z^{-1}\, \Phi(z)\, dz$$

$$I_2 = \frac{\overline{\mu_o^2}}{\overline{\mu^2}} = \frac{1}{2\pi j}\int_{\Gamma} H(z)\, H(z^{-1})\, Z^{-1}\, dz$$

where Γ is the unit circle

As stated previously,

$$H_R(z) = \frac{z(a+b) - b}{z^2 + z(a+b-2) + 1 - b} \quad \text{range}$$

$$\dot{H}_R(z) = \frac{z-1}{z^2 + z(a+b-2) + 1 - b} \quad \text{range rate}$$

Solutions of the contour integrals yield

$$I_{2R} = \frac{b + a/b + a/2}{2 - b - a/2}$$

and

$$I_{2\dot{R}} = \frac{1}{b\left(2 - b - a/2\right)}$$

so that

$$\mu_R' = \left(\frac{b+a/b+a/2}{2-b-a/2}\right)^{\frac{1}{2}} \left(\frac{M}{4}\right)\left(\frac{\tau}{\tau_o}\right) \frac{qR}{\sqrt{2\ S/N}} \quad \text{range units rms}$$

$$\mu_{\dot{R}}' = \left[\frac{1}{b\ (2-b-a/2)}\right]^{\frac{1}{2}} \left(\frac{M}{4}\right)\left(\frac{\tau}{\tau_o}\right) \frac{\dot{qR}}{\sqrt{2\ S/N}} \quad \text{range rate units rms}$$

Define B_N as the effective noise bandwidth of the range track loop where

$$B_N = \left(\frac{b+a/b+a/2}{2-b-a/2}\right) \frac{fs}{2}$$

fs = sample rate

Also, noting that $q_{\dot{R}} = a\ f_s\ q_R$ and $M\ q_R = \tau_o$, let $\frac{a}{b(b+a/b+a/2)} = \alpha^2$

so that

$$\mu_R' = \frac{\tau}{2\sqrt{2}\sqrt{2\ S/N}}\sqrt{\frac{B_N}{f_s}}$$

and $$\mu_R^{\cdot} = \frac{\alpha\tau}{2\sqrt{2}\sqrt{2\ S/N}}\sqrt{B_N f_s}$$

Now apply the appropriate parameter values for the maximum altitude case, i.e.,

$$\tau = 1.067\ \mu s$$

$$S/N = 2.2\ dB$$

$$f_s = 14.295\ Hz$$

and $$B_N = \left(\frac{b+a/b+a/2}{2-b-a/2}\right)\left(\frac{f_s}{2}\right)$$

where $a = (\frac{1}{2})^2$

and $b = \frac{1}{2}$

The one-sigma noise error is calculated to be approximately 21.1 meters. Thus, the 3σ noise error is $\pm$ 63.3 meters or $\pm$ 0.41%. Since altitude error is proportional to the reciprocal of the square root of the S/N, and since S/N is proportional to the reciprocal of altitude squared (beamwidth limited), percent error will be roughly independent of altitude.

Electronics package.-The range tracker constitutes the bulk of the electronics package. Also included is the AGC and signal conditioning circuitry for antenna beam steering. There are 260 integrated circuit chips and 175 conventional components in the package.

The integrated circuit chips will be packaged, in functional groupings of approximately 25 chips, into flat boxes as shown in the detail in Figure 39. This box is 1" by 1 1/8" by 0.070" high, and is made of ceramic. The interconnection between the chips within the boxes is deposited on the surface of the ceramic base of the box. The chips are connected to the interconnecting circuitry by small gold wires thermo-compression bonded at each end. This is the method presently used to connect transistors and integrated circuits into cans or flat packs. The outputs from the flat boxes are deposited strips (on 25-mil centers) which pass under the wall of the box. A metal lid completely hermetically seals the assembly. Twelve of these boxes will be required for the unit.

The connectional components, plus about 15 integrated circuits in flat pack form, will be made into cordwood modules. Eight modules 1.35" x 1.2"

SIZE: 2.0 x 3.2 x 5.0 in.
WEIGHT: 1.2 lb.
POWER: 5.3 watt

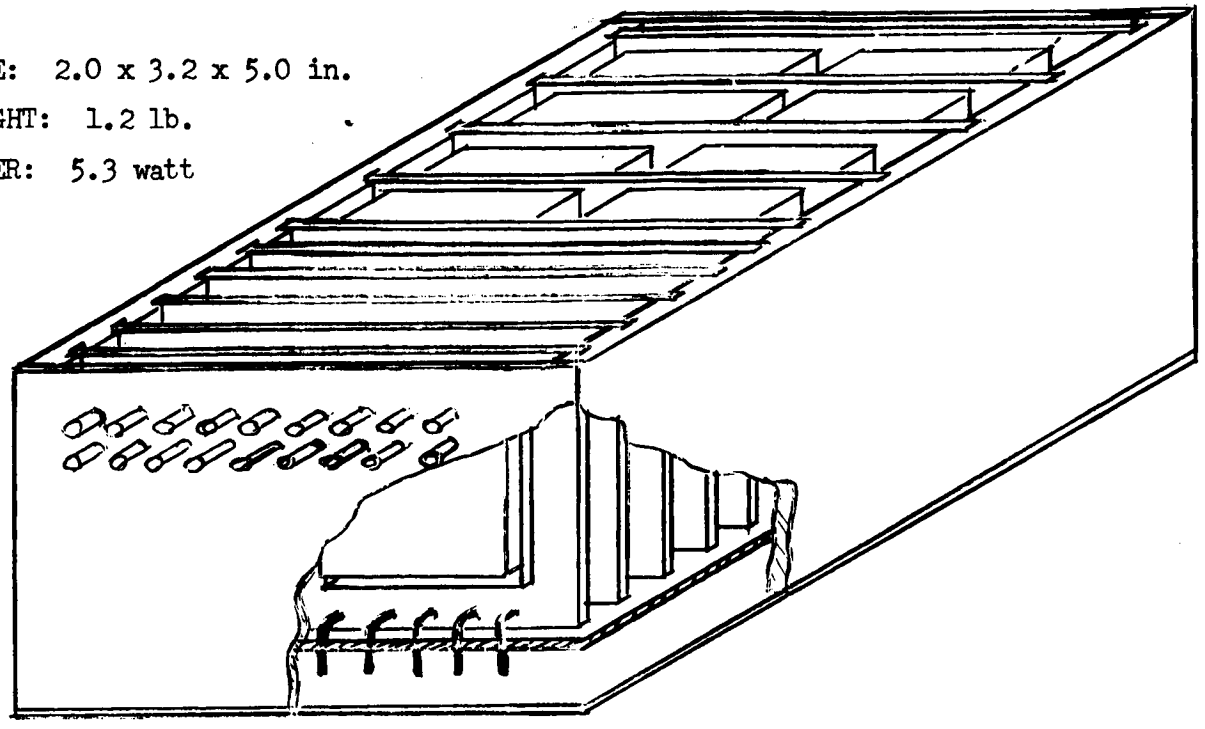

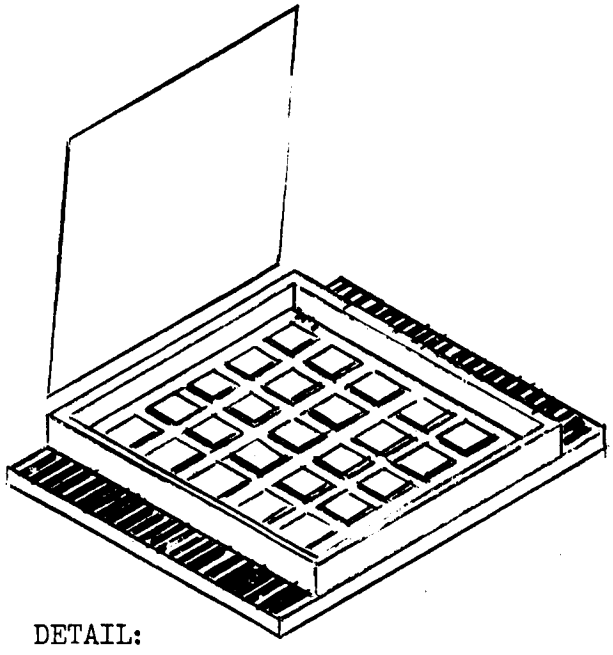

DETAIL:
INTEGRATED CIRCUIT BOX

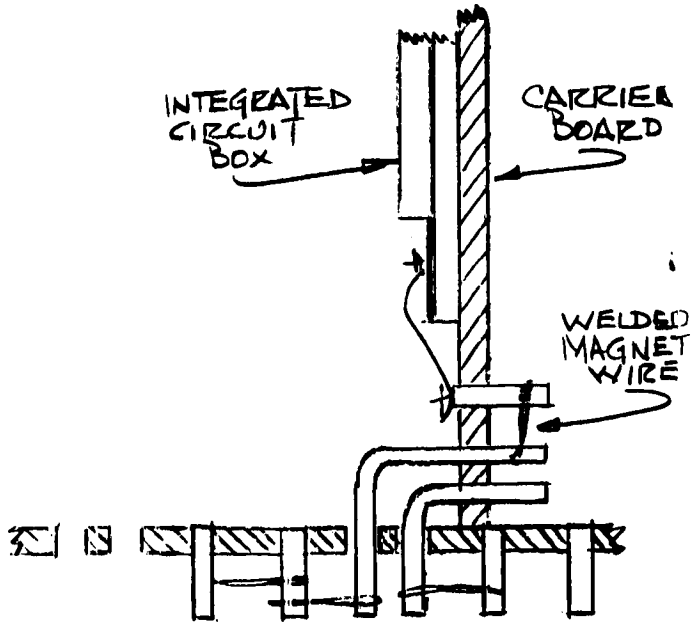

DETAIL:
INTERCONNECTION

FIGURE 39 - ELECTRONICS PACKAGE APPEARANCE

x 0.75" will be needed to contain these components.

The ceramic chip boxes are mounted onto carrier boards made of silicone fiber glass material. Two boxes are put in each carrier board, so six boards 3.20" x 1.67" are required. The cordwood modules mount on the same type of carrier boards; four boards are required here. The total of 10 carrier boards mount into a metallic case as shown, a camming arrangement securely clamping the boards.

The detail of Figure 39 shows the inter-connection between the boxes or modules on the boards and connections between the 10 carrier boards and the output pins. Through-pins are provided on the boards, one pin for each ceramic box output; connections are made from box to board pins by welding with small ribbons. Inter-connections between boxes, and to the right-angle output pins, are made by welding with insulated magnet wire. With this technique crossovers can be made as required without the fear of shorting since each wire is completely insulated.

Interconnection between carrier boards is made on the other side of the motherboard with the same technique. Here, pins are placed in a grid pattern with one pin for each bent pin from a carrier board. The actual interconnection is made between the fixed pins on the mother-board and the tie to the carrier board using a single wire bridge. With this system the mother-board can be built beforehand and tested for correctness. Then, after the carrier boards are installed, they are easily removed by cutting the wire bridge to each bent pin. Outputs from the completed package consist of solder lugs near the top at one end, and a coax connector near the bottom at the same end.

Power Supply

The power supply accepts prime power at a nominal 28 volts and provides regulated voltages for altimeter subassemblies. As shown in the block diagram of Figure 40, the inverter generates a signal synchronized to a multiple of the PRF (2927.4 Hz). This sync minimizes the effect of ripple on the power supply lines. The inverter signal is then amplified to a usable level by power transistors.

The regulator is a series type between the 28 volt input and the inverter amplifier. Regulation is achieved by comparing with a reference voltage an error signal from a separate winding on the power transformer. By using this type of sensing element, load variations on one supply will not be reflected as corrections in the entire supply.

The regulated signal feeds the primary of the main power transformer, the secondaries providing the system voltages which are rectified and filtered.

Figure 41 illustrates the power supply packaging. Transformers, power transitors, and other components are mounted on a heat sink base. After assembly and test, the unit is potted for mechanical integrity. Outputs are through solder lugs at one end.

Description of the Overall Package

The basic building block for the overall radar altimeter package is the heat-sink base structure sketched in Figure 42(a). The base consists of an aluminum angle plate forming the lower deck and a hinged panel which forms the upper deck. Threaded inserts in the lower plate permit securing the assembled unit into the spacecraft interface mounting surface. For economy in volume utilization, the unit is designed so the mounting bolts go through the spacecraft pad and screw into the altimeter base.

As shown in Figure 42(b), four of the subunits mount on the lower deck. They are the electronics package, master oscillator, HVPS/modulator, and TWT. These items represent over 60% of the power dissipation from the package and are so mounted as to give the best thermal path. In addition, this mounting position for the TWT on the heavier lower plate ensures that it will not flex and thereby degrade performance.

The rest of the subunits mount onto the hinged upper deck as shown in Figure 43. This deck rests upon the top surfaces of the electronics package and the HVPS/modulator. The whole assembly bolts together to form a unified package for minimum volume, good thermal paths, and a high level of mechanical integrity. Since each sub-assembly is designed to be resistive to harsh environments, the total assembly does not require a case or cover. Short and secure cable runs, unified construction, and the protected location of the altimeter within the spacecraft body are further indications that a cover is an unnecessary expense in weight and volume.

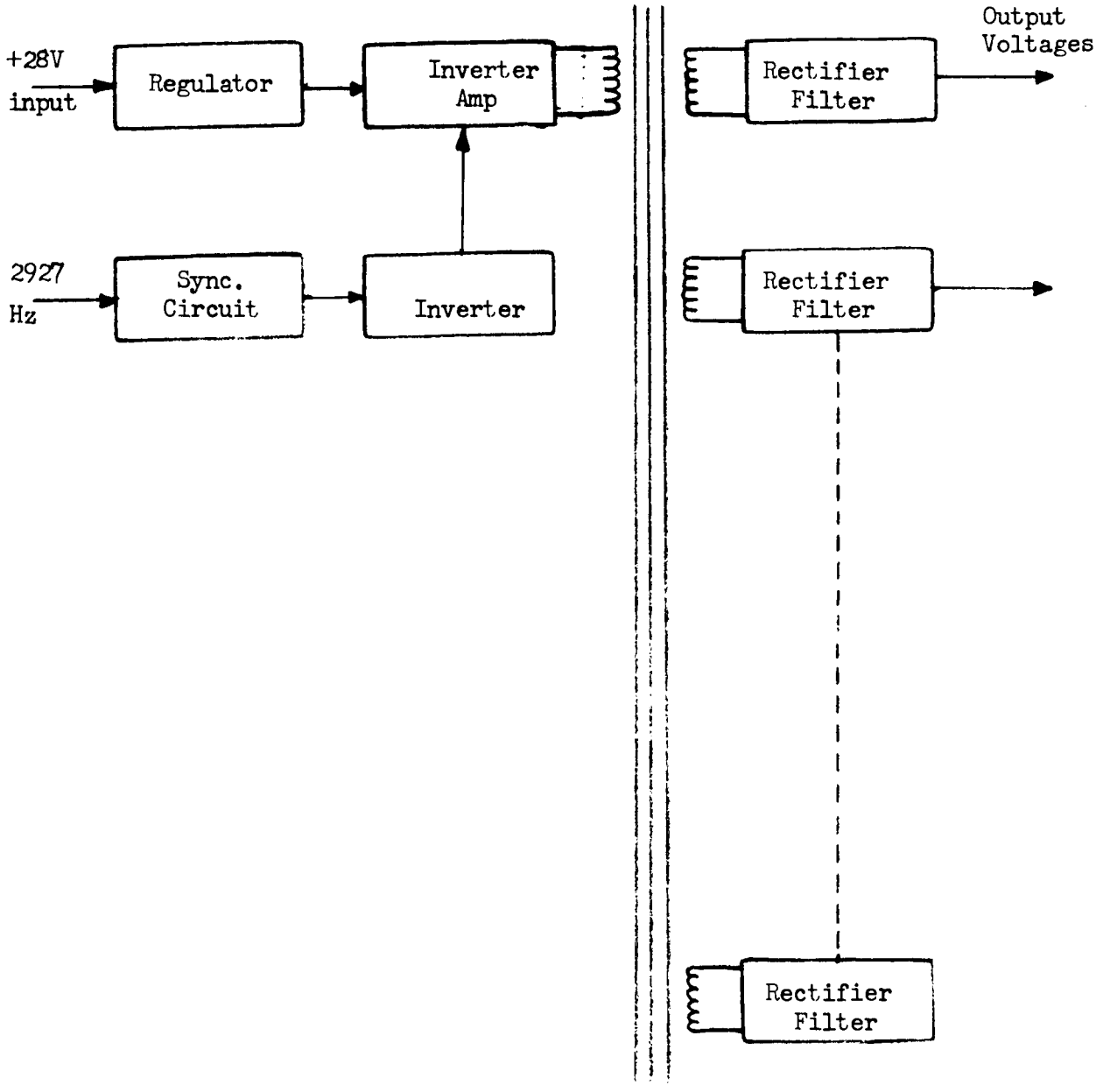

FIGURE 40 - POWER SUPPLY BLOCK DIAGRAM

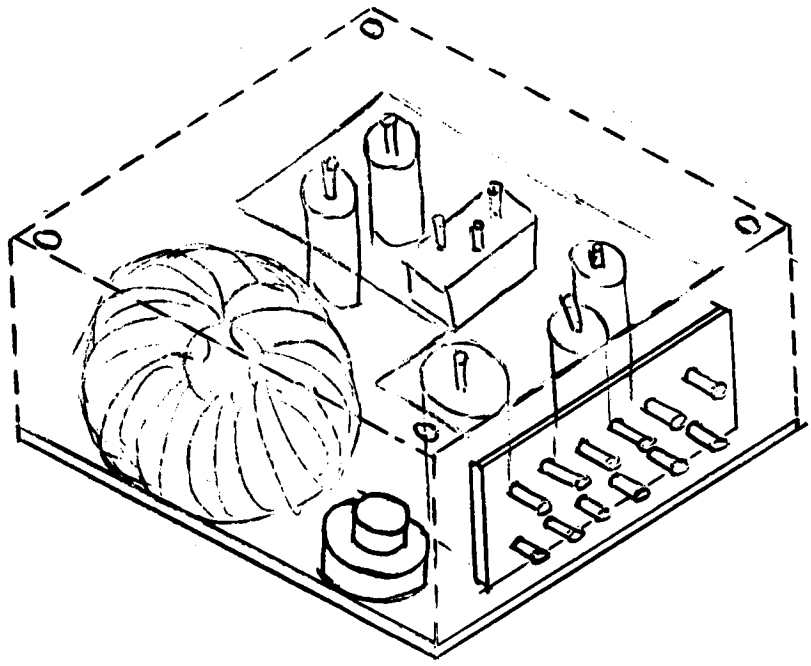

SIZE: 4.5 x 4.4 x 1.5
WEIGHT: 1.3 lb
POWER: 5.2 watt

FIGURE 41 _ POWER SUPPLY APPEARANCE

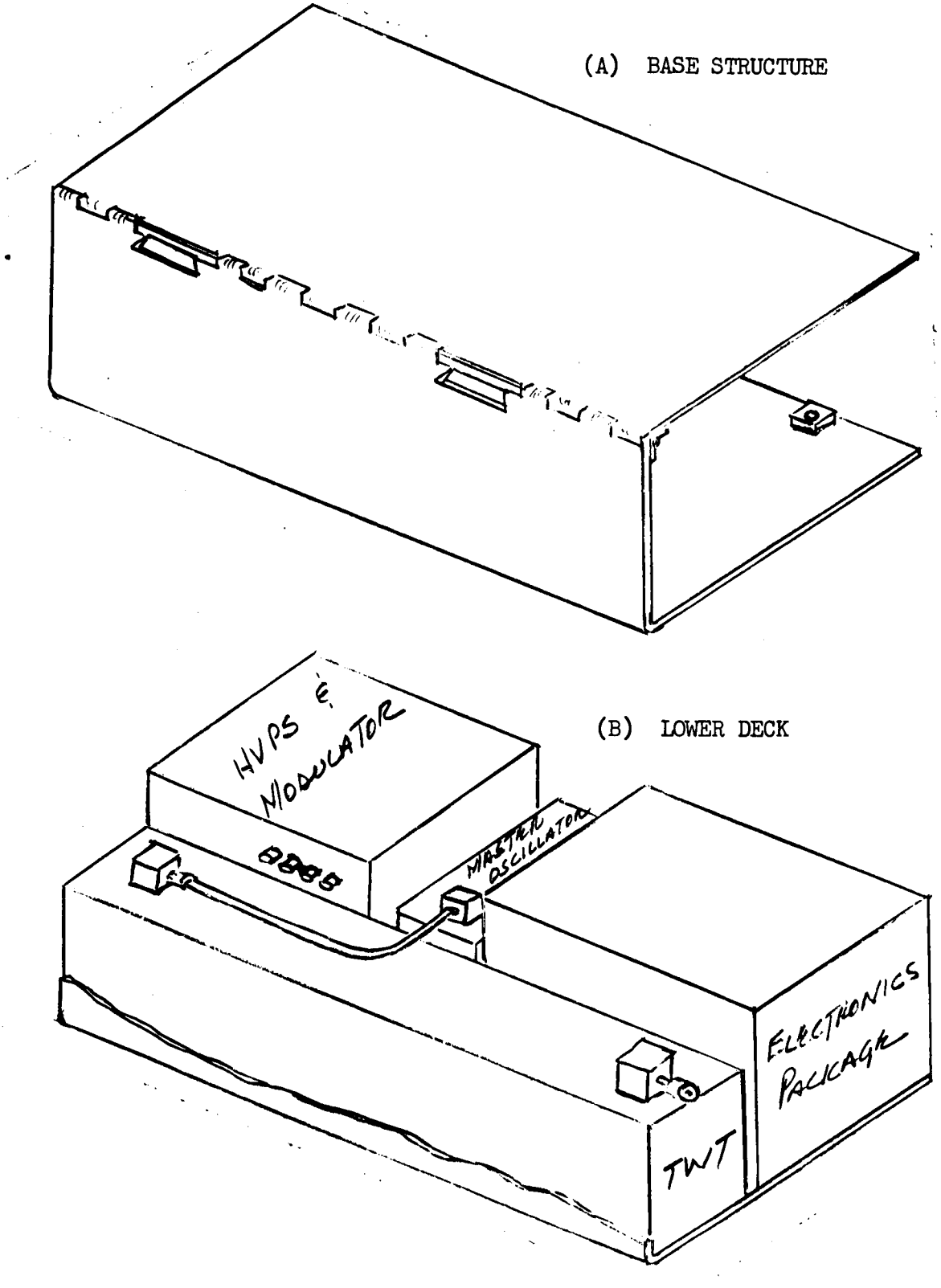

FIGURE 42 - OVERALL PACKAGE APPEARANCE

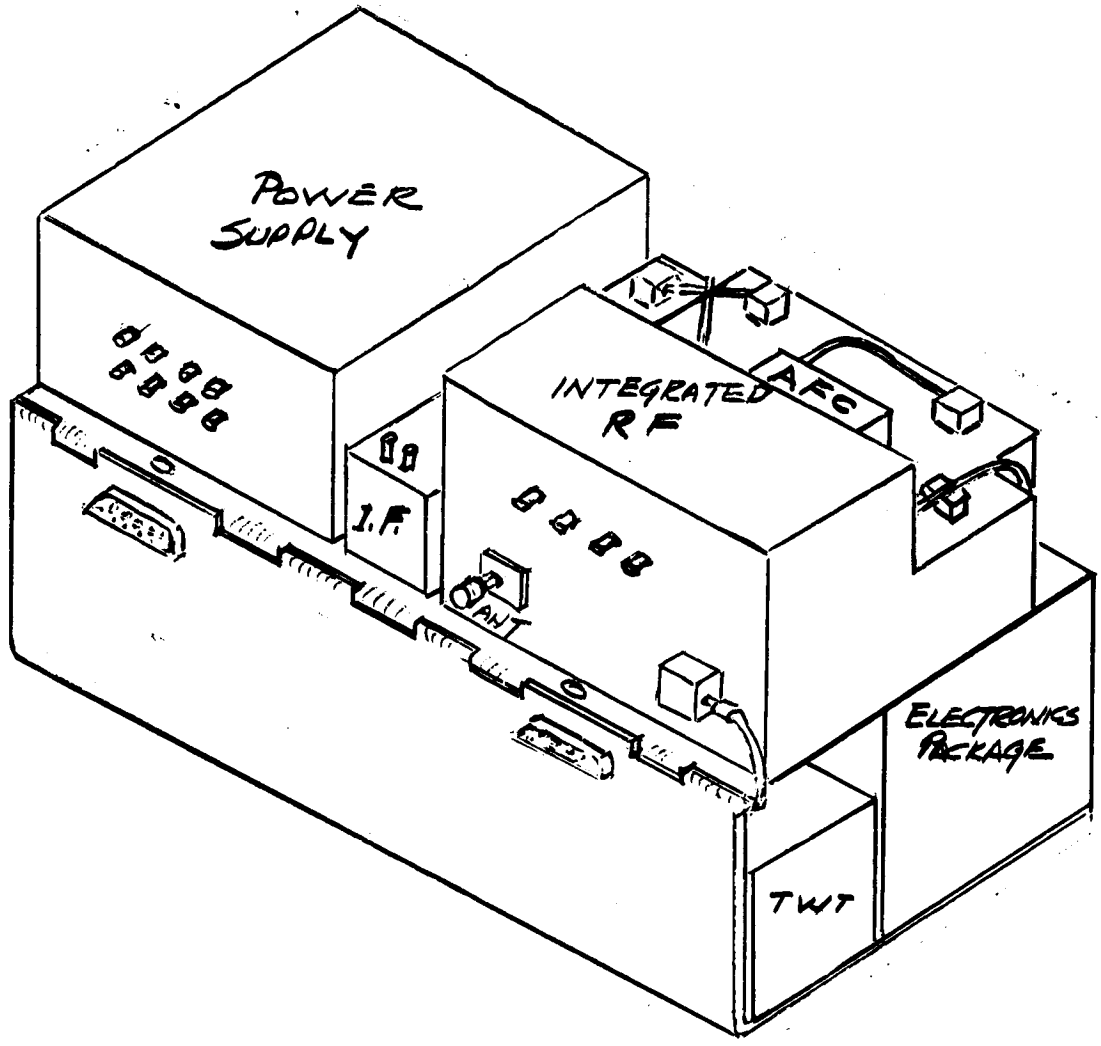

Total altimeter electronics (antenna not included)

Size: 11 X 5.38 X 4.09
Volume: 238 cu in
Weight: 10.5 lb
Power: 18.6 watt

Total, altimeter electronics plus antenna

Volume: 474 cu in
Weight: 13.88 lb
Power: 20.6 watt

FIGURE 43.- UPPER DECK COMPONENTS

Two multipin connectors are on the front face of the altimeter. One forms the electrical interface with the spacecraft, and the other the interface with the altimeter antenna. A coaxial connector on the front surface of the RF unit provides the high-frequency link to the antenna. The subassembly will perform satisfactorily with up to 3 feet separation between the altimeter electronics and the antenna.

The layout of the assembly provides a convenient space or channel just below the lower deck (over the TWT and master oscillator) for the routing of cabling between the subassemblies. Wires which connect to solder lugs on the top-deck items have very short runs to grommets through the deck to the wiring cables. Since the top deck hinges, the wiring between decks is arranged so that the cable bundle twists instead of bends when the assembly is opened. This arrangement also eliminates the need for service loops in the wiring to the subassemblies. To hinge back the top deck it is necessary to disconnect only two coax connectors, one to the TWT and one to the electronic package. Both of these are readily accessable.

Figures 44, 45 and 46 are photographs of a mock-up of the radar electronics and a sketch of the antenna.

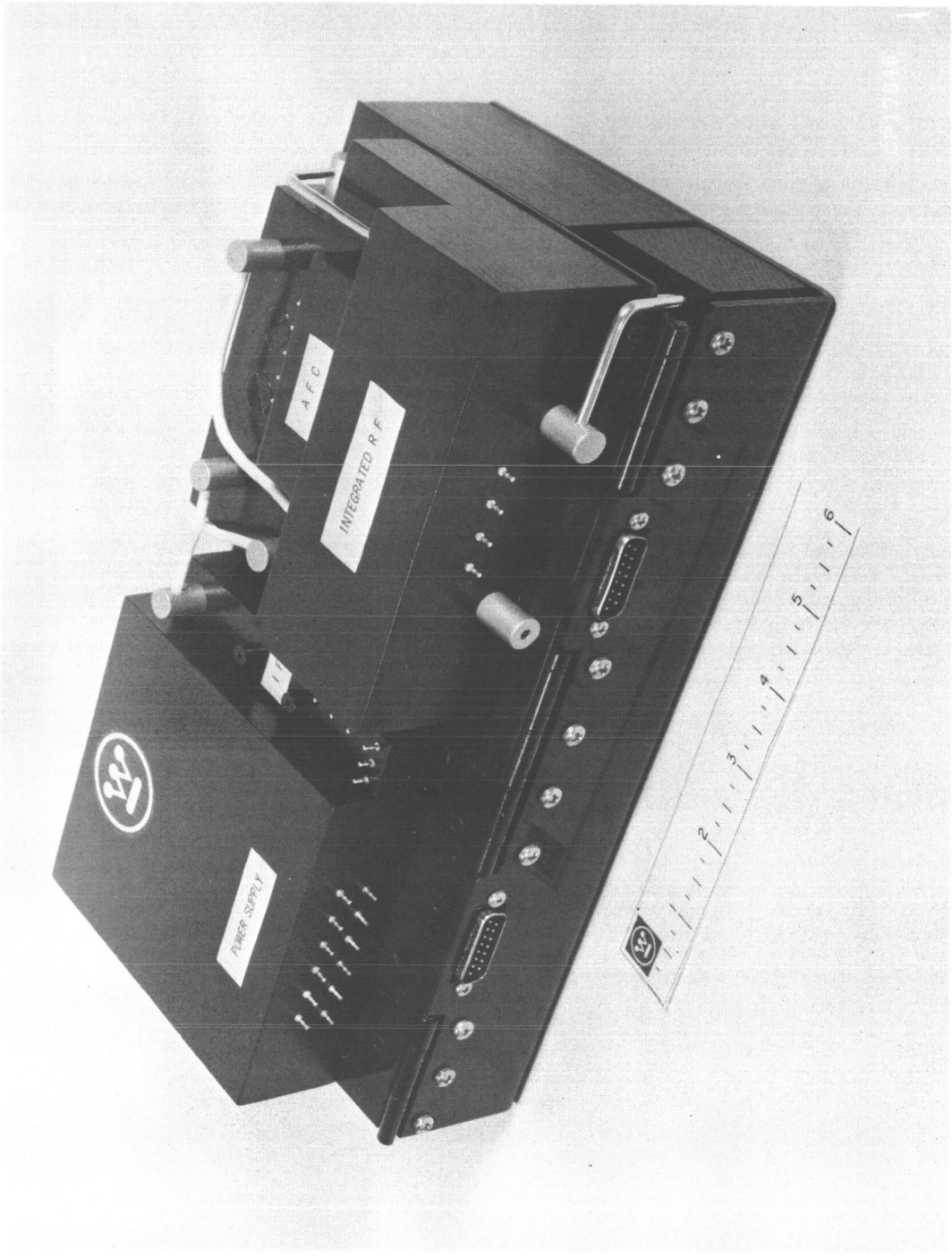

FIGURE 44.- MOCK-UP PHOTOGRAPH, UPPER DECK

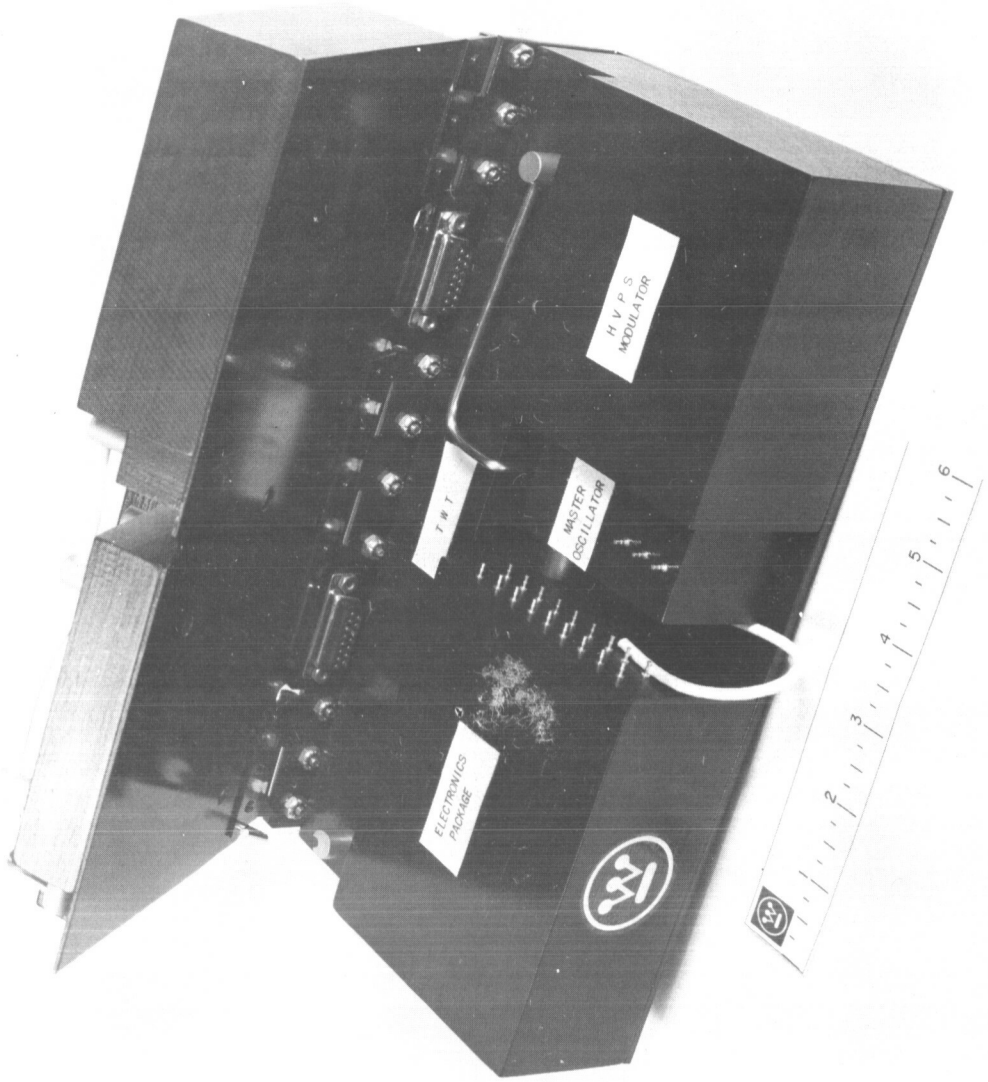

FIGURE 45.- MOCK-UP PHOTOGRAPH, LOWER DECK

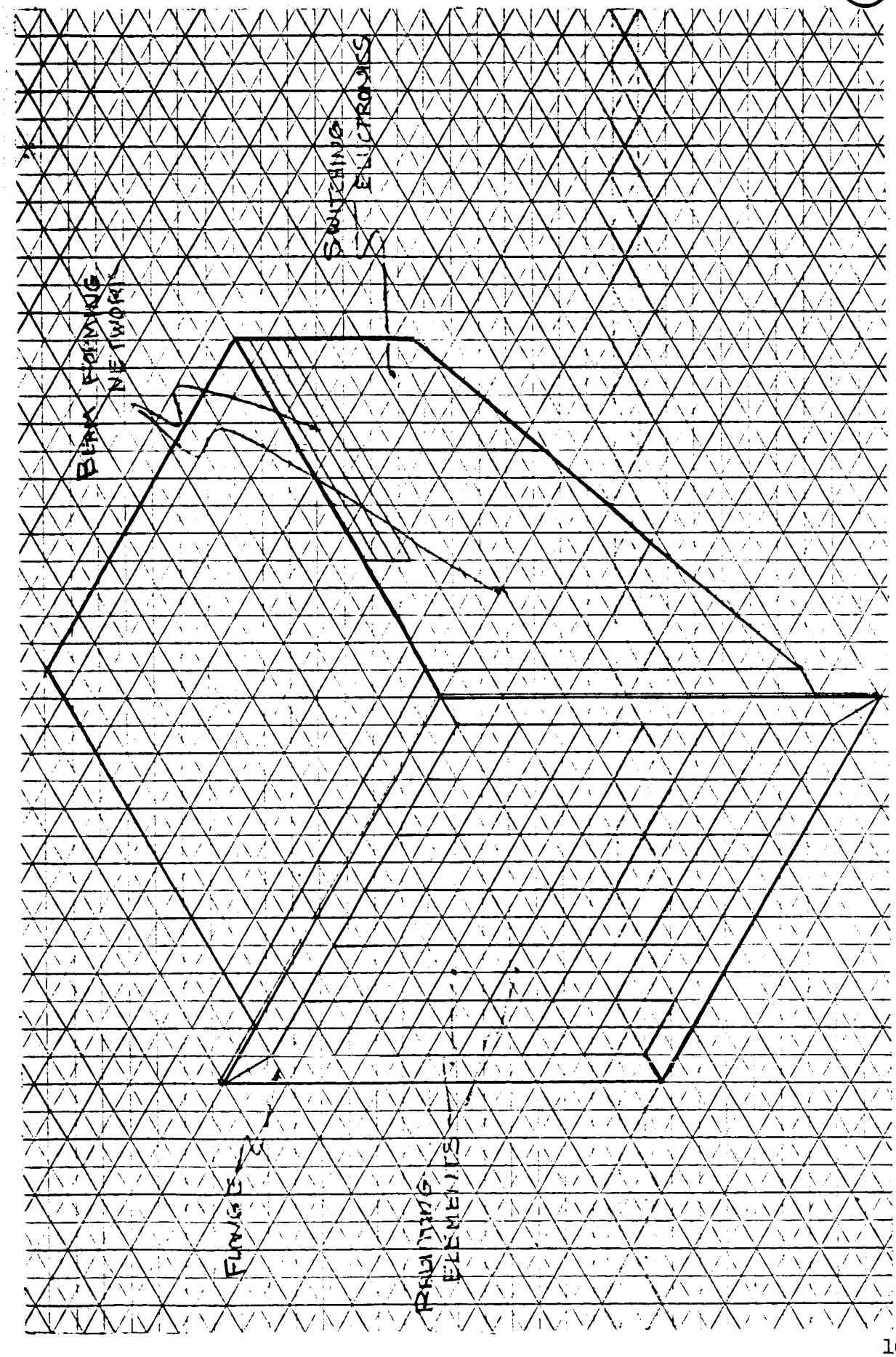

FIGURE 46.- ANTENNA APPEARANCE

Size, Weight, and Power

The weight, volume, and power of the various sub-units and of the overall subsystem are shown in Table A-1. The complete subsystem (including antenna) occupies 474 cubic inches, weighs 13.9 pounds, and dissipates 20.6 watts of power. Detailed weight calculations are given in Appendix C.

The calculations of centers of gravity and moments of inertia are given in Appendix D and are summarized below:

Altimeter Electronics -

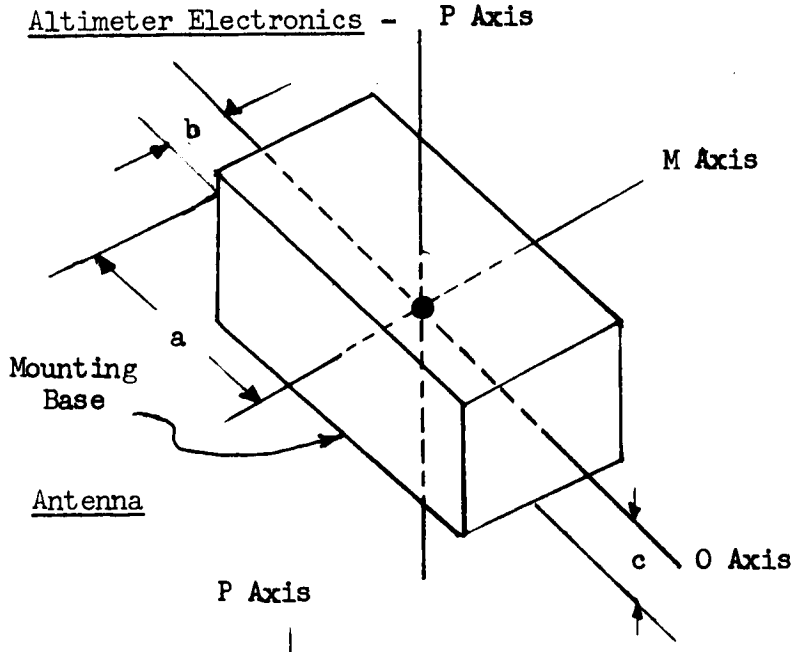

CG Location:

a = 5.45 in
b = 2.49 in
c = 1.66 in

Moment of Inertia

I_o = 38.3 lb-in^2
I^o = 120.0 lb-in^2
I^m_p = 131.0 lb-in^2

Antenna

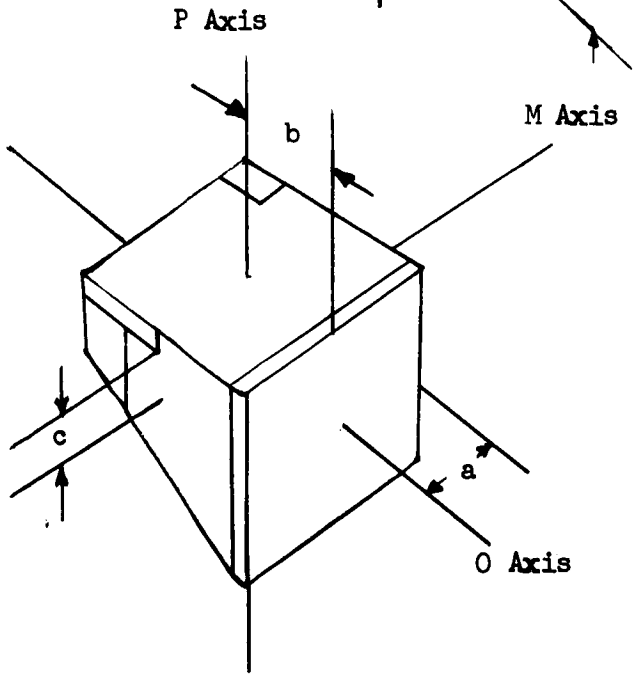

CG Location

a = 3.00 in
b = 3.26 in
c = 2.41 in

Moment of Inertia

I_m = 18.6 lb-in^2
I^m = 17.4 lb-in^2
I^o_p = 22.0 lb-in^2

TABLE VII

VOLUME, WEIGHT, AND POWER DISSIPATION

ITEM	SIZE in	VOLUME in^3	WT lb	POWER watts
IF Strip	0.75 x 0.75 x 4.25	2.4	0.25	0.40
Integrated RF	{0.9 x 5.25 x 4.75 / 1.0 x 5.25 x 2.8}	32.9	2.00	2.00
Power Supply	1.5 x 4.4 x 4.5	30.0	1.30	5.20
AFC	2.6 x 1.3 x 0.75	2.5	0.14	0.30
Master Oscillator	1.5 x 1.5 x 2.0	4.5	0.15	2.00
TWT	1.4 x 1.5 x 11	23.0	2.50	2.90
HVPS, Modulator	3.5 x 4.0 x 2.0	28.0	1.75	0.52
Electronics Package	3.2 x 5.2 x 2.0	32.5	1.20	5.30
Structure	-----	--	1.20	--
Antenna	-----	236	3.35	2.0

Total Altimeter Electronics (Antenna Not Included)
Size = 5.3 x 4.1 x 11
Volume = 238 in^3
Weight = 10.53 lb
Power = 18.6 watts

Total, Altimeter Electronics Plus Antenna
Volume = 474 in^3
Weight = 13.88 lb
Power = 20.5 watts

Thermal Considerations

Objective.-The basic objective of a thermal design is to provide thermal compatibility between equipment and its environment consistent with a high probability of success. This entails a dual endeavor in, first, controlling or at least understanding the thermal environment; and, second, after providing the best design possible, recognizing the limitations of the design to operate in that environment.

An active thermal control system appears necessary to maintain the spacecraft temperature within normal operational limits during transit from Earth to Mars, or to some more distant planet. The altimeter itself, enclosed within the spacecraft envelope, will depend upon passive means to keep component temperatures within reliable limits. The altimeter thermal design and analysis is discussed in more detail below.

Design concept.-The altimeter is designed so that the angle plate is the heat-sink base and forms the interface with the spacecraft; 60% of the heat generated is located on this level. The other sub-units mount upon the upper deck which in turn rests upon and is tightly coupled thermally to the top surface of the modulator and the electronics package. This produces a compact package with good conductive coupling between all dissipating elements and the heat-sink base.

All components and materials are to be selected from approved lists or will be tested to ensure compatibility with the 145°C sterilization temperature. This is of course a non-operating temperature, and is assumed to be the maximum non-operating temperature that will be experienced during the mission. Under operating conditions, a very conservative limiting range of -20°C to +75°C has been assigned to all conventional components to give maximum reliability. Integrated circuit chips, by their nature and construction, can of course operate at a higher temperature with no degradation.

The total power dissipation of the altimeter electronics is 18.7 watts. This gives a density of 0.078 watts/in^3 and a distribution of 31.8 watts/in^2 at the thermal interface with the spacecraft.

Thermal analysis.-A thermal analysis helped develop a basic appreciation for the thermal stability of the altimeter package. This analysis covered its operational characteristic under both transient conditions (typical of a short 30-minute operation) and under steady state conditions (typical of a mission of longer operation).

Transient operation.-For short duration operation of an hour or less, the transient analysis is important. The conservative approach taken assumes complete isolation of the altimeter electronics from the rest of the spacecraft. That is, it assumes that all the heat generated in the altimeter is absorbed by the altimeter in the form of a temperature rise. This analysis is detailed in Appendix E. From this analysis, the altimeter electronics

dissipating 18.6 watts, weighing 10.5 pounds, and operating for 1/2 hour would experience a temperature rise of only 15°F. A breakdown showing the condition of the various sub-units is given in Table VIII.

Of course the actual module temperature increases will be lower than those shown since increased mass from the connectors, wire, and structure is not included. In addition, the thermal design intimately connects the heat sources to the heat sink. A close thermal tie of this heat sink to the spacecraft will further decrease the altimeter temperature rise during operation.

Equilibrium operation.-For longer duration missions and periods of intensive testing, an equilibrium analysis is necessary. To be completely accurate this analysis should encompass the entire spacecraft thermal environment with its heat sources, heat sinks, and heat flow paths. Resultant equipment temperatures will be highly dependent on the spacecraft temperature control system. However, since these parameters are not all known at this time, the best approach is to assume conductive transfer and to establish the maximum temperature drop between components and the thermal interface with the spacecraft.

For this analysis Appendix F examined a potentially hot component on each level of the assembly. The first of these was an integrated circuit chip mounted in the ceramic box in the electronics package subassembly on the lower level. A 20-mW chip mounted here gives a temperature rise of 6°C between chip surface and box mounting surface, and there is a 15°C rise from box to altimeter base. Therefore there is a total rise of 21°C from thermal interface to chip surface. For the top deck there was an analysis of a 1/2-watt resistor potted in foam in the power supply. This was considered the worst thermal condition in this level. A total rise of 18°C above heat sink interface was determined for this case.

This means that in order to maintain the components at a maximum operating temperature of 75°C, which as noted earlier is a very conservative value, the spacecraft heat sink mount must be maintained at a maximum temperature of 55°C. This analysis is considered to be a worst case condition since the effects of convection or radiation have been neglected and would most certainly help to reduce the thermal gradients. This heat sink temperature requirement is a very reasonable one, and should not be difficult to maintain with standard thermal control procedures.

Magnetic Cleanliness

It is assumed that the space probe will fly a magnetometer; present indications are that field level measurements in the region of 0.25 gamma will be desired. To achieve this level will require a magnetrically clean spacecraft, and the altimeter is designed to have minimum stray field interference with the magnetometer.

TABLE VIII - THERMAL CONSIDERATIONS

TRANSIENT ANALYSIS

Item	Power Dissipation Watt	Weight lb	Temperature Increase After ½ hr Operation °F
IF Strip	0.40	0.25	12.6
Power Supply	5.20	1.30	28.0
AFC	0.30	0.14	13.4
TWT	2.90	2.50	10.0
Master Oscillator	2.00	0.15	113.0 *
RF unit	2.00	2.00	8.5
HVPS & Modulator	0.52	1.75	2.5
Electronics Package	5.30	1.20	37.6
TOTAL PACKAGE	18.60	10.50	15.0

* This item coupled directly to heat sink.

STEADY STATE ANALYSIS

Look at a hot spot on each deck.

Item	Temperature Rise Above Heat Sink, °C
20 mW integrated circuit chip	21
1/2 W resistor	18

Conclusion: Temperature rise = 20°C. Therefore, for maximum component temperature of 75°C, keep heat sink temperature = 75-20 = 55°C.

Requirements.-Nonmagnetic materials are used wherever possible. The structure is fabricated from aluminum and the hardware is nonmagnetic stainless steel. Electrostatic shielding cases are aluminum or brass. As far as is practical, component leads are nonmagnetic. Due to hermetic sealing problems this is not always possible on items such as transistors and integrated circuit flat packs. In these cases the shortest possible lead length is used. Interconnecting wiring is copper and cordwood modules use nonmagnetic alloy 180 for welding ribbon and output pins. The magnet wire interconnects in the electronics package is also alloy 180.

Certain of the components such as the TWT and the integrated RF depend on permanent magnets for their operation. Since these leakage fields cannot be eliminated they must be shielded against or reduced by compensation. We recommend compensation since it is much simpler from a standpoint of fabrication and structural mounting and will occupy less volume. This is best illustrated by examining the TWT, which has by far the highest residual field in the altimeter.

TWT field attenuation.-The maximum external field of the TWT is quoted to be 4 gauss at a distance of 3 feet from the tube. Using this value, it is possible to calculate the field strength at other distances and the shielding or compensation required to reduce it to a negligible value. These calculations are presented in Appendix F, but are summarized below.

The spacecraft is assumed to be about 12 feet in diameter with the altimeter located near the center. The magnetometer is assumed to be on a boom $6\frac{1}{2}$ feet long (a magnetometer boom of this length was used on the Pioneer spacecraft). This provides a magnetometer-altimeter separation of $12\frac{1}{2}$ feet, and at this distance the TWT field is reduced to 2 gamma.

A shield enclosure to attenuate this field would have a wall 4 mils thick and would weigh approximately 0.08 pounds. This is not a great weight penalty but the shield cannot be placed too close to the tube magnets or their performance will be impaired. The calculations are based on a one-inch separation, which would result in a much larger TWT package. Then too, the shield is most effective in a dead soft annealed condition, and this presents fabrication and assembly problems.

A better solution is the compensation approach in which a small magnet nulls the stray field. A magnet to do this for the altimeter TWT will be of 0.10 inch diameter by 0.50 inch long and will weigh 0.0012 pound. It is made of the same material as the TWT magnets (platinum-cobalt) and can be installed right on the tube at the time of manufacture. Compensation is of course a "line-of-sight" effect, so the exact physical relationship between altimeter and magnetometer must be known before the magnet placement can be set.

Sterilization and Decontamination

Requirements.-Two basic considerations are involved in the sterilization and decontamination procedure. The first is to ensure that the equipment is compatible with the sterilization/decontamination processes. The second is that the equipment be delivered at a level of contamination sufficiently low to ensure that the terminal sterilization process will be effective. Although these are related, they are not necessarily the same consideration.

There is a fundamental document which outlines the tests to be followed to ensure the equipment will operate satisfactorily in the expected environments. This document is JPL specification VOL-50503-ETS (12 Jan 66), which calls for a final assembly clean room at a class 100,000 level. Such a room will be provided. As a definite side effect of this test procedure, there is a significant reduction in the biological load on the equipment. This test procedure, then, coupled with clean room operation, will ensure that the altimeter operates reliably after the terminal sterilization process.

Plan.-A plan will be followed in the fabrication of the altimeter to ensure low microbe count and prove compatibility. It will consist of four basic steps:

(1) Use only approved parts and materials, or test to prove compatibility. No material problems are anticipated; a discussion of candidate materials follows in the next paragraph.

(2) Clean and store components in the clean room. Clean machined parts or subassemblies and store them in the clean room. Even if no biological load reduction resulted from following this clean room procedure, it would be followed for the phychological effect upon the personnel and the increase in reliability from operating in this environment.

(3) Assemble altimeter and perform the flight acceptance tests in the clean room. This includes sterilization/decontamination tests as outlined in VOL-50503-ETS.

(4) After final tests, package and ship the altimeter to its final destination in a container which maintains the clean room environment.

Candidate materials.-Listed below are typical materials to be used to ensure equipment compatibility with the heat/ETO processes.

Potting Material.-Candidate materials would be anhydride cured epoxy resins and RTV silicones. The epoxies would be used where rigidty is required, and where adhesion to a potting case is needed; that is, for potted modules. Silicones would be used where resilience is desired or allowable, and where reparability is needed. Also, certain of the silicones are excellent for high voltage power supplies, since their electrical properties are excellent and they resist cracking under thermal aging or thermal cycling. Where low density is required, glass microballoons could be formulated into the resin. If still lower density is desired note that certain polyurethane foam formulations have good stability at these temperature levels.

Molded plastic parts.-The best material for molded plastic parts would be glass-filled diallyl phthalate. DAP is easy to process and is widely used for molding shells, boxes, cases, headers, connectors, spacers, and practically all other moldable plastic parts. In addition to its dimensional stability, DAP has good electrical properties which are stable up to 150°C.

Wiring, cabling and sleeving (or tubing).-For hook-up wire applications TFE teflon wire would be the choice. It is stable, with respect to temperature, in nearly all properties. Where insulated copper wire (magnet wire) is required, polyimide (ML varnish) insulated wire would be the choice. Cable bundles would be composed of teflon wires. Larger cables or high voltage cables would use silicone rubber insulation. Coaxial cables would use FEP teflon. Tubing and sleeving would also be teflon, which, as in the case of hook-up wire insulation, has excellent thermal stability.

Seals, gaskets, elastomers.-Fluorinated elastomers such as Viton would be used here. These elastomers are stable up to about 200°C.

Film and sheet insulation.-Kapton polyimide film will be used where sheet and film insulation is required.

Laminates and terminal boards (including stripline).-Teflon glass or silicone glass would be the choice for laminate or terminal board applications. Where copper-clad laminates are needed, as in printed circuit boards, some suppliers have a more rigid, higher bond strength copper-clad silicone glass material, which is quite stable at 150°C.

Reliability Estimate

Analysis of system configuration.-The following analysis of the system configuration was used to determine the reliability model.

(a) The system is essentially composed of a group of elements. The failure of any element will cause the system to fail.

(b) Each element is composed of parts (e.g., resistors, capacitors, transistors), the failure of any one of which will cause the element and, in turn, the system to fail. This statement is not true for all part applications however it is used in this analysis since the few redundant applications of parts will have only a minor effect on the total reliability figure.

(c) The parts and hence the lower level elements of the system exhibit constant failure rates during their life.

From this analysis it may be seen that the system is composed of a group of elements which comprise a series system from the reliability standpoint.

Reliability model.-The reliability model of a series system is:

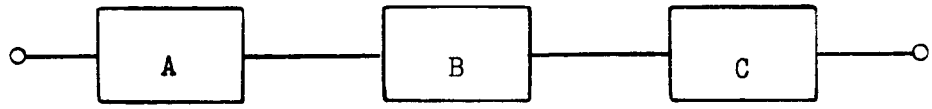

A, B & C are elements of the series system. Failure of any one of the elements results in system failure.

The reliability of any element, element A for example, may be expressed as:

$$R_A = e^{-\sum_{i=1}^{n} \lambda_i t}$$

when the parts exhibit constant failure rates,

where R_A = the reliability of element A

λ = the failure rate of each of n parts

t = the total operating time

The total reliability of the series system may be determined by the product rule for combining reliabilities,

$$R_{system} = R_A \cdot R_B \cdot R_C$$

In exponential form this becomes

$$R_{system} = e^{-(\lambda_A + \lambda_B + \lambda_C)t}$$

where λ_A, λ_B, and $\lambda_C = \sum_{i=1}^{n} \lambda_i$ for elements A, B, and C, and t is the mission time.

Therefore, the failure rate for any element in the series system is equal to the sum of the failure rates of the parts which comprise the element. Further, the failure rate of the system is equal to the sum of the failure rates of the elements which comprise the system.

Reliability calculation.-Summing the failure rates of all parts in the system, we arrive at 32.4625%/1000 hrs, using failure rates from MIL-HDBK-217A.

From the previous reliability equation,

$$R_{system} = e^{-\sum_{i=1}^{n} \lambda_i t}$$

or $$R_{system} = e^{-32.5t}$$

and $$R_{system} = 0.722$$ for a 1000-hour operating period.

Reliability requirements.-

(1) Mission lifetime
   (a) 9 months inactive or standby; 30 minutes active
   (b) 2 years inactive or standby; 2 days active
(2) Proposed reliability requirements
   (a) 0.9999 probability of surviving 9 months inactive or standby
       0.9999 probability of operating for 30 minutes
   (b) 0.99 probability of surviving 2 years inactive or standby
       0.99 probability of operating for 2 days

Table IX lists the predicted failure rates for the various units of the space probe radar altimeter, based on the rates of the component parts. The grand total is thus the failure rate for the entire altimeter.

Antenna reliability.- The antenna, being a type of phased array, has to some extent a "slow die" property. The radiating aperture consists of 64 individual elements in an 8X8 array. These are fed by a complex network of hybrids and transmission line fabricated in stripline. Within the stripline beam forming network are 64 diode switches. There is a combination of switch positions (open or shorted) for each of 64 possible beam positions. Perfect beam forming and beam steering depends upon proper operation of all switches.

Failure of a single diode (or its driver or the decoder gate which activates the driver) will result in one of many possible effects. The most likely result of a failure is antenna pattern degradation—a breakup of beam structure and a loss of gain—in some beam positions. This is because the failure of one switch influences the signals fed to many elements rather than just one.

TABLE IX

SPRA FAILURE RATE PREDICTION

UNIT	PART/TYPE	QTY.	MIL-HDBK-217A or LIFE DATA F/R	F/R %/1000 HRS.	ASSEMBLY F/R
Integrated RF Unit	Varactors	3	0.5	1.5	
	Pt. Contact Diodes	4	1.5	6.0	
	Coupler	1	.015	.015	
	Isolator	1	.015	.015	
	Transistors	3	.02	.060	
	Diodes	1	.01	.010	7.6000
Antenna/ Ant. Steering	Connectors	16	.012	.1920	
	Diodes	64	.10	6.40	
	MIC's	64	.0035	.2240	
	Gates	64	.0035	.2240	7.0400
TWT/LO	TWT	1	4.0	4.0	
	LO	1	2.0	2.0	6.0000
Range TRKR AGC	Capacitors				
	Mica	23	.007	.161	
	Tantalum	13	.0098	.0127	
	Variable	1	.031	.031	
	Resistors				
	Carbon	44	.004	.176	
	Diodes				
	Switching	9	.001	.009	
	MIC's	260	.0035	.9100	
	Inductors				
	Fixed	16	.05	.80	
	Variable	1	.05	.05	
	Crystals	1	.01	.01	
	Crystal Filters	2	.80	1.60	3.7597
Power Supply	Capacitors:				
	Ceramic	4	.01	.04	
	Tantalum	31	.0098	.304	
	Variable	1	.031	.031	
	Resistors				
	Metal Film	23	.028	.644	
	Wire Wound	10	.0032	.032	

TABLE IX (cont'd)

UNIT	PART/TYPE	QTY.	MIL-HDBK-217A or LIFE DATA F/R	F/R %/1000 HRS.	ASSEMBLY F/R
Power Supply (Continued)	Potentiometers				
	WW	2	.187	.3740	
	Transistors				
	Hi Pwr	4	.2	.8	
	Lo Pwr	16	.015	.24	
	Diodes				
	Silicon Rect.	48	.01	.48	
	Switching	7	.001	.007	
	Zener	3	.025	.075	
	Transformers				
	HF Power	3	.046	.138	
	Inductors				
	Fixed	1	.05	.05	3.215
IF Strip					
	Capacitors				
	Ceramic	26	.01	.26	
	Glass	6	.01	.06	
	Tantalum	6	.0098	.0588	
	Variable	3	.031	.093	
	Resistors				
	Metal Film	17	.028	.475	
	Potentiometers	1	.187	.187	
	Transistors				
	Low Power	1	.015	.015	
	Diodes				
	Silicon Rect.	5	.01	.05	
	MIC's	7	.0035	.0245	
	RF Coils	23	.05	1.15	2.3733
HV P/S & Mod.	Capacitors				
	Ceramic	1	.01	.01	
	Mica	2	.007	.014	
	Tantatum	3	.0098	.0294	
	Met. Paper	4	.06	.24	
	Resistors				
	Carbon	12	.004	.048	
	Transistors				
	Low Power	4	.015	.06	

TABLE IX (cont'd)

UNIT	PART/TYPE	QTY.	MIL-HDBK-217A or LIFE DATA F/R	F/R %/1000 HRS.	ASSEMBLY F/R
HV P/S & Mod. (Continued)	Diodes				
	Silicon Rect.	4	.01	.04	
	Switching	4	.001	.004	
	Zener	3	.025	.075	
	Transformers				
	Pulse	1	.046	.046	
	HF Power	3	.046	.138	.7044
AFC	Capacitors				
	Ceramic	6	.01	.06	
	Glass	8	.01	.08	
	Tantalum	12	.0098	.1176	
	Resistors				
	Metal Film	19	.028	.532	
	Pots WW	1	.187	.187	
	Transistors				
	Low Power	1	.015	.015	
	Diodes				
	Switching	9	.001	.009	
	MIC's	5	.0035	.0175	
	RF Coils	5	.05	.25	1.2681
Ext. Conn.	RF	12	.04	.480	
	AN	2	.012	.024	.504
				OVERALL	32.4625
				MTBF ≅ 3000 hrs.	

However, the failure may be such that the correct switch position is present for many beam position (i.e., the diode could open, presenting an open circuit all the time--a correct situation for many beam positions). The worst case, severe degradation, would reduce altimeter effective altitude, probably by a factor of four or more.

Another possible effect is a steering error or an improper positioning of the beam. This would merely introduce an altitude error (if the beam still illuminates the surface). But it is perhaps more probable that the beam would be pointed such that only sidelobes illuminate the surface. Then the effective altitude would again be reduced.

A final possibility is the loss of correct phasing of the signals feeding a single row of 8 elements. This is the least damaging failure. It would result in a small loss of gain and a minor reduction of performance. Total failure due to a combination of semiconductor failures is virtually impossible. The antenna will always radiate, even though the pattern may become distorted. The only way to suffer a total failure is by failure of the RF feed (coaxial connector or the coaxial line from transmitter to antenna) or by physical destruction of the antenna beam forming network.

Surface Roughness

A rudimentary measure of surface roughness can be made by correlating altitude measurements made by the altimeter with the trajectory profile. By taking advantage of its horizontal motion, the lander can determine surface roughness along the projection of the lander flight path on the surface. The amount of data thus obtained is sharply limited, but it is available without modifying the basic altimeter. A more comprehensive surface roughness measurement (e.g., via a mapping radar) would require a considerable increase in system size, weight and complexity .

Method of measurement.-An estimate of the resolution of the surface roughness information can be obtained as follows. Three quantities are measured: (1) descent rate, Vh, by a surface-independent sensor (an accelerometer, for example); (2) altitude rate, hm, as meauured by the altimeter (either by using altitude rate from the range tracker or by differentiating altitude measurements); and (3) horizontal rate, Vx (again, an integrating accelerometer might be used).

For purposes of resolution estimation, a sinusoidal surface model is assumed. If the surface is described by

$$K \sin \alpha x$$

where K is the peak surface variation in feet
x is the horizontal displacement in feet
and α is the rate of variation in radians/foot,

The measured altitude rate is then

$$\dot{h}_m(t) = V_h(t) + \frac{dh}{dx} \cdot \frac{dx}{dt}$$

$$= V_h(t) + (K \alpha \cos \alpha x)(V_x).$$

The quantity descriptive of the surface features is

$$S(t) = K \alpha \cos \alpha x = \frac{\dot{h}_m(t) - V_h(t)}{V_x}.$$

Error and resolution.-Resolution will be influenced by the angular resolution and accuracy of the various measurements required for computing S(t). These errors are designated as follows:

rms error in $\dot{h}_m(t) = \mathcal{E}_{hm}$

rms error in $V_h = \mathcal{E}_{vh}$

rms error in $V_x = \mathcal{E}_{vx}$

Inserting these terms in the equation for S(t) and manipulating, the per-unit rms error in measuring surface roughness is obtained:

$$\text{per-unit error} = \frac{\sqrt{2}\,\mathcal{E}_R}{K\alpha},$$

where $$\mathcal{E}_R = \frac{\sqrt{\mathcal{E}_{hm}^2 + \mathcal{E}_{vh}^2}}{V_x}.$$

The limit of roughness resolution is defined as the point at which the error is one-half the quantity $K\alpha$, i.e.,

$$\frac{\sqrt{2}\,E_R}{K\alpha} = \tfrac{1}{2}.$$

This quantity is plotted on Figure 47 as a function of V_x and

$$\mathcal{E}_T = \sqrt{\mathcal{E}_{hm}^2 + \mathcal{E}_{vh}^2}.$$

Ability to determine roughness can be estimated from this figure. For example, if the rms error, E_T, is 100 feet/second (a representative value), and horizontal velocity, V_x, is 1000 feet/second, a $K\alpha$ of 0.28 can be resolved. If one cycle of a sinusoidal terrain feature extends 2000 feet, then $\alpha = 2\pi/2000$ and resolvable $K \geq \frac{0.28}{2\pi/2000}$ or 90 feet.

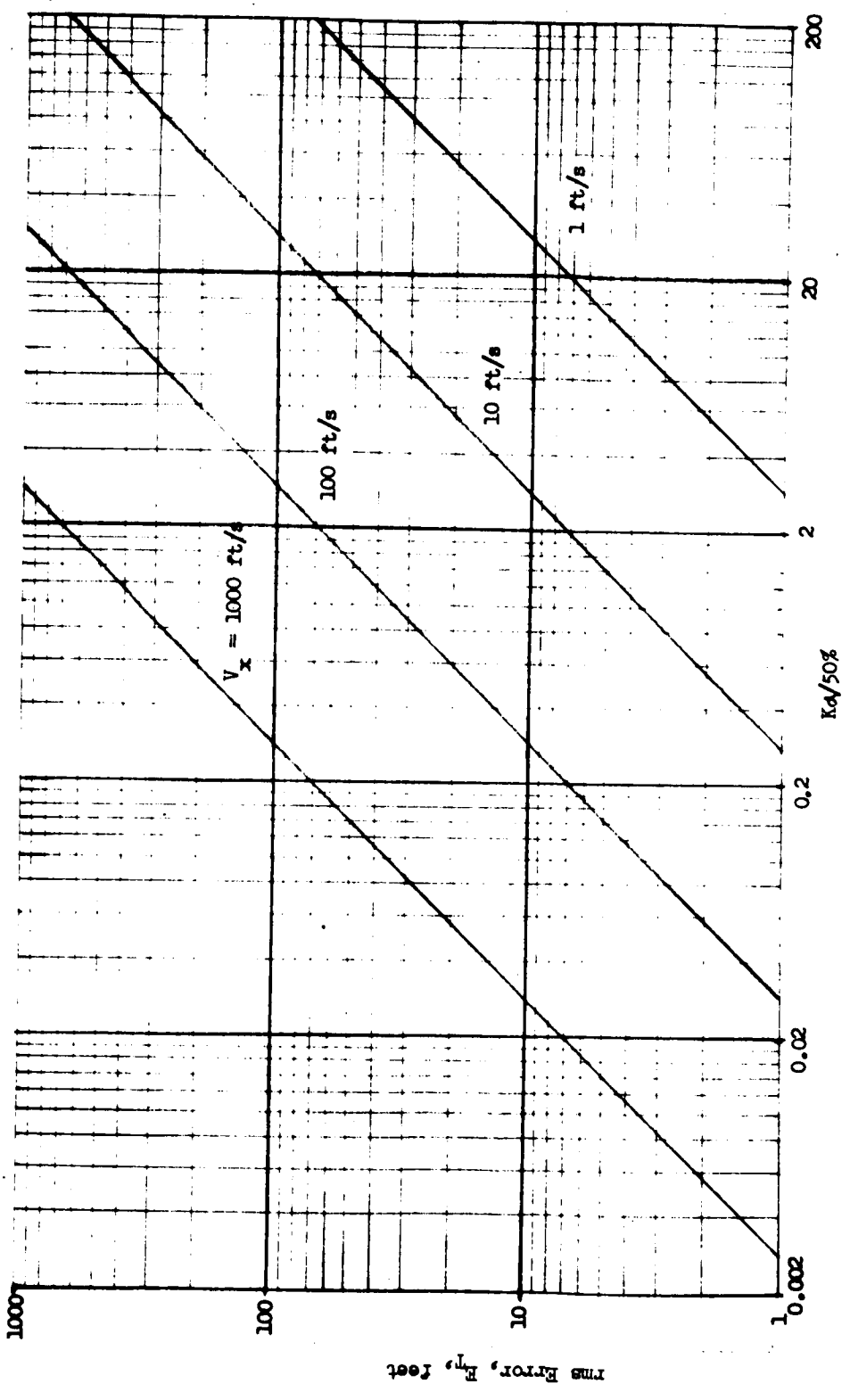

FIGURE 47.- ERROR-LIMITED RESOLUTION

The second resolution limitation is due to the extent of the surface illuminated by the antenna beamwidth. With a six inch-aperture (and 8.0 GHz), the resolution limit is about 0.2 times the altitude. For example, at 10,000 feet features extending over less than 2000 feet along the surface cannot be resolved.

Figure 48 combines the effects of measurement errors and angular resolution. In plotting Figure 48, the following assumptions were made:

(1) Antenna beamwidth =0.05 radian, corresponding to the 24 inch antenna which might be used in a system for future application.

(2) Error in hm and V_h are both assumed to be 100 feet/second at a 50,000 foot altitude, decreasing linearly with altitude to a minimum of 10 feet per second. Thus $\mathbf{E}_T = \sqrt{2}$ X 100 feet/second decreasing to $\sqrt{2}$ X 10 feet/second at 5000 feet, and constant thereafter.

(3) The minimum resolvable α is determined by altitude and antenna beamwidth, and is equal to $\pi/h\theta$, where h = altitude and θ = beamwidth.

(4) The smallest resolvable terrain variation (K in Figure 48) is calculated using the minimum resolvable α. If α is larger, resolvable K diminishes as the reciprocal of α. Thus Figure 48 is a most favorable case.

Advanced Requirements

Requirements placed on an altimeter for future applications were considered principally from the standpoint of required modifications to the basic altimeter. Design goals for future applications were given in the contract work statement and are summarized in Table X.

To accomodate these requirements, a number of changes must be made in the basic system. Some of these would not result in significantly greater weight and volume. But others, in particular the higher altitude, will have a major impact. Required modifications are discussed below.

Short range mode.-A technique for short range tracking can be incorporated without adding a great deal of extra equipment. In this mode, a short pulse is transmitted and tracked by centroiding a narrow, swept tracking gate over the signal return. Tracking is done at microwave, the microwave-diode TR switch accomplishing the range gating. It is swept over the return in a manner similar to that used in the conventional tracking mode. Tracking is accomplished by observing the return in each of the swept gate positions (for example, 8 positions might be used). The gate is then positioned so that it sweeps an equal distance on either side of the return. The existing range tracker can be used in this mode.

Higher altitude.-Greater maximum altitude capability must be incorporated in the range tracker. This will involve an increase in the number of molecular integrated chips composing the digital tracker. The PRF of the basic system are sufficiently high and need not be changed.

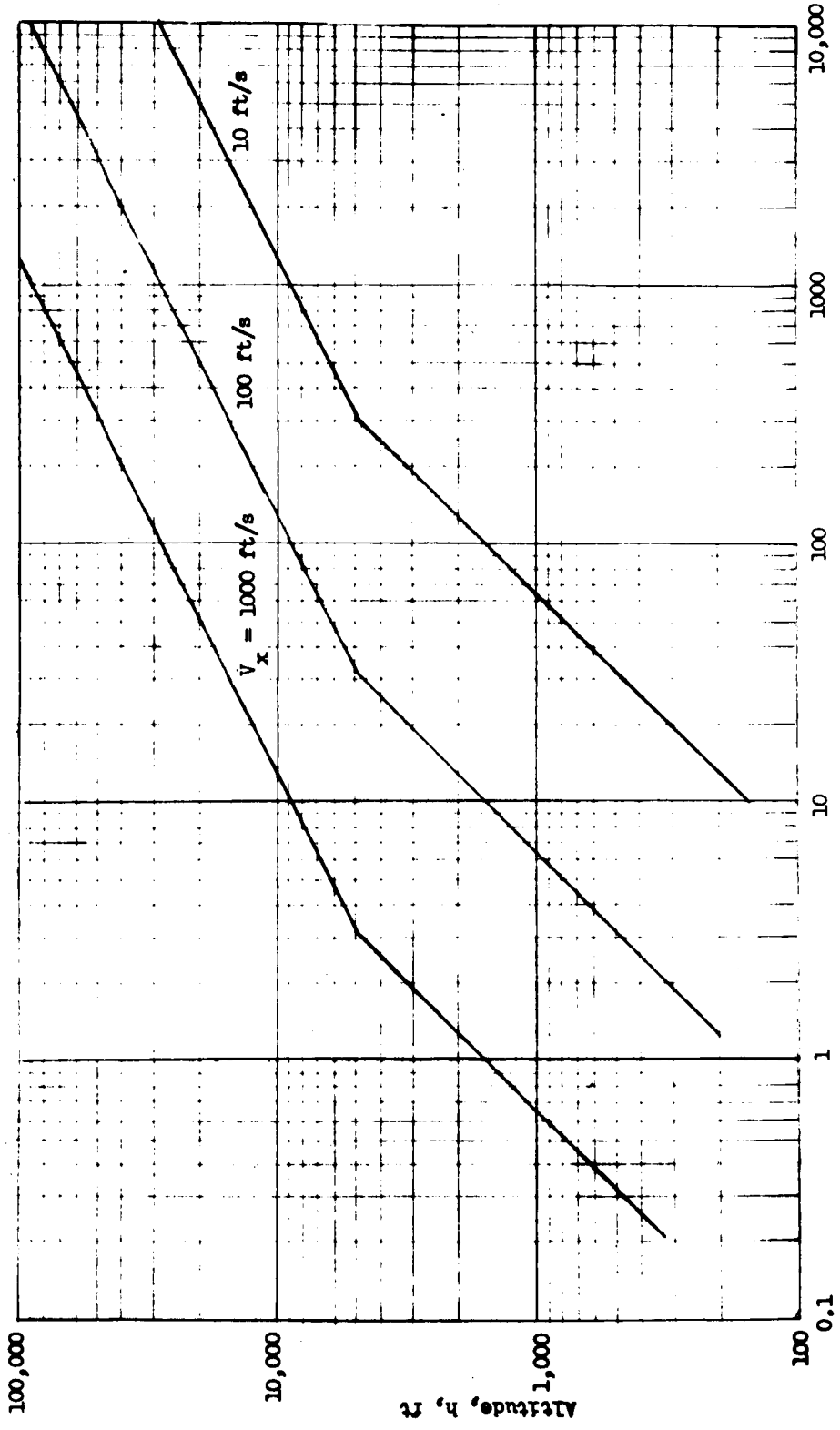

FIGURE 48.- SURFACE ROUGHNESS RESOLUTION

TABLE X - DESIGN GOALS FOR FUTURE APPLICATIONS

Parameter	Performance
Altitude range	30 m to 100 km
Accuracy	±5 m or ±1%
Frequency	X-band, 8-10 GHz
Velocity	10 km/s (max)
Acceleration	250 g (max)
Antenna size, diameter	24 inches (max)
Power required	20 watts (max)
Size	500 cubic inches (including antenna)
Weight	10 lb (including antenna)
Quantization	3 m
Lifetime	2 years inactive, 2 days active

Signal dynamic range will increase as a consequence of the greater altitude range. Consequently the dynamic range capability of the receiver must be greater.

Finally, transmitted power and/or antenna gain must be increased. This will be discussed subsequently.

Accuracy and quantization.-As shown earlier present accuracy is well within the more stringent future requirement as long as return S/N ratio is not severely degraded. Data quantization must be finer, however. Again, this will entail an increase in the number of parts and complexity in the range tracker, but not a significant increase in size and weight.

Acquisition time.-Higher altitude and approach velocity complicate the problem of rapidly acquiring the surface return. A solution which does not require a great amount of hardware is the use of multiple acquisition channels. Several channels would split the altitude interval, thus permitting simultaneous search at several range gate positions. This in turn would keep the acquisition time within acceptable bounds.

Power and antenna gain.-Increased power and/or antenna gain is necessary to maintain adequate S/N at the higher altitude. A slight reduction (to 0 dB) in the IF S/N is acceptable because of the inclusion of multiple acquisition channels. Work statement guidelines allow for an antenna aperture as large as 24 inches. However the optimum balance of weight, size and power consumption will not necessarily be reached by using the entire available aperture. For the basic system, it was concluded that all of the available 6 inches should be used. But since antenna weight grows rapidly with aperture size (largely because of the large scan angles), a more favorable balance can be achieved by using a smaller antenna. Several combinations of power and antenna size adequate for providing a 0-dB S/N at maximum altitude (100 km) are given below:

Antenna Size	Peak Power
12"	20 kW
17"	5 kW
24"	1.25 kW

Total system weight and antenna weight are estimated as follows using three antenna sizes:

Array Size (in)	Antenna Weight (lb)	Total Weight (lb)
12	17	42
17	29	43.5
24	48	60.5

Again, weights are strongly dependent upon angular coverage. The above values are based upon 120° x 120° coverage requirements. By reducing the antenna field of view, 35 to 40% of the antenna weight could be eliminated. The weight of a 24" x 24" antenna with a ± 60° line scan is estimated to be 9 pounds.

With a 120° x 120° field of view requirement, an antenna size of approximately 17" x 17" would offer the most favorable compromise between weight, volume, and power consumption. Although the weight of the system using a 12 inch antenna would be slightly less, its power consumption would be excessive. Power consumption of the system using a 17 inch antenna would be approximately 32 watts.

CONCLUSION

The space probe radar altimeter study has demonstrated that the operational and performance objectives of the altimeter can be met, although size and weight goals will be exceeded. Sterilization and decontamination procedures, while constraining component and materials selection, will not present significant difficulty. It is felt that the altimeter design is sufficiently reliable to ensure mission success, although unknowns are presented by the long storage period in space due to lack of data.

Major conclusions of the study program are summarized here:

- Pulse radar is the technique best suited for the space probe altimeter.
- Greater weight, volume, and power consumption will exceed design goals if the system is to meet reliability and performance goals and development time is limited to conform with a 1971 launch.
- Angular coverage required of the antenna has a very significant impact on weight and volume. A reduction in coverage requirements will greatly simplify antenna complexity.
- Sterilization and decontamination requirements are not reflected appreciably in system weight, size, performance, or reliability.
- Requirements placed on an altimeter for future applications (e.g., higher altitude, better accuracy) could be met with a number of minor changes plus major changes in the transmitter and antenna.
- Surface roughness information can be derived from altimeter data. This information would be limited but perhaps useful, and it is available without additional equipment.
- Principal development items incorporated in the altimeter are the antenna, TWT transmitter, and integrated microwave circuit.

The altimeter design which has been developed under the study program uses a TWT amplifier in the transmitter. Although the TWT was chosen primarily for its inherent high reliability, it should be noted that relatively minor changes could be incorporated to permit fully coherent operation. This facility could be useful in adapting the basic altimeter for a soft-landing vehicle. Also possible would be a further extension of system capability to incorporate a rudimentary synthetic aperture

mapping function. Such a system might be used in an orbiting vehicle or a lander having a very shallow trajectory. Coherent mapping functions would require more sweeping changes than a horizontal velocity sensing function, but the basic radar can be regarded as a building block.

Appendix A

ZERO CROSSINGS FOR A SINE WAVE PLUS BAND-LIMITED NOISE

Assume a sine wave plus white noise passes through an ideal bandpass filter, where the filter characteristic is

$$G(\omega) = \begin{cases} K, & 0 \leq a\,\omega_o \leq |\omega| \leq b\,\omega_o \\ 0, & \text{elsewhere} \end{cases} \qquad (A\text{-}1)$$

and where ω_o is the radian frequency of the sine wave. The expected number of zero-crossings per second of the signal plus noise is then given by *

$$\overline{N_o} = 2 f_o \left[\frac{S/N + (a^2 + ab + b^2)/3}{S/N + 1} \right] 1/2 \qquad (A\text{-}2)$$

For an ideal low-pass filter with bandwidth BW such that $b f_o = BW$, the mean number of zero-crossings is given by

$$\overline{N_o} = 2 f_o \left[\frac{S/N + (BW/f_o)^2/3}{S/N + 1} \right] 1/2 \qquad (A\text{-}3)$$

The term in the bracket is the error factor due to noise.

Figure A-1, shows the deviation in zero-crossing counts, normalized to $2 f_o$, as a function of BW/f_o for different values of signal-to-noise ratios. Note that at $\overline{N_o} / 2 f_o = 1$, the number of zero-crossings is due to the sine wave only. Also note that at $BW/f_o = 1.73$ the deviation from the $2 f_o$ zero-crossing count is zero for all S/N ratios. This occurs because this point is the apparent frequency of the noise alone equal to $f_N = BW/1.73 = 0.58\ BW$.

If the mean number of zero-crossings due to the sine wave only is

$$\overline{N_{o\,o}} = 2 f_o,$$

then the error term due to noise is

$$\% \text{ Error in } \overline{N_o} = \frac{\overline{N_o} - \overline{N_{o\,o}}}{\overline{N_{o\,o}}} \times 100\% = \left\{ \left[\frac{S/N + (BW/f_o)^2/3}{S/N + 1} \right]^{\frac{1}{2}} - 1 \right\} \times 100\% \qquad (A\text{-}4)$$

* J.S. Bendat, "Principles and Applications of Random Noise Theory," John Wiley and Sons, Incorporated, New York; 1958.

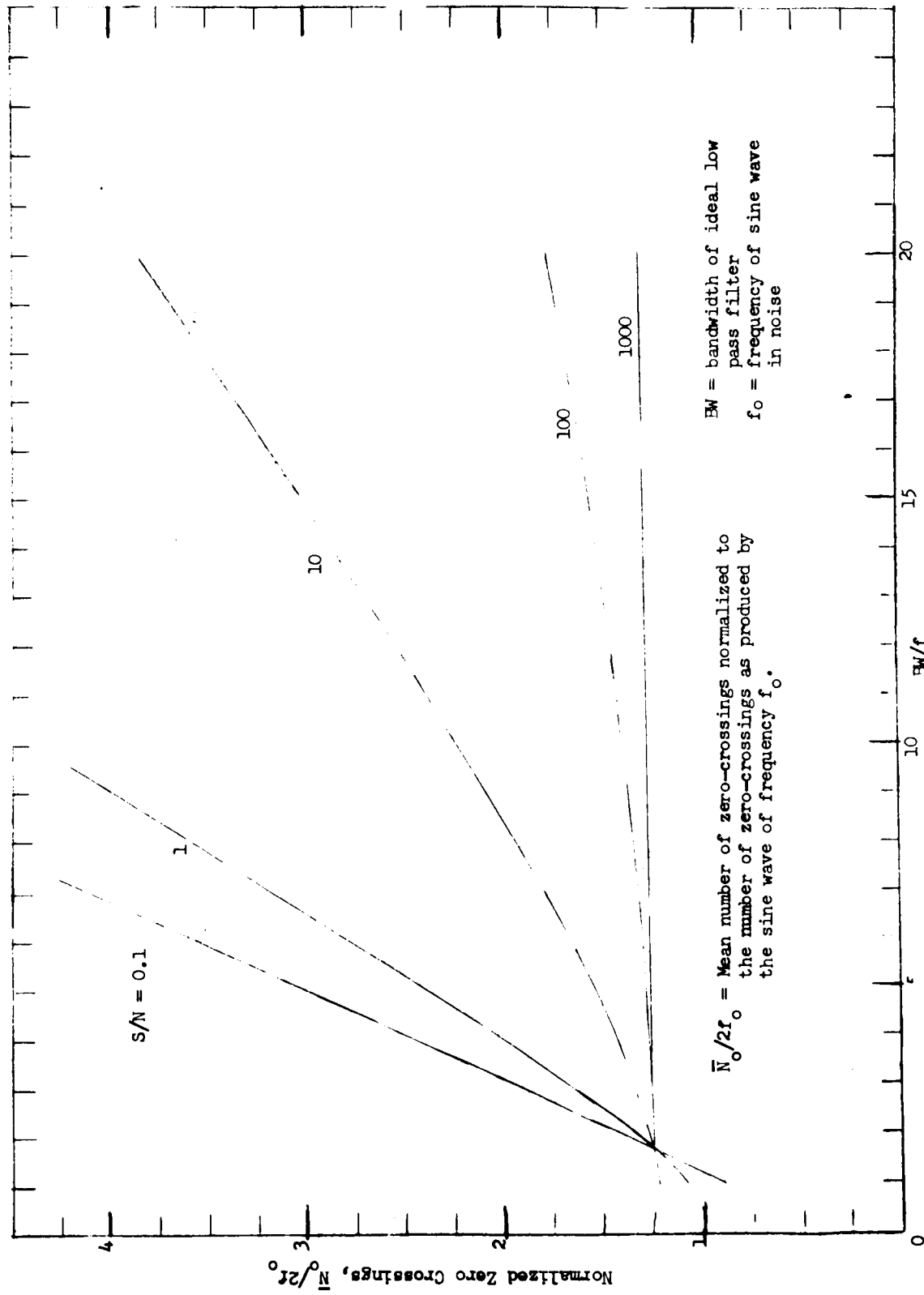

FIGURE A-1. DEVIATION IN ZERO-CROSSINGS

The S/N ratio required for a Δ % accuracy in zero-crossing count, as a function of BW/f_o, is shown to be

$$S/N = \frac{3[1 + (0.1)(\Delta\%)]^2 + (BW/f_o)^2}{6[(0.1)(\Delta\%) + 3[(0.1)(\Delta\%)]^2} \quad \text{for } BW/f_o < \sqrt{3} \qquad (A\text{-}5)$$

and

$$S/N = \frac{-3[1 + (0.1)(\Delta\%)]^2 + (BW/f_o)^2}{6[(0.1)(\Delta\%)] + 3[(0.1)(\Delta\%)]^2} \quad \text{for } \frac{BW}{f_o} \geq \sqrt{3} \qquad (A\text{-}6)$$

Equations (A-5) and (A-6) were solved for Δ % = 1% and 5% and the results shown as Figure 12 of the main text of this volume.

Appendix B

SIGNAL-TO-NOISE ANALYSIS FOR SIDEBAND SQUARING ALTIMETER

A description of the sideband squaring, or sidetone ranging, FW/CW altimeter is given in the main text of this volume. Some of the signal spectrum deviation given there is repeated here. Referring to Figure B-1, the transmitted signal is

$$e_r = E_T \sin (\omega_o + m \cos \omega_m T) \tag{B-1}$$

where ω_o = RF angular frequency

m = transmit modulation index = $\Delta F / f_m$

ΔF = transmit peak deviation

f_m = modulation frequency

The reference for the first mixer is

$$e_L = E_L \sin [(\omega_o + \omega_1)t + m \cos \omega_m t] \tag{B-2}$$

where ω_1 = intermediate angular frequency

A return delayed by τ seconds,

$$e_R = E_R \sin [\omega_o (t-\tau) + m \cos \omega_m (t-\tau)] \tag{B-3}$$

is mixed with the reference signal, e_L. The product of interest is

$$\begin{aligned} e_R e_L &= E_o \sin [\omega_1 t + \omega_o \tau + m \cos \omega_m t - m \cos \omega_m (t-\tau)] \\ &= E_o \sin [\omega_1 t + \omega_o \tau - \mu \sin (\omega_m t - \omega_m \tau/2)] \qquad \text{(B-4)} \\ &= E_o \{ J_o(\mu) \sin (\omega_1 t + \omega_o \tau) + J_1 (\mu) [\sin (\omega_1 t + \omega_o \tau + \omega_m t - \tfrac{\omega_m \tau}{2}) \\ &\qquad - \sin (\omega_1 t + \omega_o \tau - \omega_m t + \tfrac{\omega_m \tau}{2})] \\ &\qquad + J_2 (\mu) [\sin (\omega_1 t + \omega_o \tau + 2\omega_m t - \omega_m \tau) \\ &\qquad + \sin (\omega_1 t + \omega_o \tau - 2\omega_m t + \omega_m \tau)] \\ &\qquad + \ldots \} \quad , \qquad \text{(B-5)} \end{aligned}$$

where $J_n (\mu)$ is the Bessel function of order n and argument μ, and where

$$\mu = 2m \sin \frac{\omega_m \tau}{2} .$$

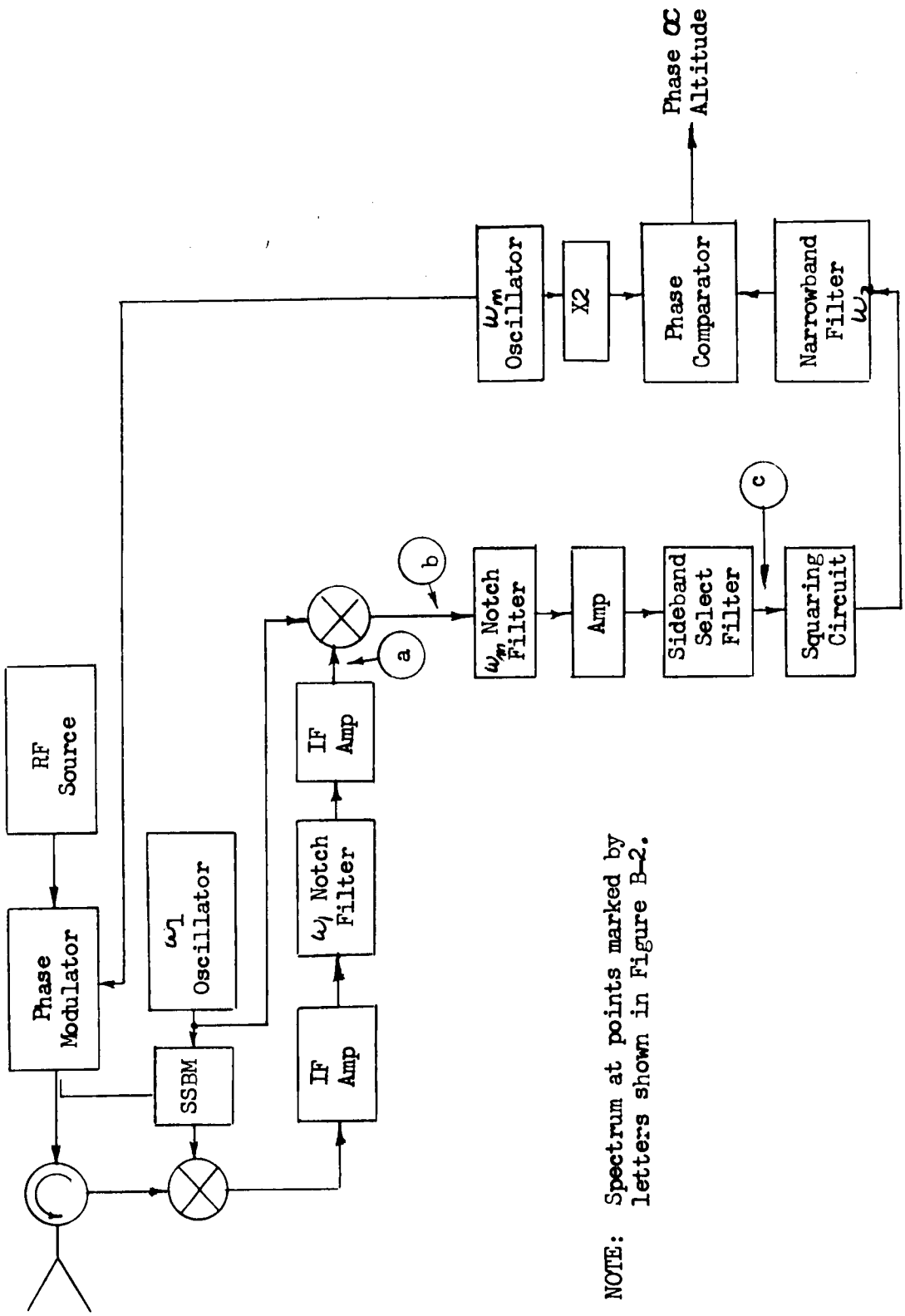

NOTE: Spectrum at points marked by letters shown in Figure B-2.

FIGURE B-1. SIDETONE RANGING ALTIMETER

Since the time delay, τ, associated with the leakage signal is small, the μ associated with the leakage will be small and most of the leakage power will be in the carrier term $E_o J_o(\mu) \sin(\omega_1 t + \omega_o \tau)$. This term is largely removed by the notch filter at angular frequency ω_1 in the IF strip.

Following the notching operation and amplification, the signal spectrum is folded about the IF, ω_1. The spectrum before and after folding is shown in igure B-2. After folding, the doppler shifted and smeared sidebands are symmetrically located about the modulating frequency, ω_m. At this point, a notch filter at ω_m attenuates the first-order leakage sideband, providing further immunity from leakage (Figure B-2b). The fact that the return signal is doppler shifted permits this operation.

The doppler shift is derived from the phase term $\omega_o \tau$ is changing, producing a doppler shift equal to

$$\frac{1}{2\pi}\frac{d\phi}{dt} = \frac{1}{2\pi}\frac{d}{dt}(\omega_o \tau) = \frac{2f_o}{c}\frac{dh}{dt} = f_d$$

The doppler shift, f_d, is the mean doppler. As shown in Figure B-2, the signal sidebands are also broadened by the doppler smear produced by the horizontal velocity component.

The sidebands of interest are the upper and lower first sidebands of the signal spectrum. These are filtered out, leaving the spectrum shown in Figure B-2c. Also shown (cross-hatched) is the noise spectrum. (Actually, a small amount of noise is notched out at ω_m by the first leakage sideband notch filter, but this may be neglected since it is as a small portion of the total. The signal and noise remaining are passed through a square-law device.

The input to the square-law device consists of:

(1) a uniform noise spectrum having bandwidth $2W$ and a Gaussian amplitude distribution with variance σ^2

(2) a sinusoid, $e_1 = E_o J_1(\mu) \sin(\omega_m t - \omega_d t - \frac{\omega_m \tau}{2})$

(3) a sinusoid, $e_2 = E_o J_1(\mu) \sin(\omega_m t + \omega_{dt} - \frac{\omega_m \tau}{2})$.

In (2) and (3) the doppler dispersion has been omitted for simplification. This ommission will not appreciably change the results of the analysis.

Following the squaring operation the signal becomes

$$(e_1 + e_2 + n)^2 = e_1^2 + e_2^2 + 2e_1e_2 + n^2 + 2e_1n + 2e_2n, \qquad \text{(B-6)}$$

where n = noise

The frequency components contributing to the output spectrum by the first three terms in (B-6) are derived as follows:

$$\begin{aligned} e_1^2 + e_2^2 + 2e_1e_2 &= E_o^2 J_1^2(\mu)\left[\sin^2\phi_1 + \sin^2\phi_2 + 2\sin\phi_1 \sin\phi_2\right] \\ &= E_o^2 J_1^2(\mu)\left[1 - \tfrac{1}{2}\cos 2\phi_1 - \tfrac{1}{2}\cos 2\phi_2 + \cos(\phi_1 - \phi_2) - \right. \\ &\quad \left. \cos(\phi_1 + \phi_2)\right] \end{aligned} \qquad \text{(B-7)}$$

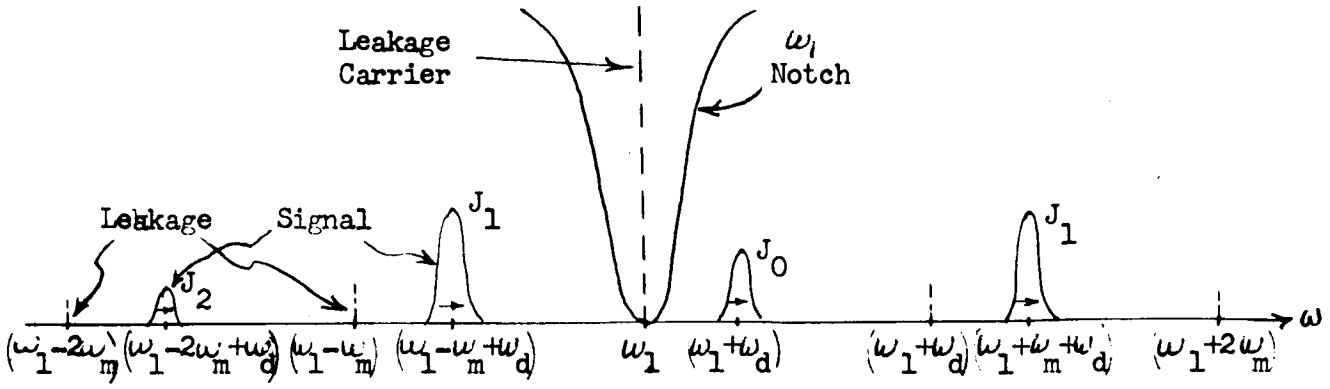

a - Before Folding

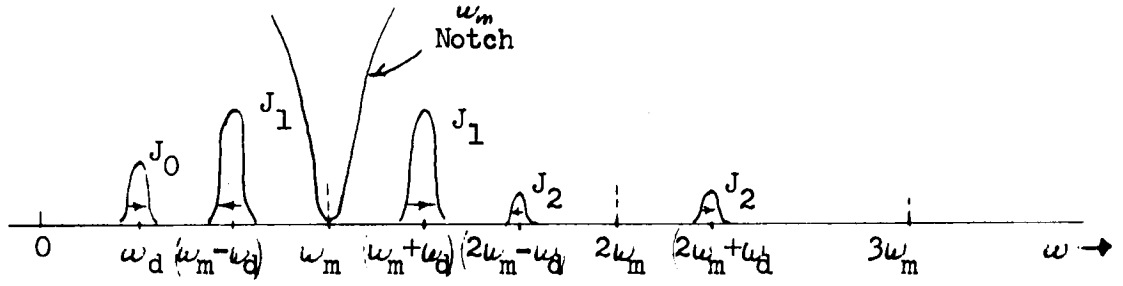

b - After Folding

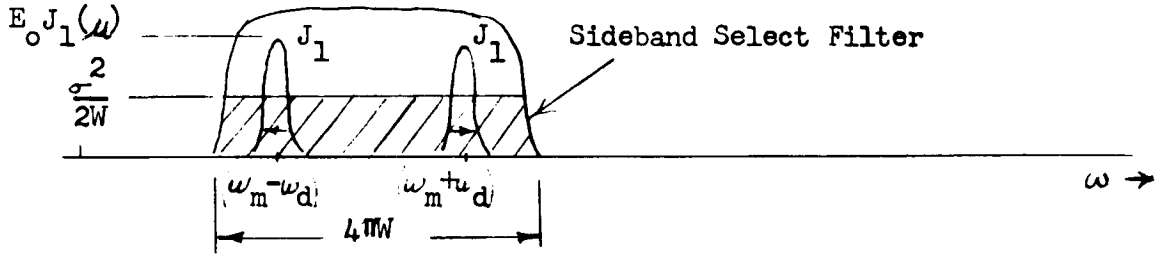

c - Before Squaring

FIGURE B-2. FREQUENCY SPECTRA

where $\phi_1 = \omega_m t - \omega_d t - \frac{\omega_m \tau}{2}$

$\phi_2 = \omega_m t + \omega_d t - \frac{\omega_m \tau}{2}$

These are represented in the frequency domain as follows

$$E_o^2 J_1^2(\mu)[\delta(o) - \tfrac{1}{2}\delta(2\omega_m - 2\omega_d) - \tfrac{1}{2}\delta(2\omega_m + \omega_d) + \delta(2\omega_d) - \delta(2\omega_m)] \quad (B\text{-}8)$$

where $\delta(x) = 1 \quad , \omega = x$

$\delta(x) = 0 \quad , \omega \neq x$

The last terms in (B-7) and (B-8) represent the information-bearing signal,

$$E_o^2 J_1^2(\mu) \cos(2\omega_m t - \omega_m \tau) \quad (B\text{-}9)$$

Note that the doppler shift has been removed in the squaring operation (this is also true of the doppler dispersion), leaving a sideband at twice the modulating frequency having a phase shift proportional to delay, τ, and hence to the altitude. The other terms in (B-7) and (B-8) are sufficiently removed from $2\omega_m$, the frequency of interest, that they may be ignored.

Now consider the output spectral contributions of the noise terms n^2, $2e_1 n$, and $2e_2 n$. Considering first the n^2 term, the autocorrelation function of the input noise process is

$$\varphi(\mu) = \frac{\sigma^2}{2\omega} \cdot \frac{1}{2\pi} \int_{\omega_m - 2\pi W}^{\omega_m + 2\pi W} e^{j\omega\tau} \, d\omega, \quad (B\text{-}10)$$

where W is one half the sideband-select filter bandwidth in Hz. Equation (B-10) reduces to

$$\varphi(\tau) = \sigma^2 e^{j\omega_m \tau} \frac{\sin 2\pi W\tau}{2\pi W\tau}. \quad (B\text{-}11)$$

Here it is assumed that the noise spectrum is rectangular and symmetrically located about angular frequency ω_m.

With a square law operation, the autocorrelation function of the output process is *

$$\varphi_o(\tau) = \sigma^4 (1 + 2\rho^2), \quad (B\text{-}12)$$

where ρ = normalized autocorrelation function of the input process. For a Gaussian process, **

$$\rho(\tau) = \frac{\varphi(\tau)}{\sigma^2}. \quad (B\text{-}13)$$

---

* Povejsil, Raven, and Waterman, "Airborne Radar," D. Van Nostrand Company, Inc., 1961; page 254.

** op. cit., page 248

Therefore, from (A-11) and A-13),

$$\rho(\tau) = e^{j\omega_m \tau} \frac{\sin 2\pi W\tau}{2\pi W\tau} . \qquad (B\text{-}14)$$

The power density spectrum is the Fourier transform of the autocorrelation function,

$$\overline{N_T(\omega)} = \int_{-\infty}^{\infty} \varphi_o(\tau)\, e^{-j\omega\tau} d\tau, \qquad (B\text{-}15)$$

where, from (A-12) and (A-14),

$$\varphi_o(\tau) = \sigma^4 + 2\sigma^4 e^{j2\omega_m \tau} \left(\frac{\sin 2\pi W\tau}{2\pi W\tau}\right)^2 \qquad (B\text{-}16)$$

The continuous portion of $\overline{N_T(\omega)}$ is recognized as a triangular spectrum, having a peak power density of σ^4/W and centered at $2\omega_m$, as represented in Figure B-3. The dc term is of amplitude σ^4.

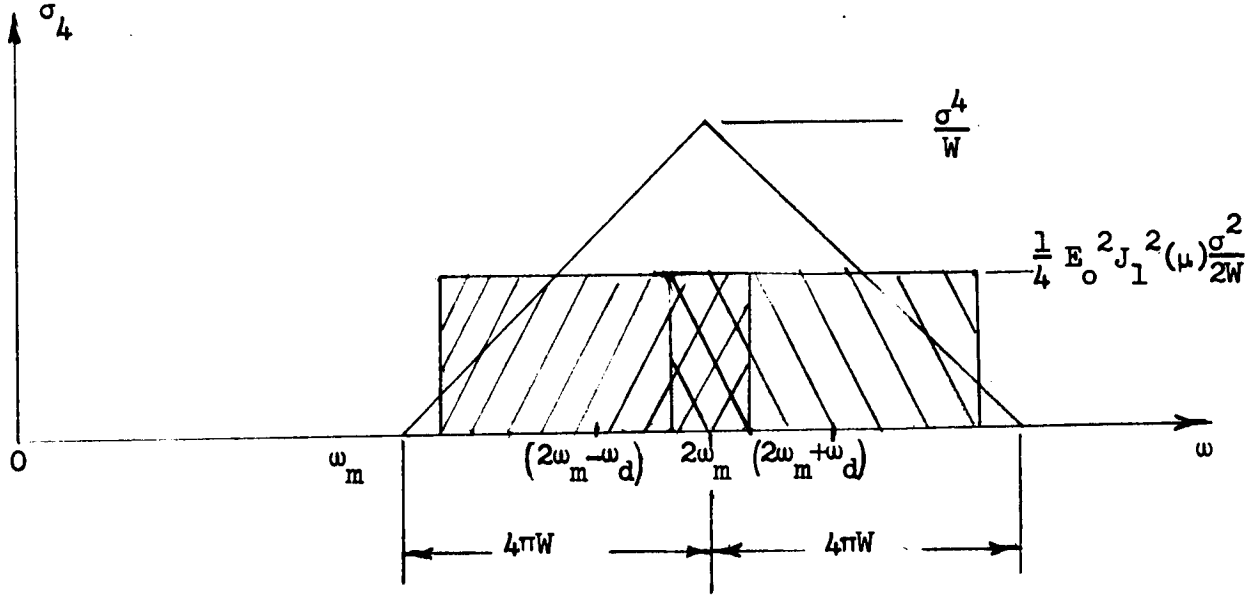

FIGURE B-3. POWER DENSITY SPECTRUM

The other two noise terms in (B-6), $2e_1 n$ and $2e_2 n$, represent the beat frequencies between the input noise spectrum and the two sinusoids. Translations of the input noise spectrum are centered at frequencies $2\omega_m - \omega_d$, ω_d and $2\omega_m + \omega_d$.

Since the modulating frequency, ω_m, is necessarily larger than the doppler shift, ω_d, only two of the translated noise spectra have components in the vicinity of the signal of interest, at $2\omega_m$. These overlapping spectra, shown cross-hatched in Figure B-3, are centered at $2\omega_m - \omega_d$ and $2\omega_m + \omega_d$, and have power densities of $\frac{1}{4} E_o^2 J_1^2(\mu) \frac{\sigma^2}{2\omega}$.

The total noise power in a small rectangular bandwidth, B, centered at $2\omega_m$ is given by

$$N_o = 2[B]\left[\tfrac{1}{4} E_o^2 J_1^2(\mu)\frac{\sigma^2}{2\omega}\right] + \frac{2}{2\pi}\int_{2\omega_m - \pi B}^{2\omega_m} \frac{\sigma^2}{4\pi\omega} 2(\omega - 2\omega_m + 4\pi W)\, d\omega$$

$$= \tfrac{1}{4} B E_o^2 J_1^2(\mu)\frac{\sigma^2}{W} + \frac{\sigma^4 B}{W}\left[1 - \frac{B}{8W}\right]$$

$$= \frac{\sigma^4 B}{W}\left[\tfrac{1}{4}\frac{E_o^2 J_1^2(\mu)}{\sigma^2} + (1 - B/8W)\right] \qquad \text{(B-17)}$$

The output signal power is given by $\frac{E_o^4 J_1^4(\mu)}{2}$.

Therefore, the output S/N is

$$(S/N)_o = \frac{E_o^4 J_1^4(\mu)}{2} \cdot \frac{W}{\sigma^4 B\left[\frac{1}{2} \cdot \frac{E_o^2 J_1^2(\mu)}{2\sigma^2} + 1 - \frac{B}{8W}\right]}$$

$$= \left(\frac{S}{N}\right)^2_{in} \cdot \frac{2W}{B\left[\frac{1}{2}(S/N)_{in} + 1 - B/8W\right]}$$

For very low input S/N, the output S/N is

$$(S/N)_o \lessapprox \frac{2W}{B}\left(\frac{S}{N}\right)^2_{in}, \qquad (S/N)_{in} \ll I$$

whereas for high input S/N, the output S/N is

$$(S/N)_o \lessapprox \frac{4W}{B}\left(\frac{S}{N}\right)_{in}, \qquad (S/N)_{in} \gg I.$$

In both cases it is assumed that $W \gg B$.

Appendix C

VOLUME AND WEIGHT DETERMINATION

A. Altimeter Electronics

1. IF Strip - Small cordwood modules in their metal shielding case.

The IF strip used here is the same as that previously used in the L-band altimeter, except that one extra stage is to be added consisting of one flat-pack and 2 to 3 trimmer resistors. This will add 0.20 inch to the length. The weight of the L-band IF section was 0.23 lb; its size is 3/4 x 3/4 x 4 inches.

Volume = 3/4 x 3/4 x $4\frac{1}{4}$ in = 2.4 in^3

Connectors and hold-down are outside this envelope and not included in the volume.

Weight = $\frac{2.4}{2.25}$ x 0.23 = 0.25 lb

2. Integrated RF - Lower section, strip line board.
Upper section, components in metal case.

Volume = (0.9 x 5.25 x 4.75) + (1 x 5.25 x 2) = 32.9 in^3

Weight (Quoted by supplier) = 2 lb

3. Power Supply - Components mounted on heat sink base; assembly foamed.

This will use the same schematic as the PS in the L-band Altimeter, but the loading will be only one-half as great. Smaller, lower rated components can be used. The L-band PS volume was 43 cubic inches and its weight was 2.3 pounds.

Volume = 1.5 x 4.4 x 4.5 = 30 in^3

Weight - Since the volume reduction is primarily in the heat sink thickness and component size, use 55% of the L-band weight.

Weight = 0.55 x 2.3 = 1.3 lb

4. AFC - Cordwood module of conventional components potted in foam.

This unit contains 61 conventional components and 5 flat-packs. Using standard procedure for sizing cordwood modules gives

Volume = 2.6 x 1.3 x 0.75 = 2.5 in^3

Assuming the unit is potted in foam, from weight estimation curve we have:

Weight = 2.5 x 0.055 = 0.14 lb.

5. Master Oscillator - Solid State devices, integral isolator and other components in shielding case.

Volume = 1.5 x 1.5 x 2 = 4.5 in^3

Since the unit has considerable case and structure in relation to its volume, assume its density is 60 lb/ft^3.

Weight = $\frac{4.5}{1728}$ x 60 = 0.15 lb

6. TWT - Ceramic vacuum tube with circular magnets potted in case.

Volume (quoted by supplier) = 2.5 lb

7. HVPS and Modulator - Relatively large components mounted in shielded case. Approximately one-half of these operate at 7 kV.

Due to the high voltages involved, parts must be placed in relatively open construction. Layout indicates case size to be

Volume = 3.5 x 4.0 x 2.0 = 28 in^3

Since the components are large and of high mass (toroidal transformers, power resistors, etc.) assume the package density is 85 lb/ft^3. This gives a weight of 28 x 85/1728 = 1.4 lb. But the lower half of the assembly must be potted in silicone to prevent breakdown due to high voltage. Assume potting will occupy one-half of the lower space and that its density is 1.4.

Weight of potting = $\frac{28}{2}$ x $\frac{1}{2}$ x 1.4 x $\frac{62.4}{1728}$ = 0.35 lb

So the total

Weight = 1.4 + 0.35 = 1.75 lb

8. Electronics Package - 260 integrated circuit chips in boxes, 175 conventional components in cordwood modules. Mounted on small carrier boards in shielding case.

Volume = 3.2 x 5.2 x 2.0 = 32.5 in^3

Weight

a.	Flat boxes = 1.2 x 0.008 =	0.09
b.	Cordwood modules = 7 x 1.2 x 0.055 =	0.46
c.	Carrier boards (0.03 Silicone fiberglass @0.065 lb/in^3 10 x (3.2 x 1.7 x 0.03) x 0.065 =	0.10
d.	Mother board (same as above) (3.25 x 5.2 x 0.03) x 0.065 =	0.03
e.	Case (aluminum, 0.09 lb/in^3.) walls volume = 2 x (5.2 x 2 x 0.2) = 4.16 cu.in. ends = 2 x (3.25 x 2 x 0.02) = 0.26 cover = 3.25 x 5.2 x 0.02 = 0.33 4.75 cu.in. weight = 4.75 x 0.09	0.43
f.	Wire, terminals, adhesives (estimated)	0.09
	Total Weight = 1.20 lb.	

9. Overall Structure (aluminum, 0.09 lb/in^3)

Volume = 5.3 x 4.1 x 11 = 238 cu.in.

Weight

Structure

Base = 11 x (2 + 5) x 0.09	=	6.9 cu.in.
Deck = 11 . 5 x 0.05	=	2.75
Hinge = 7 x 0.5 x 0.04	=	0.14
Total		9.79 in^3

weight = 9.79 x 0.09 = 0.90 lb

Connectors (Cannon; 15 Pin = 0.3 oz)

2 x 0.3 x 0.0625 = 0.04 lb

Coax lines (fittings = 4 gm; line = 12.5 gm/10 in)

Fittings = 10 x 4 gm	=	0.088 lb
Line = 12" x 12.5/10	=	0.033 lb
		0.111 lb

Wire (#24 shielded, 6 lb/1000 ft)

18 x 6/1000 = 0.10 lb

Screws, Hardware, coatings = 0.07 lb (estimated)

TOTAL WEIGHT = 1.23 lb

B. Antenna

Weights

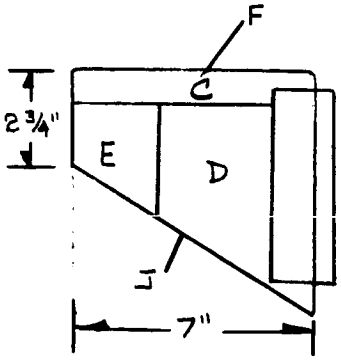

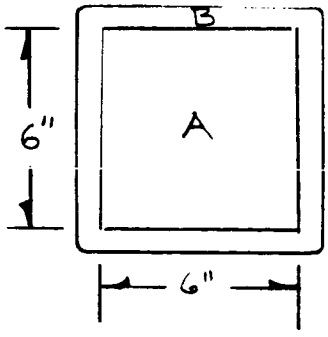

Section A

Foam

$6" \times 6" \times 1" \ (0.00521 \frac{lb}{in^3} = 0.1875 \text{ lb}$

Section B

Frame (Aluminum)

$4(6.5 \text{ in}) (0.9 \text{ in}) (0.060 \text{ in}) (0.1 \text{ lb/ in}^3) = 0.14 \text{ lb}$

Section C

Upper PC Boards (PPO-AL Sandwidh, Composite Density = 0.07 lb/in^3)

$(5 \text{ in}) (4 \text{ in}) (0.25 \text{ in}) (.07 \frac{lb}{in^3}) = 0.35 \text{ lb}$

Section D

Main PC Boards (Composite Density = 0.07 lb/in^3)

$8[4 \text{ in}(3 \text{ in}) + .5 (4 \text{ in}) 2.5 \text{ in}] (\frac{3}{16} \text{ in}) (0.07 \frac{lb}{in} 3) = 1.79 \text{ lb}$

Section E

Electronics Compartment (Density = 45 lb/ft^3)

$[1.8 \text{ in} (1.8 \text{ in}) + 0.5 (1.8 \text{ in}) 1.1 \text{ in}] 6 \text{ in}(\frac{0.026 \text{ lb}}{in^3}) = 0.572 \text{ lb}$

Section F

Upper Cover (Aluminum)

$[0.040 \text{ in} (6 \text{ in}) (8 \text{ in})] 0.1 \frac{lb}{in^3} = 0.192 \text{ lb}$

Section J

Lower Plate (Aluminium)

$[0.040 \text{ in} (6 \text{ in}) 4.75 \text{ in}] 0.1 \frac{lb}{in} = 0.114 \text{ lb}$

Total Weight = 3.35 lb

Total Volume = 236 in^3

Appendix D

CENTER OF GRAVITY AND MOMENT OF INERTIA

Altimeter Electronics

Using the weights calculated in Appendix C and measuring dimensions directly from the layout, the following table of CG calculations can be developed:

TABLE D-1.- ELECTRONICS CG

Unit	Weight lb	O-O Arm in	Moment in-lb	M-M Arm in	Moment in-lb	P-P Arm in	Moment in-lb
Power supply	1.30	2.88	3.75	2.25	2.93	3.13	4.07
Integrated RF	2.00	2.75	5.50	8.38	16.75	2.54	5.08
TWT source	0.15	0.88	0.13	4.75	0.71	4.81	0.72
AFC	0.14	2.56	0.36	8.68	1.21	3.06	0.43
IF strip	0.25	2.56	0.64	4.94	1.24	2.88	0.72
Electronics package	1.20	1.13	1.36	8.50	10.20	3.63	4.36
High voltage power supply	1.75	1.13	1.98	2.00	3.50	3.63	6.85
TWT	2.50	0.83	2.08	5.50	13.75	1.06	2.65
Structure							
Base	0.41	0.04	0.02	5.50	2.25	2.50	1.00
Side and hinge	0.23	1.00	0.23	5.50	1.27	0.04	0.00
Int deck	0.26	2.54	0.66	5.50	1.42	2.68	0.70
Ass. hardware	0.33	2.25	0.74	5.50	1.82	2.68	0.88
Total Weight	10.50	Total Moment	17.46	Total Moment	57.05	Total Moment	26.05
		$\bar{y}$	1.66		5.45		2.49

Sketched in relation to the unit, this data appears on the next page. For the moment of inertia calculations, the actual CG is close enough to that of a homogenous body that equations of that form may be used.

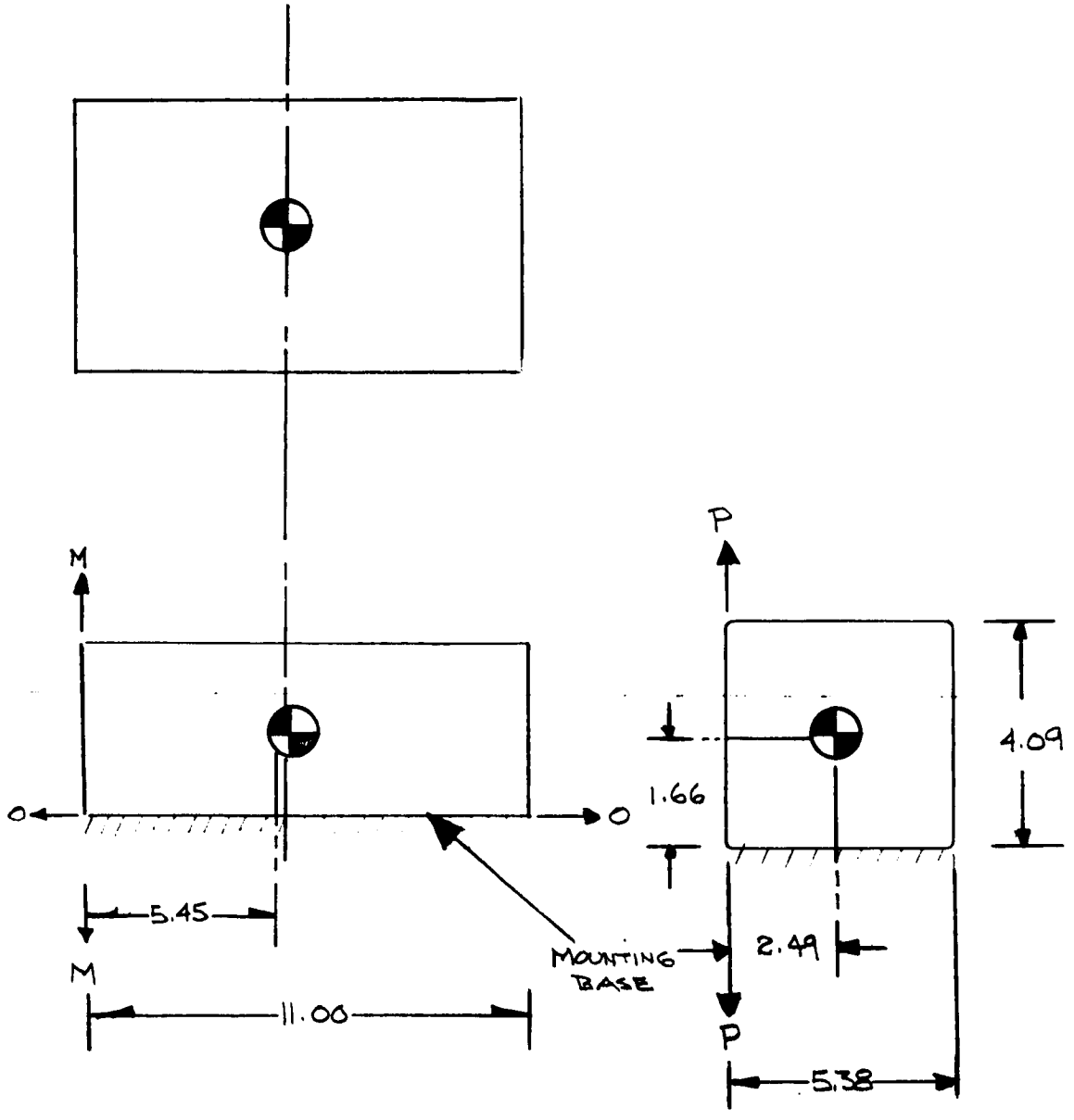
M
O
O
5.45
M
11.00
MOUNTING BASE
P
1.66
4.09
2.49
P
5.38

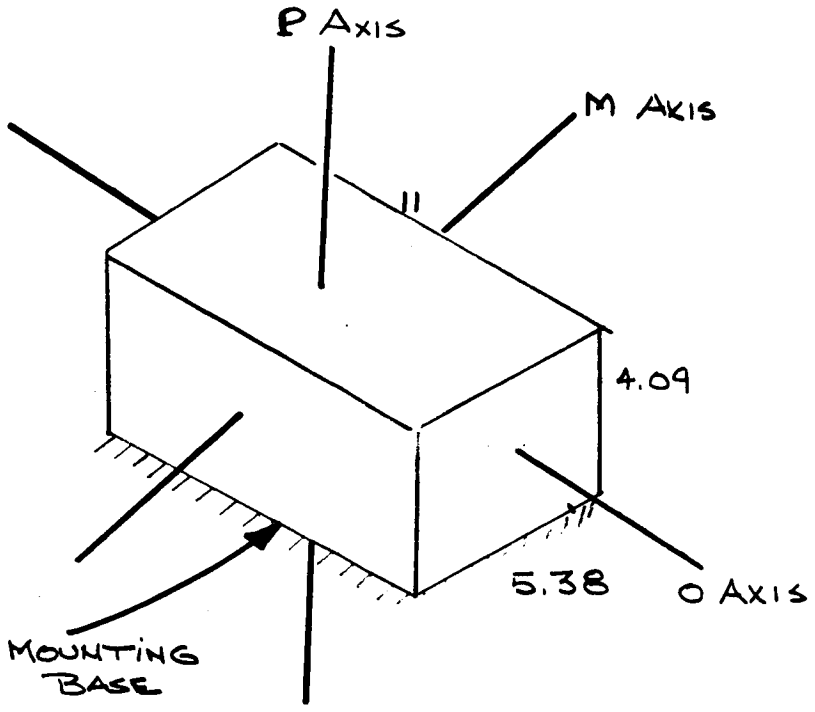

$$I_o = \frac{1}{12}(10.5)(5.38^2 + 4.09^2)$$

$$= \frac{10.5}{12}(45.8) = 38.3 \text{ lb-in}^2$$

$$I_M = \frac{1}{12}(10.5)(11.0^2 + 4.09^2)$$

$$= \frac{10.5}{12}(138) = 120.0 \text{ lb-in}^2$$

$$I_P = \frac{1}{12}(10.5)(11.0^2 + 5.38^2)$$

$$= \frac{10.5}{12}(150) = 131.0 \text{ lb-in}^2$$

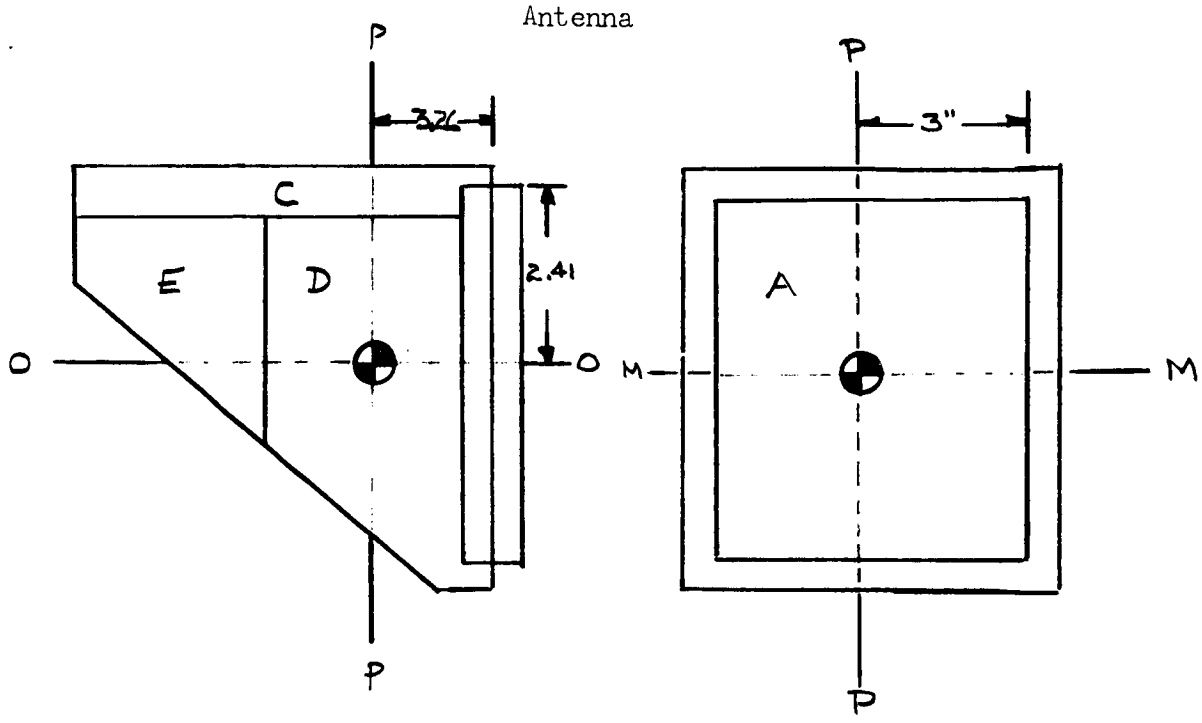

Assume homogeneously distributed mass in each section.

Section A - Foam and Frame $W = 0.3275$ lb

M Axis

$$I_{section} = \frac{1}{12} W (1 + 38.4) = 1.075 \text{ in}^2 \text{ lb}$$

$$I_M = 1.075 + (d^2 \times W) = 1.075 + (2.76^2 \times 0.39^2) W$$

$$I_m = 3.615 \text{ lb in}^2$$

O Axis

$$I_{section} = \frac{1}{12} (0.3275)(76.8) = 2.1 \text{ in}^2 \text{ lb}$$

$$I_o = 2.1 + 0.152 (0.3275) = 2.15 \text{ in lb}$$

P Axis

$I_{section} = 1.075$

$I_P = 1.075 + (2.76)^2 (0.3275) = 3.565 \text{ lb in}^2$

Section C - Upper PC Board and Cover W = 0.542 lb

M Axis

$I_{section} = \frac{1}{12} 0.542 (36 + 0.81) = 1.66 \text{ in}^2 \text{ lb}$

$I_M = 1.66 + (0.563 + 4.0) 0.542 = 4.13 \text{ in}^2 \text{ lb}$

O Axis

$I_{section} = \frac{1}{12} 0.542 (37.2 + 0.81) = 1.72 \text{ in}^2 \text{ lb}$

$I_o = 1.72 + (4.00) 0.542 = 3.88 \text{ lb in}^2$

P Axis

$I_{section} = \frac{1}{12} (0.542)(36 + 37.2) = 3.30 \text{ lb in}^2$

$I_P = 3.30 + (0.542) 0.563 = 3.61 \text{ lb in}^2$

Section D - Main PC Boards and Lower Plate W = 1.904 lbs

M Axis

$I_{section} = \frac{1.904}{12} (16.0 + 18) = 5.4 \text{ lb in}^2$

$I_M = 5.4 + 1.904 (0.202 + 0.25) = 6.26 \text{ lb in}^2$

O Axis

$I_{section} = \frac{1.904}{12} (37.2 + 18) = 8.76 \text{ lb in}^2$

$I_o = 8.76 + 1.904 (0.25) = 9.236 \text{ lb in}^2$

P Axis

$I_{section} = \frac{1.904}{12} (37.2 + 16) = 8.45 \text{ lb in}^2$

$I_P = 8.45 + 1.904 (0.202) = 8.834 \text{ lb in}^2$

Section E - Electronics Compartment W = .572 lbs

M Axis

$I_{section} = \frac{0.572}{12} (5.76 + 4.41) = 0.510 \text{ lb in}^2$

$$I_M = 0.510 + 0.572\ (0.160 + 7.02) = 4.62 \text{ lb in}^2$$

O Axis

$$I_{section} = \frac{0.572}{12}\ (5.76 + 37.2) = 2.04 \text{ lb in}^2$$

$$I_o = 2.04 + 0.572\ (0.16) = 2.13 \text{ lb in}^2$$

P Axis

$$I_{section} = \frac{0.572}{12}\ (37.2 + 4.41) = 1.985 \text{ lb in}^2$$

$$I_o = 1.985 + 0.572\ (7.02) = 6.005 \text{ lb in}^2$$

TABLE D-2. - ANTENNA CENTER OF GRAVITY

SECTION	VOLUME	DENSITY	WEIGHT	MOMENT ARM AXIS			MOMENTS		
				1	2	3	1	2	3
	in^3	lb/in^3	lb	in	in	in	in/lb	in/lb	in/lb
A. Foam	36.0	0.00521	0.1875	0	0.5	3.0	0	0.0937	0.562
B. Frame	1.4	0.1	0.14	0	0.5	3.0	0	0.070	0.42
C. Upper PC Boards	5.0	0.07	0.35	0	0.5	0.5	0	1.4	0.175
D. Main PC Boards	25.5	0.07	1.79	0	2.75	2.9	0	4.93	5.20
E. Electronics Comp	25.3	0.026	0.572	0	5.85	2.0	0	3.34	1.14
F. Upper Cover	1.92	0.1	0.192	0	3.7	0	0	0.71	0
J. Lower Plate	1.14	0.1	0.114	0	3.0	4.9	0	0.342	0.559
TOTALS:	236*		3.3455				0	10.8857	8.056
PACKAGE CG LOCATION:							0 in	3.26 in	2.41 in

* Envelope Volume

NOTE: See moments of inertia for CG location.

TABLE D-3. - ANTENNA MOMENTS OF INERTIA

SECTION	WEIGHT	M AXIS				O AXIS				P AXIS			
		I Section	Distance		Moment of Inertia	I Section	Distance		Moment of Inertia	I Section	Distance		Moment of Inertia
			O	P			M	P			M	O	
	lb	lb/in^2	in	in	lb/in^2	lb/in^2	in	in	lb/in^2	lb/in^2	in	in	lb/in^2
A. Foam Frame	0.3275	1.075	2.76	0.39	3.615	2.1	0	0.39	2.15	1.075	0	2.76	3.565
C. Upper PC Board and Cover	0.542	1.66	0.75	2.00	4.13	1.72	0	2.00	3.88	3.30	0	0.75	3.16
D. Main PC Boards & Lower Plate	1.904	5.4	0.45	0.50	6.26	8.76	0	0.50	9.236	8.45	0	0.45	8.834
E. Electronic Compart	0.572	0.510	2.65	0.40	4.62	2.04	0	0.40	2.13	1.985	0	2.65	6.005
TOTAL	3.35				$I_M = 18.6$				$I_o = 17.4$				$I_p = 22.0$

APPENDIX E

THERMAL ANALYSIS

Transient Analysis

Assume that the altimeter is thermally isolated so that all generated heat is absorbed by the altimeter mass in the form of a temperature rise. The governing equation for a conservative analysis is:

$$\frac{\Delta T}{t} = \frac{\dot{Q}}{CM} \times \left[\begin{matrix}\text{Conversion} \\ \text{Factors}\end{matrix}\right]$$

Where:

t = time, hr
ΔT = temperature rise, °F
$\dot{Q}$ = heat generated, watts
C = Specific heat
= 0.20 BTU/lb °F
M = mass, lb

The above equation is usually a straight line as noted below:

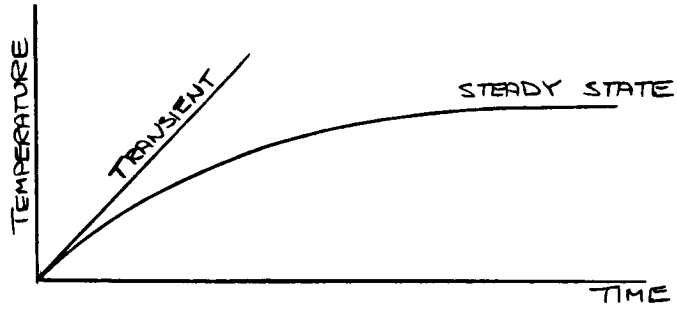

Simplifying the equation, to solve for ΔT gives:

$$\Delta T = \frac{\dot{Q}t}{CM} = \frac{W}{M}\left[\frac{3.41\ (0.5)}{0.2}\right] = 8.53\ \frac{W}{M}\ °F$$

Using the values for power dissipated, (W) and weight (M) as given in the first two columns below and substituting in the above equation, the sub-unit temperature increases can be obtained as tabulated below:

Sub-Unit	Power Dissipation (W) Watts	Weight (M) lb	Temperature Increase After ½ hour operation
IF	0.40	0.25	12.6
Power Supply	5.20	1.30	28.0
AFC	0.30	0.14	13.4
TWT	2.90	2.50	10.0
Master Oscillator	2.00	0.15	113.0 *
Integrated RF	2.00	2.00	8.5
HVPS & Modulator	0.52	1.75	2.5
Electronics Package	5.30	1.20	37.6
Overall, Including Structure	18.6	11.46	13.8

*NOTE: The temperature rise of the Master Oscillator appears very high, but this would not in actual fact occur, since this unit is mounted directly onto the heat sink and the structural mass (as reflected in the overall temperature rise) would keep this temperature down.

Note from the table that the total sub-system temperature rise above the starting ambient would be only 14 °F for a 30-minute operation in a thermally isolated condition.

Equilibrium Analysis

Assume that only conductive heat transfer will apply to obtain a worst-case condition. Then look at a potential hot component on each deck to determine the temperature rise (steady state) between the component and the heat sink at the spacecraft interface. On the lower deck, consider an integrated circuit chip in the Electronics Package. On the upper deck examine a ½-watt resistor in the potted power supply.

Integrated Circuit Chip - This is a 20-mW chip mounted 25 to a ceramic box. The ceramic box adheres to a silicone-glass carrier board which has a 2-ounce copper strip beneath the box to enhance heat transfer. The board is clamped into an aluminum case firmly fixed to the lower deck, which is the basic sub-assembly heat sink.

From work previously done to study the thermal properties of this package we have plotted Figure E-1 on page 161. From the curve for this power level, the temperature drop from chip to ceramic box mounting surface is found to be 6 °C.

For the drop from mounting surface to aluminum case, use:

$$Q = KA \frac{\Delta T}{\Delta x} \cdot \left[\text{Conversion Factors}\right]$$

$$\Delta T = \frac{Q \Delta X}{KA}$$

Also, $R = \frac{\Delta T}{Q} = \frac{\Delta X}{KA}$

So that, $R = \frac{1}{0.92 \times 0.0028 \times 2.54} = 36.5\ ^{\circ}C/_{watt}$

Where:

Q = Power, watts
ΔT = Temperature Difference, °C
Δx = Length of Heat Path = 1 in
K = Thermal Conductivity = 0.92 $^{cal}/_{sec\ cm\ ^{\circ}C}$
A = Cross-Sectional Area of Heat Path = 0.0028 in^2
R = $^{\circ}C/_{watt}$

In this package, approximately 5 watts of the 5.3-watt sub-unit dissipation is in the integrated circuit chips. Assuming this distributed equally between the 12 boxes, temperature rise is:

$$R = \frac{5}{12} \ (36.5\ ^{\circ}C/watt) = 15.1\ ^{\circ}C$$

Assuming negligible temperature differential between the aluminum case and the heat sink (a valid assumption since the wall is relatively massive and is well secured to the base), the total temperature drop from the circuit chip and the heat sink interface is: 6° + 15° = 21 °C.

Resistor in Power Supply - The Power Supply is mounted on the second level deck. It has components formed in cordwood style and potted in foam onto an alumimum base. The thermal path is from resistor to foam to plate to HVPS case below to sub-system sink.

Assume:
Power = 0.5 watt
Size = 3/4" long x 0.3" diameter
Foam potting is scotch cast, thermal conductivity is 5.2 $^{BTU\ in}/_{hr\ ^{\circ}F\ ft^2}$

If the resistor is embedded in ½-inch of the potting compound, the thermal resistance is then:

$$R = \frac{1}{2\pi LK} \ln_e \frac{2L}{D} \left[1 + \frac{\ln_e \frac{L}{2z}}{\ln_e \frac{2L}{D}} \right]$$

Where:

L = length of resistor = 0.75 in.
K = thermal conductivity of potting material = 5.2 $\frac{BTU\ in.}{ft^2\ °F\ hr}$
D = diameter of resistor = 0.3 in.
z = distance from resistor to potting material surface = 0.5 in.

Substituting and simplifying,

$$R = 20.1 \left[\ln_e 5 \left(1 + \frac{\ln_e \frac{0.75}{5}}{\ln_e 5} \right) \right]$$

$$= 20.1 \left[1.609 \left(1 + \frac{0.287}{1.609} \right) \right]$$

$$= 26.5\ °F/watt = 14.7\ °C/watt$$

For the $\frac{1}{2}$-watt resistor, the temperature drop from the component to the power supply base is:

$$\Delta T = 0.5\ \ (14.7) = 7.35\ °C\ \ \text{(use 8 °C)}$$

To determine the rise from the Power Supply base through the HVPS/Modulator to the spacecraft heat sink interface,

Assume:

Power = 5.2 watt
Size = 4.5 x 4.5
HVPS = 0.02" wall, 2" high
Perimeter HVPS = 4.0" x 3.5"
Thermal Conductivity = 80 BTU/hr-ft-°F (Aluminum Alloy)

$$R = \frac{\Delta T}{Q} = \frac{\Delta x}{KA}$$

Through the HVPS Case, then, the rise is:

$$R = \frac{(2)(12)}{80\ (0.02)\ 15} = 1.0\ \frac{°F\ hr}{BTU}$$

$$= 3.41\ \frac{°F}{watt}$$

and the rise is

$$\Delta T = 5.2\ (3.41) = 17.7\ °F = 10\ °C$$

The total drop here is then, $\Delta T_{total} = 8 + 10 = 18°C$

Time for Altimeter to Reach Sterilization Temperature

Determine how rapidly the altimeter will reach sterilization temperature (135 °C) when tested per JPL Specification VOL - 50503 ETS (12 January 1966).

$$mCp \frac{dT_2}{dt} = \dot{Q}_{in}$$

$$= \frac{T_1 - T_2}{R}$$

$$\text{let } \theta = T_1 - T_2$$

$$\frac{d\theta}{dt} = \frac{dT_2}{dt}$$

Substituting, we get

$$-mCp \frac{d\theta}{dt} = \frac{\theta}{R}$$

or

$$+ \frac{d\theta}{dt} + \frac{\theta}{mCpR} = 0$$

$$e^{+\int \frac{dt}{mCpR}} = e^{+\frac{t}{mCpr}}$$

$$\theta e^{+ t/mCpR} = \text{Const}$$

$$@ \; t = 0, \; \theta = 135 - 25 \; °C$$

$$\therefore \text{ const} = 110$$

Where:

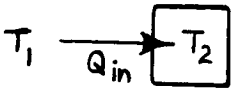

$\dot{Q}_{in}$ = heat flow to component
t = time
m = weight of component
Cp = specific heat of component
T_2 = component temperature
T_1 = heat sink temperature (step function from 25°C @ t = 0 to 135°C at $t \geq 0$
$\theta = T_2 - T_1$
R = thermal resistance between spacecraft heat sink and component

For example, consider the power supply module (a typical component within the PS).

$$mCp = 0.06 \; \frac{\text{BTU lb hr watt 9 °F}}{\text{°F lb 3.41 BTU 5°C}}$$

$$= 0.0316 \; \frac{\text{hr watt}}{\text{°C}}$$

$$R = 3.5 + 15 = 18.5 \; °C/\text{watt}$$

$$(135 - T_2)e^{t/0.0316\,(18.5)} = (135 - T_2)e^{1.7t} = \text{const} = 110$$

$$T_2 = \frac{-110}{e^{1.7t}} + 135 = -F(t) + 135$$

t = hours
T = °C

t hrs	1.7t	$e^{1.7t}$	$F(t) = \frac{110}{e^{1.7t}}$	$-F(t) + 135$ °C
0	0	1	110	25.0
0.5	.85	2.34	47.0	88.0
1	1.7	5.47	20.1	114.9
2	3.4	30.0	3.66	131.34
3	5.1	165.0	.666	134.334
4	6.8	900	.1225	134.8775
5	8.5	5000	.022	134.978

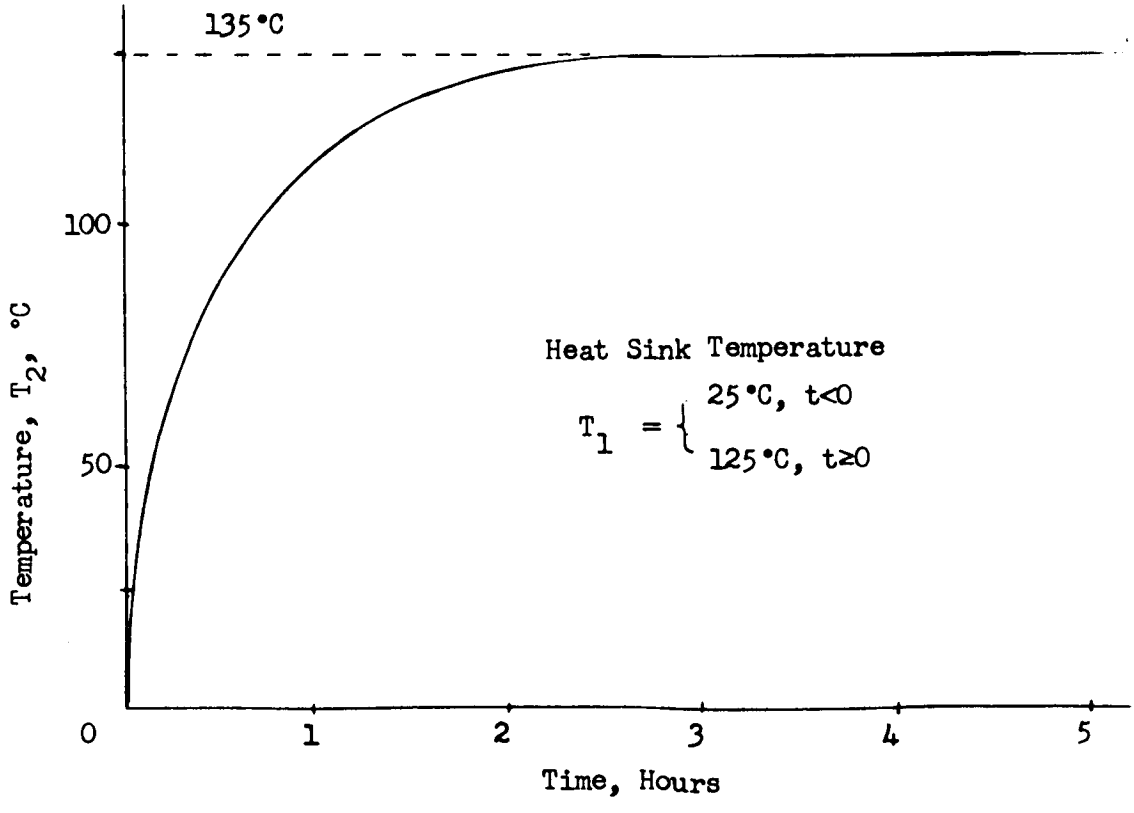

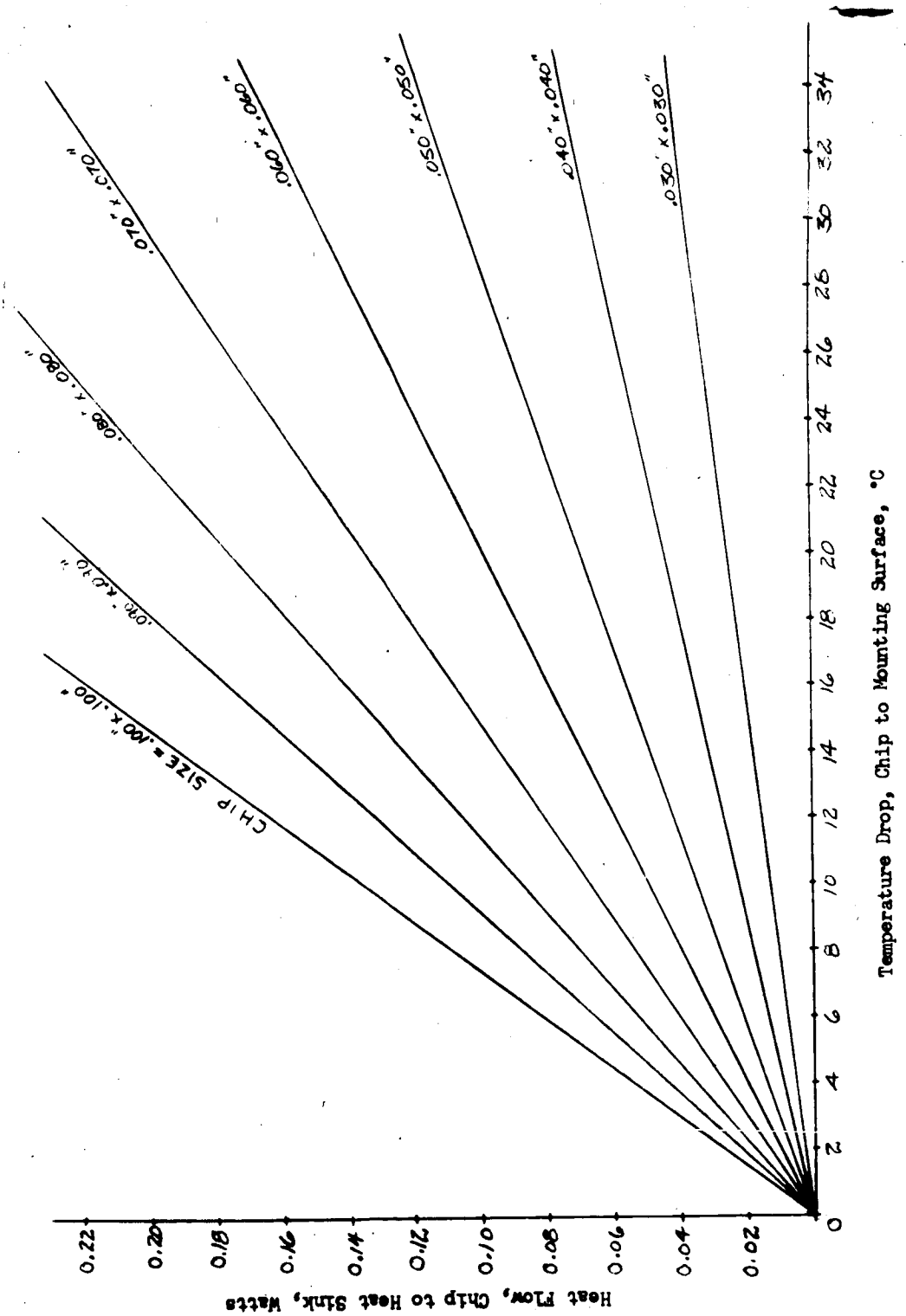

FIGURE E-1. - THERMAL PROPERTIES OF IC CHIP

APPENDIX F

MAGNETIC SHIELDING AND COMPENSATION FOR TWT

As a basis for examining the level of shielding or compensation required to eliminate stray fields from the altimeter TWT, two assumptions were made:

(1) The flight spacecraft will be 12 feet in diameter. This appears reasonable based on present data. (See "Landing on Mars", L. P. Thompson, JPL -- Aeronautics and Astronautics, July 1966; pg 69). Also the altimeter will be located somewhere near the center, or approximately 6 feet from the surface.

(2) The magnetometer is located on a $6\frac{1}{2}$-foot boom. Although there is some difference of opinion as to the mechanical implications of a boom, it appears that to get good magnetic isolation with reasonable weight and design expense, a boom is indicated. Booms of this type previously used have been about 80 inches long (JPL Technical Memorandum No. 33-216, "Proceedings of the Magnetic Workshop", September 15, 1966).

From these two assumptions, the separation distance from altimeter to magnetometer is $12\frac{1}{2}$ feet.

The maximum field strength of the TWT is quoted as being 4 gauss at 3 inches from the tube. In the far-field regions, the field intensity decays with the cube of distance. Although there may be some slight error involved since the 3-inch intensity value is probably still in the near-field region, the best estimate of the field at greater distances can be calculated on the $1/d^3$ relationship, and plotted as shown in Figure F-1.

From this curve we can see that the field at the magnetron contributed by the TWT is 2 gamma. For distances closer to the tube, values can be obtained by comparing with other sources for which the near-field strengths are known. Approximations in this region for the TWT are:

Distance	Field
3"	4 gauss
2"	9 gauss
1"	30 gauss

The TWT is essentially a ceramic tube 11 inches long and $1\frac{1}{2}$ inches in diameter with a series of circular magnets along its length. For the purposes of calculating shield requirements, assume the magnets to be about 1 inch apart (worst case condition). Also assume that the shield is placed 1 inch away from the O.D. of the magnets in the form of a long cylinder. (Much closer might give operational problems.)

Field quoted at 4 Gauss (400,000 gamma) at 3 inches.
Other distances calculated as shown.

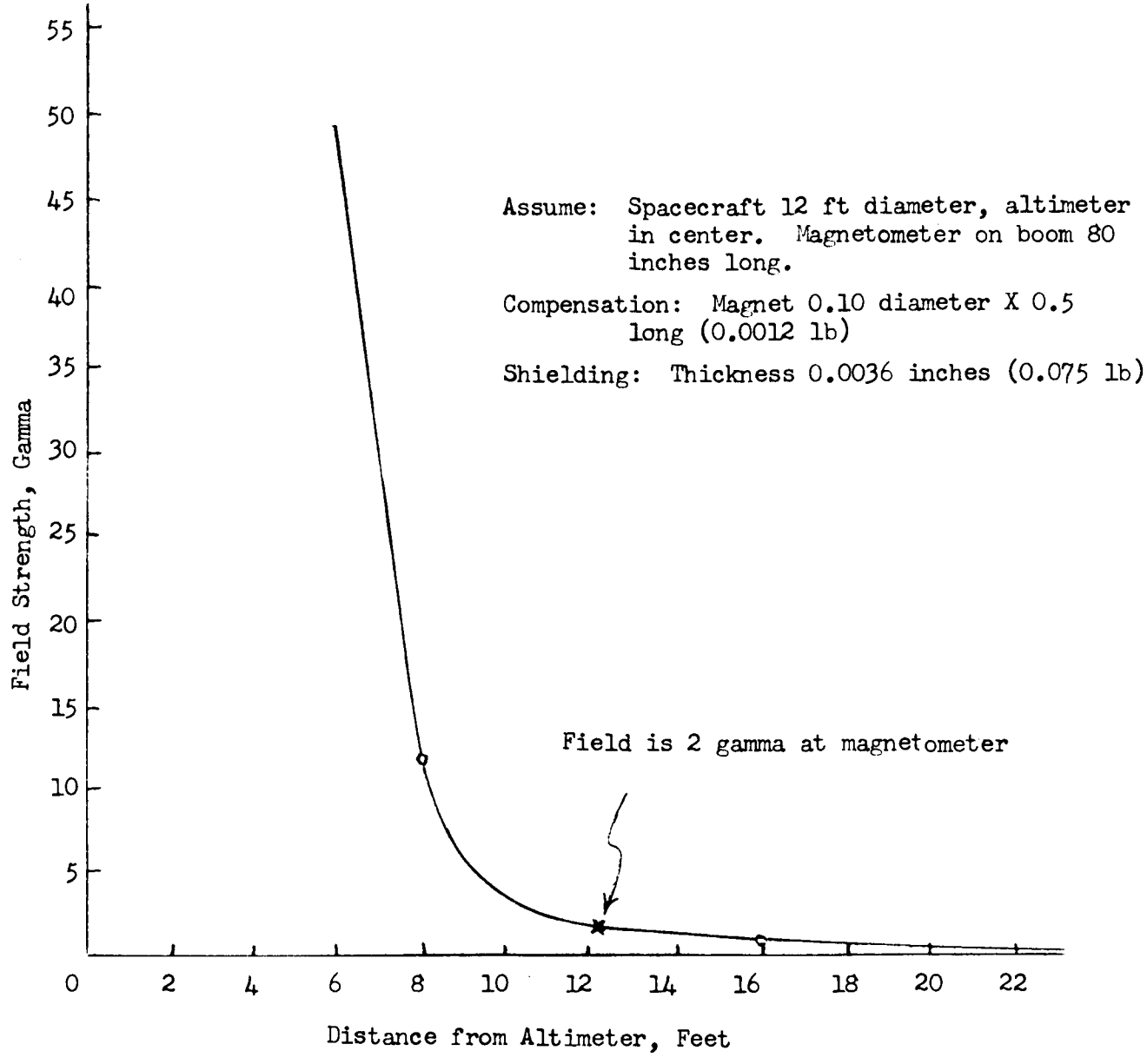

FIGURE F-1. - MAGNETIC CLEANLINESS

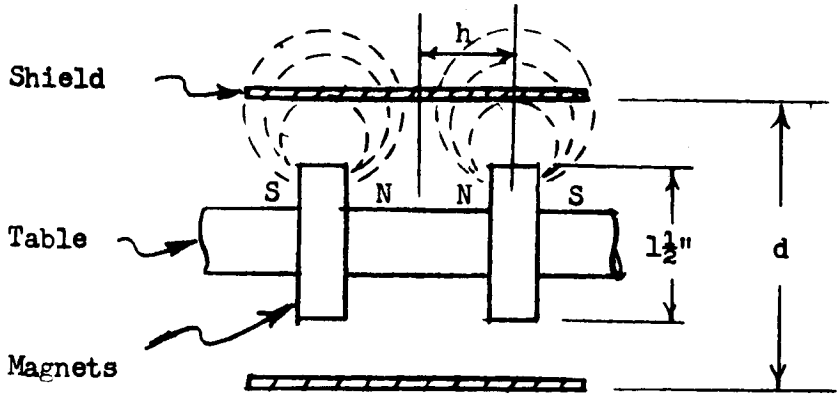

h = ½ distance between magnets

d = shield diameter

In the shield we want to absorb the field which is outside of the shield and to shunt it over to the other pole. Examine a circular shell of the shield which is in length equal to one-half the distance between magnets. The area of this shell is:

$$A = \pi dh = 3.142 \times 3.5 \times 0.5$$

$$= 5.5 \text{ in}^2 = 35.5 \text{ cm}^2$$

We have previously approximated the flux density at one inch to be 30 gauss. Therefore the

$$\text{Flux at shield} = 35.5 \times 30 = 1070 \text{ Maxwells}$$

Most magnetic shielding materials (Mumetal, HY MU 80, etc.) saturate at levels of 7000-8000 gauss. However, since we do not have sufficient driving force here to saturate, assume that the material will work around 4150 gauss. The cross-section area of the shield should then be

$$A_s = \frac{1070}{4150} = 0.258 \text{ cm}^2$$

The shield circumference is:

$$C = \pi \times 3.5 \text{ in} \times 2.54 = 28 \text{ cm}$$

And the shield thickness calculates to be

$$t = \frac{0.258}{28} = 0.0092 \text{ cm}$$

$$= 0.0036 \text{ in}$$

The weight of this shield will then be

$$W = \pi d l t \sigma$$

$$W = \pi \times 3.5 \times 13 \times 0.004 \times 0.288$$

$$= 0.08 \text{ lb}$$

where
d = diameter of shield, in
l = length of shield, in
t = thickness of shield, in
σ = density of shield material, lb/in^3

From the above, the variation in isolation with shielding weight can be plotted as shown in Figure F-2. Calculations have estimated what the shield weight would be if its diameter were varied. They show that, within the realm of operating possibility, the shield weight remains essentially constant for the same protection. Although the weight of the shield is not too great, its occupied volume would result in a considerable increase in overall package size.

A more economical approach is to use a small magnet to compensate or null out the stray field. But compensation is possible only at a specific location both in distance and placement. Therefore, the spatial relationship between altimeter and magnetometer must be established before making the final compensation design.

The actual compensation is a cut-and-try process requiring some experimentation to obtain the best field null. But, once established, the null magnet can easily be applied by the TWT supplier. Since this is a null condition, care must be taken that the compensating field is firmly fixed and does not shift with time. It should be made of the same material as the source so that temperature variations, natural decay, and induced fields will affect both equally to maintain the null.

The following formula gives the first approximation for the compensating magnet. It is about as close as can be determined without experimentation.

$$M_x = \frac{H_x D^3}{2}$$

$$M_x = \beta V$$

$$V = H_x D^3 / 2\beta$$

H_x = field at magnetometer, gamma
D = distance from compensating magnet to magnetometer, feet
β = flux density of compensating magnet, gamma
V = volume of magnet, ft^3

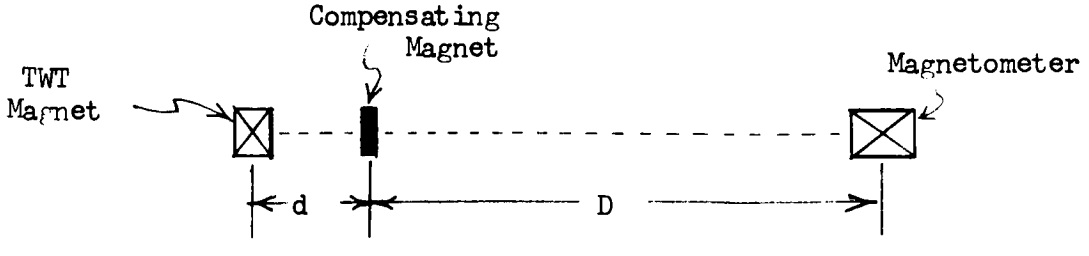

NOTE: The distance d above is made as short as possible without interfering with TWT operation. This, of course, gives the greatest latitude in placement relationship between the TWT and magnetometer.

For this case:

H_x = 2 gamma (see Figure F-1)

D = $12\frac{1}{2}$ feet. It is assumed that d will be small compared to d; use worst case conditions.

= 8000 gauss = 8×10^8 gamma

$M_x = H_x D^3 / 2\beta$

$= 2 \times \overline{12.5}^3 / 2 \times 8 \times 10^8$

$= 24 \times 10^{-7}$ ft^3

$= 0.0042$ in^3

The magnet weight

$$W = 0.0042 \times \frac{500}{1728} = 0.0012 \text{ lb.}$$

For most effective operation, the ℓ/d ratio of the compensating magnet should be about 5, so that

$$V = \frac{\pi d^2}{4} \times 5d$$

Or $$d^3 = \frac{4V}{5\pi} = 4 \times \frac{.0042}{5\pi}$$

d = 0.103 inch diameter

ℓ = 5 d = 0.515 inch long

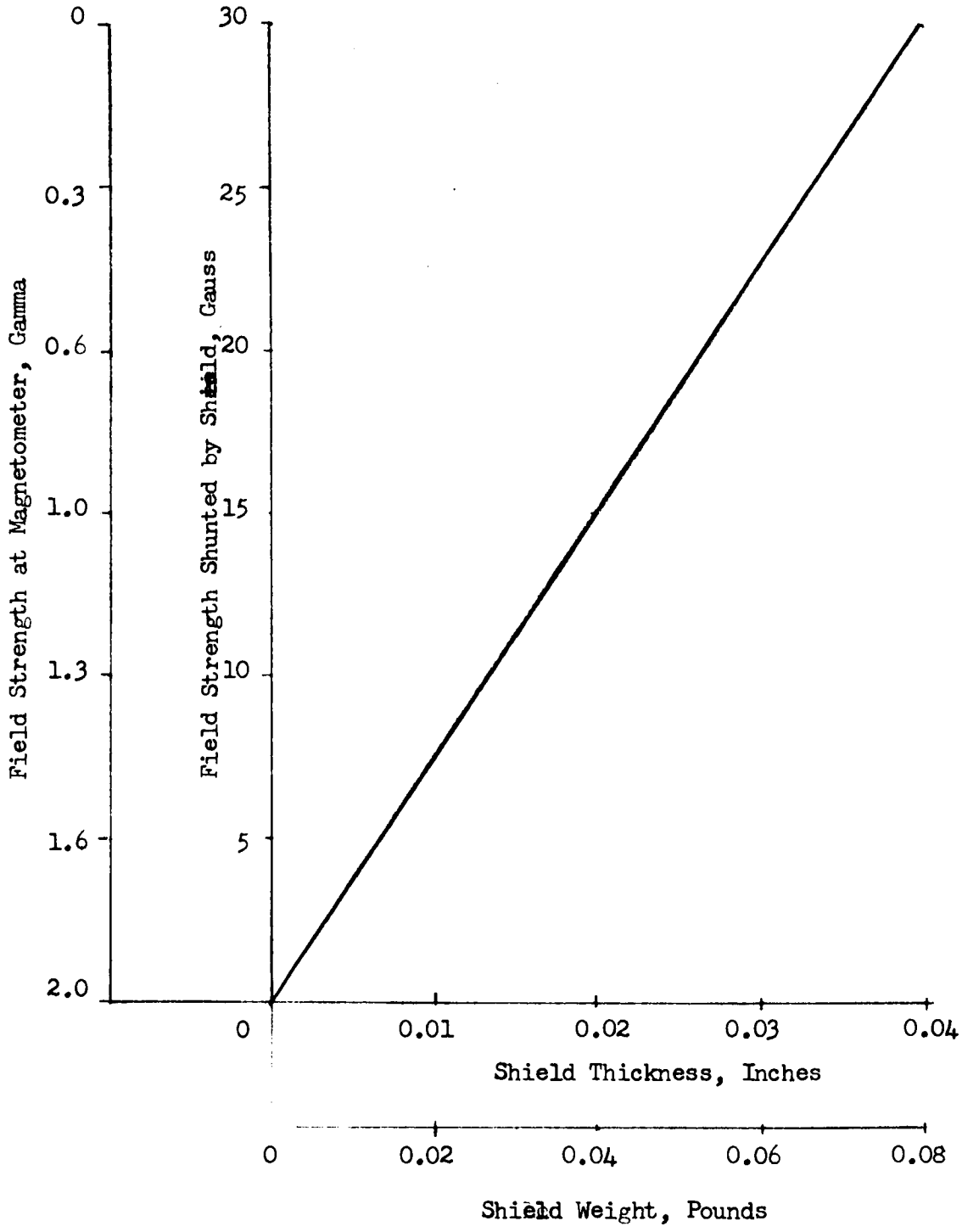

FIGURE F-2. - SHIELD WEIGHT AT TWT VS. FIELD STRENGTH AT MAGNETOMETER